ZEBRAFISH MAGNETITE AND LONG-LIVED ROHON-BEARD NEURONS: EXPANDING OUR VIEW OF TWO ZEBRAFISH SENSORY SYSTEMS IN DEVELOPMENT AND ADULTHOOD

Thesis by

Alana Dixson

In Partial Fulfillment of the Requirements for the

degree of

Doctor of Philosophy

CALIFORNIA INSTITUTE OF TECHNOLOGY

Pasadena, California

2012

(Defended September 8, 2011)

DEDICATION

This dissertation is dedicated to my cute Caltech baby, Kizashi James. Please learn to love God and to seek knowledge in your youth; dream well all your life; work hard so that you may achieve and provide; and never, ever, compromise your integrity.

ACKNOWLEDGEMENTS

I extend a special thanks to Drs. Joe Kirschvink, Bruce Hay, Kai Zinn, Henry Lester, David Prober, and Tim Raub, Dean Joseph Shepherd, Bishop Randy Muhlestein, Lillian Dixson, and Adam Robinson for supporting and encouraging me to move forward despite challenges and setbacks. I also recognize Drs. Marianne Bronner and Scott Fraser for training and financial support for the first four years of my doctoral work; Debbie Marshall, Drs. Le Trinh and Sean Megason, and the CEGS Screen Team for technical assistance; Drs. David Koos, Max Ezin, Rasheeda Hawk, Thai Ngyuen, and Aidyl Gonzalez-Serrichio for helpful scientific discussions and encouragement; and Drs. Alvaro Sagasti, Angeles Ribera, and Eduardo Rosa-Molinar for informative discussions about Rohon-Beard neurons and zebrafish in general. I would also like to acknowledge the entire Bronner and Fraser labs during my tenure in the Fraser group for encouragement and friendship, and especially Dr. Bronner for supporting me and my zebrafish work. Funding was provided by the National Human Genome Research Institute (NHGRI) Center of Excellence in Genomic Science (CEGS) Grant: P50 HG004071, the National Science Foundation (NSF) Human Frontiers Science Program (HFSP) Grant: RGP0028 to JLK for the paleomagnetic and FMR work, and the Achievement Rewards to College Scientists (ARCS) Foundation for the ARCS Fellowship that allowed me to complete my doctoral work and be a mother.

ABSTRACT

During embryogenesis, the central nervous system (CNS) transforms from what seems like an amorphous mass of cells to a rod-like structure, and then to a fully functional and complex system of tissues composed of multiple cell types. Using confocal laser scanning microscopy (CLSM), I demonstrate a modified version of *in toto* imaging to track normal spinal cord organization in zebrafish from bud stage, ~ 11 hours post-fertilization (hpf), to 48 hpf. I also assisted in identifying several transgenic lines using a gene trap vector, the FlipTrap (FT), which creates a normally localized and functional fluorescent fusion protein for *in vivo* analysis of gene expression throughout development. I used two FT lines along with a modified version of *in toto* imaging to study sensory cells in the dorsal spinal cord.

With the FT tool, I discovered a subset of Rohon-Beard (RB) neurons that perdures into the adult. These uniquely transient chemo- and mechano-sensory cells have been well characterized in the dorsal spinal cord of lower vertebrates; however, the notion of persistent RBs contrasts with dogma suggesting that the entire population disappears during the early larval period. The coexistence of RB-like neurons with dorsal root ganglia (DRG) suggests that zebrafish have two post-embryonic sensory systems, challenging the previous notion that only peripheral sensory neurons survive.

In the second part of my dissertation I describe my studies of biogenic magnetite which has been detected in a broad range of organisms, including magnetotactic bacteria, migratory fish and birds, invertebrates, and humans. Magnetite mediates magnetosensation in many species through the effects of pulse-remagnetization on behavior. The mechanisms of

magnetite biomineralization are not well characterized in higher organisms. Previous studies have shown deposits of magnetite in projections of the trigeminal nerve, alongside behavioral evidence suggesting that both optical pumping and magnetite-based mechanisms may operate simultaneously. Subsequent efforts to identify the anatomical seat of magnetoreceptors have focused on the same locations in new organisms, excluding other areas. Here I report the unexpected presence of biogenic magnetite in the lateral line region of the genetically and physiologically tractable vertebrate model organism, *Danio rerio*.

TABLE OF CONTENTS

LIST OF ILLUSTRATIONS AND/OR TABLES

CHAPTER I

Introduction

AUTHOR

Alana D. Dixson

A Brief Review of Early Spinal Cord Patterning in Zebrafish

The spinal cord in mammals, birds, and zebrafish begins as the caudal extension of rostral-caudal patterning of the neural tube (Appel, 2000). The forebrain is the first CNS organ to form, followed successively by the midbrain and hindbrain, and finally, the spinal cord (Appel, 2000; Jessell, 2000). As these posteriorizing events proceed, neurogenesis begins along the dorsoventral (DV) axis of the new spinal cord (Appel, 2000; Jessell, 2000). The product of DV patterning which involves cues (Guillemot, 2007; Helms, Battiste, Henke, Nakada, Simplicio, Guillemot and Johnson, 2005; Jessell, 2000; Lewis, 2005; Lewis and Eisen, 2003) from the roof and floor plates, neuroectoderm, and the notochord are the specific neuronal cell types of the spinal cord (Appel, 2000; Jessell, 2000). This process of neurogenesis proceeds via the creation of genetically programmed neuronal progenitor domains (Guillemot, 2007; Helms Amy W., 2003; Jessell, 2000; Lewis Katharine E., 2003; Lewis, 2005), which contain the precursors of the full spectrum of motoneurons (MNs), sensory neurons (SNs), and interneurons (INs), as well as other cell types, such as radial glia (Guillemot, 2007; Helms et al., 2005; Jessell, 2000; Lewis, 2005; Lewis and Eisen, 2003).

In previous studies in the embryonic zebrafish spinal cord, workers have shown that primary neurons with distinctive soma morphology, position, and axonal extension precede secondary neurons (Kimmel and Westerfield, 1990; Kuwada, Bernhardt and Nguyen, 1990; Lewis and Eisen, 2003). As early as 15-17 hpf growth cones of these earliest spinal neurons are visible and they begin to prepare the tissues within the spinal cord for neuronal tracts, which then will carry motor and sensory information (Kuwada et

al., 1990; Lewis and Eisen, 2003). For example, in the SN system, Rohon-Beard (RB) cell axons pioneer the dorsolateral funiculus (DLF) and then reportedly are functionally replaced by dorsal root ganglion (DRG) axons (Kuwada et al., 1990; Lewis and Eisen, 2003; Sipple, 1998b). Among MNs, secondary and primary MN progeny persist together and are found in the adult animal. As the spinal cord continues to develop, the new neurons complete axonal projections to their CNS or extra-CNS targets, such as hindbrain, other neurons, or muscles, and begin to form more identifiable axonal tracts (Kuwada et al., 1990; Lewis, 2005; Lewis and Eisen, 2003).

At this point, spinal neuron identities become more clearly defined anatomically, molecularly, functionally, and morphologically. The general organization of the spinal cord, coupling of MN to IN, and the role of each spinal neuron subtype come into clearer focus using electrophysiological recordings to characterize cell-type-specific neuronal firing patterns that can be elicited by ectopic stimuli (Jankowska, 2001; Lewis and Eisen, 2003; McLean, Fan, Higashijima, Hale and Fetcho, 2007).

Investigators have shown that spinal neuron subtypes are already specified by the time they make their axonal projections, but they retain some plasticity. For example, *in vitro* exposure to different signaling molecules can change progenitor identities, causing them to specify different post-mitotic neurons (Guillemot, 2007; Jessell, 2000). Notwithstanding their potentially flexible identity early on, we can distinguish spinal neurons by their progenitor domains of origin and signature mRNA expression profiles of transcription factors (TFs) (Briscoe, Pierani, Jessell and Ericson, 2000; Guillemot, 2007;

Jessell, 2000; Sapir, Geiman, Wang, Velasquez, Mitsui, Yoshihara, Frank, Alvarez and Goulding, 2004; Saueressig, Burrill and Goulding, 1999; Shirasaki and Pfaff, 2002; Zhou, Yamamoto and Engel, 2000).

Jessell and others have constructed a model of the genetic signaling mechanisms that underlie DV patterning of the vertebrate spinal cord (Appel, 2000; Helms et al., 2005; Helms and Johnson, 2003; Jessell, 2000). These signaling gradients are composed of bone morphogenetic proteins (BMPs) and Sonic hedgehog (Shh) that act on TFs in a concentration-dependent manner. In turn, each TF in the dorsal and ventral spinal cord has a distinct boundary that allows tight spatial control of neuronal progenitor domains. Once the domains are established under the influence of the domain-specific TFs, neuronal subtypes are specified. Figure 1, taken from Lewis (2005), shows these gradients in the dorsal and ventral cord and the progenitor domains they establish.

Transcription factors responsible for neuronal progenitor domains can be broken up into two groups, Class I and Class II (Jessell, 2000). Depending on the class, the TFs are either induced or inhibited by the BMP and Shh gradients to which they are subjected (Jessell, 2000). For example, decreasing levels of BMPs lead to expanded IN populations but fewer or absent neural crest and RB cells (Lewis and Eisen, 2003). The downstream effects of these actions allow spatial constriction of neuronal subtype despite the close proximity of these progenitor domains to each other in the small space of the embryonic spinal cord.

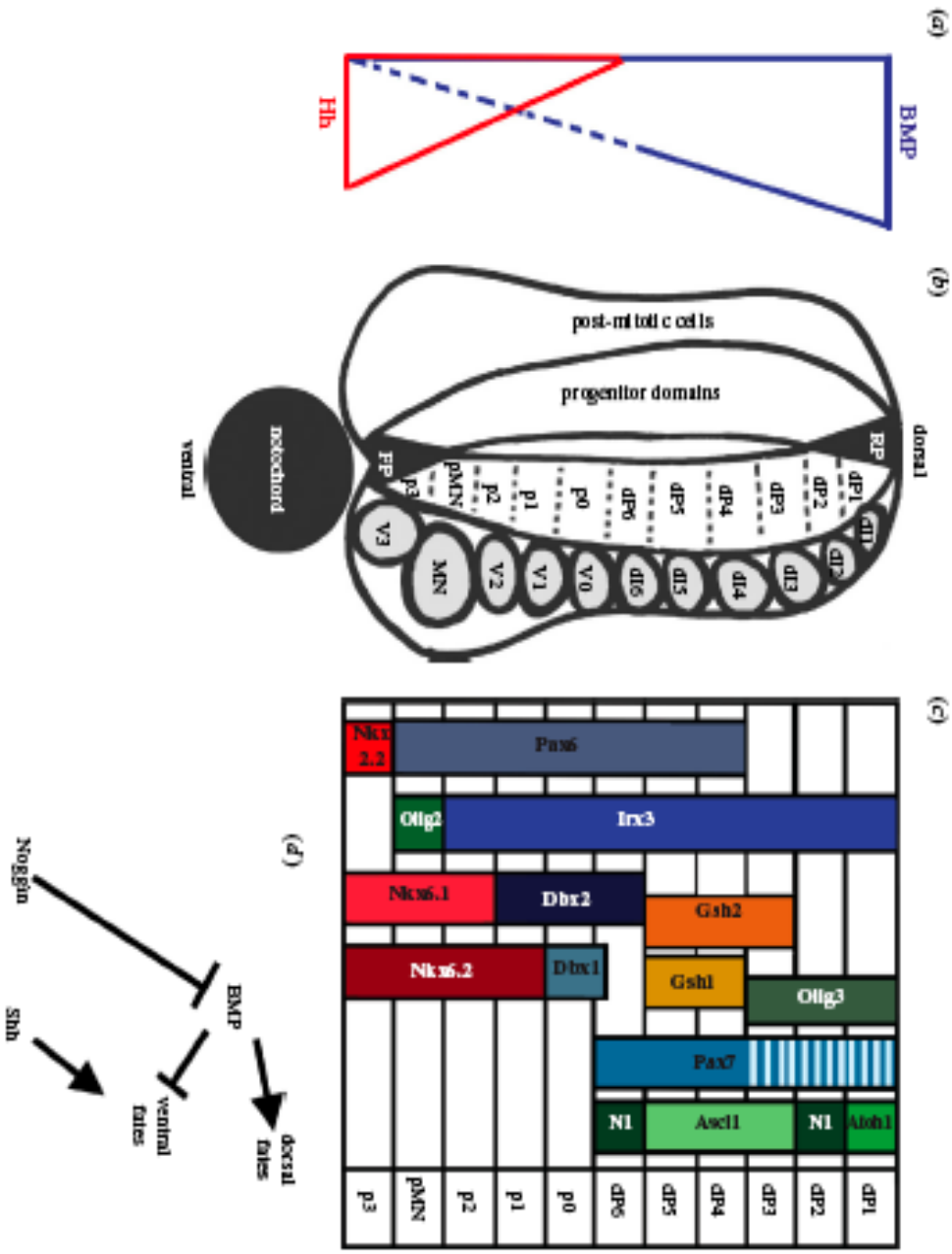

Figure 1 Patterning of the Mammalian Spinal Cord

Figure 1 Patterning of the Mammalian Spinal Cord

Schematic showing gradients of Hh and BMP signaling in the embryonic vertebrate spinal cord. BMP signaling is highest in the dorsal spinal cord and Shh signaling is highest in the ventral spinal cord. In all cases, dorsal is up and ventral is down. The dotted blue line indicates that the influence of BMP signaling may extend to the ventral spinal cord. (b) Schematic cross-section through the embryonic mammalian spinal cord. Progenitor domains are located medially in the ventricular zone and post-mitotic cells are located at the lateral edges of the spinal cord. RP, roof plate; FP, floor plate; dP1--dP6, pMN, and p1-3 are different progenitor domains. dI1-dI6, MN, and V0--V3 are different populations of post-mitotic neurons. (c) Schematic showing the transcription factors expressed in particular progenitor domains. N1 refers to neurogenin 1. bHLH proteins are in green, Class I homeodomain proteins are in blue, Class II homeodomain proteins are in red, and dorsal homeodomain proteins that have not been shown to be Class I proteins are in orange. Proteins that share an expression boundary and cross-repress each other are vertically aligned. (d) A model of how BMP and Shh signaling may interact to specify dorsal and ventral spinal cord fates. Ventrally expressed Shh induces ventral fates, whereas dorsally expressed BMPs induce dorsal fates and repress ventral fates. The repression of ventral fates by BMPs is removed in the ventral spinal cord by ventrally expressed BMP inhibitors such as Noggin (Lewis and Eisen, 2003).

The presence of TFs alone does not explain the temporal control of neuronal subtype specification and the fact that more than one spinal cord cell type can be produced from a small number of progenitors. TFs act at different times on progenitor domains to direct

cell differentiation in neural and glial directions, and then more specifically in MN or IN directions, depending on the location in the developing spinal cord (Briscoe et al., 2000; Guillemot, 2007; Lee and Pfaff, 2001). More recent work has begun to unravel the transcriptional code that itself relies on a combinatorial code to execute neuronal and non-neuronal cell specification using largely the same proteins (Briscoe et al., 2000; Guillemot, 2007; Lee and Pfaff, 2001).

Dynamic *In Vivo* Imaging of Vertebrate Spinal Cord Development

While many of these classical pathways are understood, how other genes contribute to vertebrate neural tube formation is not. Following gene expression in real time can reveal the temporal and spatial arrangement of developmentally important molecules throughout this process to generate the entire mature spinal cord. The goal of developmental biologists is to resolve the process of epigenesis on the cellular level, and this can be addressed with *in vivo* imaging techniques (Megason and Fraser, 2003). In addition to those signaling pathways discussed above, other genes may factor into this process and interact with these classical mechanisms in a manner that will be difficult to parse without dynamic imaging. Typically, tools such as immunohistochemistry with static imaging explain changes in morphology and help characterize gene expression or protein interactions, but they are limited to the time point studied and cannot describe dynamic processes that may happen in between selections. Creating fluorescence patterns that are easily identified and in locations in the CNS that are accessible by light microscopy techniques can add to what we already know; confocal laser scanning microscopy is capable of doing this in high throughput or, on the scale of individual embryos, with high

resolution (Megason, 2009; Megason and Fraser, 2003). The dorsal spinal cord and the large, primary sensory cells, Rohon-Beard (RB) neurons, are a good target for such studies.

Zebrafish are ideally suited for CLSM because the limitations of tissue thickness and opacity present with other vertebrate embryos are eliminated by their relatively small size and optical transparency (Megason, 2009; Megason and Fraser, 2003). Fluorescent labels such as variants of the naturally occurring green fluorescent protein (GFP) are easily introduced into zebrafish (Gong, Ju and Wan, 2001) and highlight cells of the spinal cord by creating fusion proteins with endogenous genes (Blader, Plessy and Strähle, 2003; Kimura, Okamura and Higashijima, 2006; Park, Kim, Bae, Yeo, Kim, Hong, Shin, Yoo, Hibi, Hirano, Miki, Chitnis and Huh, 2000). Fluorescence imaging may give way to label-free methods, such as generation of second- and third-harmonic (SHG and THG, respectively) signals to study cell division and morphogenesis (Olivier, Luengo-Oroz, Duloquin, Faure, Savy, Veilleux, Solinas, Debarre, Bourgine, Santos, Peyrieras and Beaurepaire, 2010), but for gene- and protein-level expression, dynamic imaging with fluorescent proteins is still the most powerful technique.

Rohon-Beard Neurons

In the 1880s Rohon and Beard (Beard, 1889; Rohon, 1884) identified a set of large neurons in the dorsal spinal cord of skates, which were later named Rohon-Beard (RB) neurons. Stereotypical anatomical features among RBs form the basis of their characterization, including a large, granular cytoplasm, a central axon that pioneers and

subsequently heavily invests the dorsolateral tract (DLT), and a peripheral axonal arbor that innervates skin and muscle. These cells are specified during gastrulation via delta/notch signaling (Cornell and Eisen, 2000) before a true spinal cord exists, and migrate from the lateral neural plate to take up their position in a bilateral row along the full rostral-to-caudal extent of the developing cord. RB neurons form the first, rudimentary sensory system in the embryo, allowing it to avoid predation and potentially harmful environmental stimuli by mediating escape reflexes such as C- and S-startle in zebrafish. We find evidence of RB neuron conservation throughout vertebrate taxa, including xenopus, newt, lamprey, zebrafish, and even humans.

Rohon-Beard neurons are completely eliminated during embryonic development (Lamborghini, 1987) in several species of anamniotes. In zebrafish, and other species, the function of RBs is to provide a first defense against predation before the mature sensory system mediated by the DRG arrives and differentiates from its neural crest origins.

Several reports have indicated that caspase-mediated apoptosis alters key neurotrophins and other factors that contribute to RB death in zebrafish (Williams, 2000). For example, comparing the caspase inhibitor, zVADfmk, and a control treatment with sFAfmk, which is not an inhibitor, Williams and colleagues observed a 5% versus 20% death rate in the inhibitor group compared to controls between 19 hpf and 3.5 dpf, with a decline in changes associated with zVADfmk around 48 hpf. Also, at 48 hpf, the caspase-inhibitor-treated embryos failed to show a change in the number of dying RBs. In embryos that

were continually treated by 3.5 dpf, the authors again saw complete, or near complete RB death; they postulated that RBs die via a mechanism other than caspase-mediated programmed cell death (PCD), or that the inhibitor was unable to penetrate the spinal cord. It is also possible that different waves of RB death exist that involves diverse mechanisms depending on the type of RB cell involved. Following this logic, in zebrafish early-dying RBs may be removed via a caspase mechanism, while later-dying RBs are autophagocytosed (Lamborghini, 1987).

Next, Williams and colleagues showed that depletion of neurotrophin-3 (NT3) also seems to play an important role. In cultured spinal cord explants, administration of NT-3 antibodies lead to increased death among RB neurons, while treatment with NT-3 increased the number of trkC1-positive RB neurons. Interestingly, among the RB cells as a population, although cell death was reduced, it was not eliminated. Using these results the authors conclude that NT-3 is necessary, but not sufficient for RB survival and that other factors are likely to be involved in regulating RB lifespan.

Zebrafish Possess A Magnetic Sense

In contrast to the RB neuron, almost nothing is known about magnetoreceptor cells in zebrafish. The fact that these animals can be trained to respond to magnetic fields (Shcherbakov, Winklhofer, Petersen, Steidle, Hilbig and Blum, 2005) is evidence that some form of magnetoreceptive system exists, but as in many organisms that have successfully been conditioned to respond to changes in magnetic field direction, intensity, or oscillations, no definitive receptor or cell has been identified. Zebrafish possess

several peripheral sensory structures, each of which could convey magnetic field information to the CNS.

It is possible that a separate magnetosensation apparatus exists, but more likely, another structure has been co-opted to perform this function. Several candidates include the trigeminal ganglion (TG) and its projections, the lateral line, the DRG, and in early embryos the RB neurons. A mechanoreceptor-coupled cell is the most likely neuronal subtype and a sensory system that synapses on CNS targets would be the most elegant and efficient transducer of magnetic field stimuli. In zebrafish we can study each of these sensory neuronal subtypes in both embryos and adults, to understand magnetosensation capabilities from their earliest time points through the mature adult.

A Special Connection: Rohon-Beard Neurons and the Trigeminal Ganglion Neurons

The early zebrafish embryo possesses a unique population of neurons called RB cells that form and disappear during the first 18 - 48 hours post fertilization (hpf) (Sipple, 1998a). RB neurons (Figure 1) are large, bipolar mechanosensory cells with granular cytoplasm in the dorsal spinal cord of embryonic vertebrates, including zebrafish, which can also be identified by a combination of molecular markers, location, and morphology. These "primary" neurons are born first and provide sensation throughout the head and trunk during early embryogenesis (Kimmel 1990, Sipple 1998).

RB cells, though not technically part of the peripheral nervous system (PNS), send branching axons throughout the skin of the dorsal side of the embryo to locations that

will later be innervated by the DRG to form a true PNS. From their location within the spinal cord, RBs are mechanosensors that, in their role as the precursor PNS, mediate the escape reflex and detect noxious stimuli from 20 hpf until establishment of the mature DRG sensory system (Sipple 1998). Past researchers have shown that RB elimination via apoptosis coincides with the formation and maturation of the DRG (Cole 2001, Sipple 1998, Williams 2000) and functional DRG and their arbors reportedly begin to replace RB cells by 48 hpf (Sipple, 1998b).

RB neurons also participate in reflexes such as swimming away from a stimulus in 21 hpf zebrafish embryos whose tails are touched and they are essential to spinal cord development, in particular formation of the dorsolateral fascicle (DLF). The importance of the RB contribution to the DLF is notable because many other neurons use this fascicle to connect to the hindbrain and contribute to motor behaviors in both embryonic and adult zebrafish (Sipple, 1998b).

In contrast, the TG is believed to form from both neural crest and placode elements in the first few stages of embryogenesis (D'Amico-Martel and Noden, 1983) The fully formed TG then persists as a permanent ganglion throughout the remainder of embryonic and adult life in vertebrate species (D'Amico-Martel and Noden, 1983). The cellular origins of the TG in zebrafish are less well studied, but believed to follow a similar developmental process, arising from neural crest and placode cells (D'Amico-Martel and Noden, 1983).

The TG has an important sensory function in the developing embryo (Kimmel and Westerfield, 1990; Saint-Amant and Drapeau, 1998). Sensory neurons of the bilateral TG are among the first neurons in vertebrates. Their arborization throughout the skin of the head by 16 hpf provide the early network of sensory axons that respond to touch by 21 hpf. Various stereotyped behaviors and reflexes are observed in young zebrafish embryos within the first day of embryogenesis, including those associated with the TG (Kimmel and Westerfield, 1990; Saint-Amant and Drapeau, 1998). Embryos respond to physical stimuli even before they form a mature nervous system. By 21 hpf a zebrafish embryo can quickly move in a direction opposite from a predator that touches the side of its head in an "escape" response mediated by TG arbors (Kimmel and Westerfield, 1990).

Both populations of cells are sensory neurons whose early development relies on specific interactions that take place both across the midline and in the rostral-to-caudal direction (Sagasti, Guido, Raible and Schier, 2005). The TG forms as the normal ganglia grow and project arbors to the midline but are repulsed by contralateral TG sensory neuron axons (Sagasti et al., 2005). The same repulsion across the midline has been observed for RB axons. Rostro-caudal repulsion ensures that TG sensory axons and RB axons are segregated to the head and spinal cord region, respectively (Sagasti et al., 2005). Chemokine signaling also appears to be important in the migration and proper positioning of TG neurons within the ganglion itself (Knaut, Blader, Strahle and Schier, 2005).

In zebrafish embryos with unilaterally ablated TG, axons from the contralateral TG expand across the midline to arborize the ablated side (Sagasti et al., 2005). In these

cases, reflexes normally associated with the TG, such as escape behaviors, are altered (Sagasti et al., 2005). In contrast, in embryos with bilaterally ablated TG, neurons of RB origin have been shown to migrate from the dorsal aspect of the fish and innervate both their normal spinal cord regions and the anterior cephalic region of the TG sensory neurons (Sagasti et al., 2005).

Overlapping molecular markers also link these two populations; RB and TG neurons are almost indistinguishable by traditional immunohistochemical techniques. These methods identify cells according to antigens on proteins or cellular components that can be uniquely labeled by fluorescently conjugated antibodies. In almost all categories, the same markers that label RBs label TG neurons *en masse*. These cell populations sense environmental stimuli in very similar ways, and in zebrafish it may be possible to link both to magnetosensation.

RESEARCH CHAPTER SUMMARIES

Chapter II

Here I describe a method to produce confocal laser scanning microscope (CLSM) time-lapse movies of the developing neural tube that can be used over the first 72 hours post-fertilization in zebrafish embryos, capturing optically sliced z-stacks of the dorsal-to-ventral diameter of the spinal cord. My goal was to demonstrate a method to produce multi-spectral fluorescent labeling of the cell membrane, nuclei, and a developmentally important gene to provide spatial and temporal information about gene expression and morphogenetic movements during this critical period of spinal cord development.

Building on the work done by Sean Megason, a former post-doctoral fellow in the Fraser laboratory, I developed a method for mounting and imaging very young zebrafish embryos (10 hpf onward) to produce time lapse movies with 7–10 minute full z-stack acquisition times and still images of *in vivo* neural tube development and gene expression. I was concurrently a member of the CEGS FlipTrap screen team, a multi-year project that identified over 150 developmentally important genes and proteins with the FlipTrap vector. In the second half of this chapter I use the previously devised *in vivo* imaging techniques with two FlipTrap lines.

Chapter III

This chapter is devoted to the RB neuron. I discuss the history of this cell type, its known function in early embryos and larvae, and its previously reported removal from the larval spinal cord through apoptosis between 24 and 48 hours after fertilization. Using the two FlipTrap transgenic lines from Chapter 2, I discuss my observations of a subset of fluorescent-protein-labeled RB neurons that survive past the first week of development, persisting up to 30 days after fertilization.

Chapter IV

In 2010 I began a project with Joseph Kirschvink and subsequently transferred to his group to complete my doctoral work. We set out to use my FlipTrap lines, which both express a fluorescent protein in the TG and its projections, to look for the presence of magnetite in zebrafish embryos, larvae, and adults. We began our collaboration with CLSM reflectance-mode imaging and quickly realized that, given the part-per-billion

concentration of biogenic magnetite found in other organisms, light microscopy is a poor screening tool to find trace amounts of magnetite in young, highly reflective zebrafish embryos. In adult zebrafish, the large volume of tissue and lack of optical transparency also made the initial search for magnetite via an optical method less than ideal. I decided to postpone confocal imaging to identify areas of relatively high magnetite concentration. We then turned our efforts to validated and reliable rock magnetism and spectroscopic methods that had yielded good results on bacterially produced biogenic magnetite in work by previous members of the Kirschvink group. Here I report on the results of these studies and the use of a magnetic imaging technique that led us to magnetite stores, which unexpectedly turned out to be in the trunk of adult samples.

BIBLIOGRAPHY

Appel, B. (2000). Zebrafish Neural Induction and Patterning. *Developmental Dynamics* **203**, 155-168.

Beard, J. (1889). On the early development of Lepidosteus osseous. *Proceedings of the Royal Society of London* **46**, 1108-1118.

Blader, P., Plessy, C. and Stra¨hle, U. (2003). Multiple regulatory elements with spatially and temporally distinct activities control *neurogenin1* expression in primary neurons of the zebrafish embryo. *Mechanisms of Development* **120**, 211-218.

Briscoe, J., Pierani, A., Jessell, T. M. and Ericson, J. (2000). A Homeodomain Protein Code Specifies Progenitor Cell Identity and Neuronal Fate in The Ventral Neural Tube. *Cell* **101**, 435-445.

Cornell, R. A. and Eisen, J. S. (2000). Delta signaling mediates segregation of neural crest and spinal sensory neurons from zebrafish lateral neural plate. *Development* **127**, 2873-2882.

D'Amico-Martel, A. and Noden, D. M. (1983). Contributions of Placodal and Neural Crest to Avian Cranial Peripheral Ganglia. *The American Journal of Anatomy* **166**, 445-468.

Gong, Z., Ju, B. and Wan, H. (2001). Green fluorescent protein (GFP) transgenic fish and their applications. *Genetica* **111**, 213-225.

Griesbeck, O., Baird, G. S., Campbell, R. E., Zacharias, D. A. and Tsien, R. Y. (2001). Reducing the Environmental Sensitivity of Yellow Fluorescent Protein. *the Journal of Biological Chemistry* **276**.

Guillemot, F. (2007). Spatial and temporal specification of neural fates by transcription factor codes. *Development* **134**, 3771-3780.

Helms, A. W., Battiste, J., Henke, R. M., Nakada, Y., Simplicio, N., Guillemot, F. and Johnson, J. E. (2005). Sequential Roles for Mash1 and Ngn2 in the Generation of Dorsal Spinal Cord Interneurons. *Development* **132**, 2709-2719.

Helms, A. W. and Johnson, J. E. (2003). Specification of dorsal spinal cord interneurons. *Current Opinion in Neurobiology* **13**, 42-49.

Jankowska, E. (2001). Spinal Interneuronal systems: identification, multifunctional character and reconfiguration in mammals. *The Journal of Physiology* **533**, 31-40.

Jessell, T. M. (2000). Neuronal Specification in the Spinal Cord: Inductive Signals and Transcriptional Codes. *Nature Reviews: Genetics* **1**, 20-29.

Kimmel, C. B. and Westerfield, M. (1990). Primary Neurons of The Zebrafish. In *Signals and Sense*, (ed. G. W), pp. 561-588. New York: Wiley Liss.

Kimura, Y., Okamura, Y. and Higashijima, S. (2006). alx, a Zebrafish Homology of Chx10, Marks Ipsilateral Descending Excitatory Interneurons That Participate in The Regulation of Spinal Locomotor Circuits. *The Journal of Neuroscience* **26**, 5684-5697.

Knaut, H., Blader, P., Strahle, U. and Schier, A. F. (2005). Assembly of Trigeminal Sensory Ganglia by Chemokine Signaling. *Neuron* **47**, 653-666.

Kuwada, J. Y., Bernhardt, R. R. and Nguyen, N. (1990). Development of Spinal Neurons and Tracts in the Zebrafish Embryo. *The Journal of Comparative Neurology* **302**, 617-628.

Lamborghini, J. E. (1987). Disappearance of Rohon-Beard Neurons From the Spinal Cord of Larval *Xenopus laevis*. *The Journal of Comparative Neurology* **264**, 47-55.

Lee, S. K. and Pfaff, S. L. (2001). Transcriptional networks regulating neuronal identity in the developing spinal cord. *Nature Neuroscience* **4**, 1183-1191.

Lewis, K. E. (2005). How do genes regulate simple behaviours? Understanding how different neurons in the vertebrate spinal cord are genetically specified. *Philosophical Transactions of The Royal Society B* **361**, 45-66.

Lewis, K. E. and Eisen, J. S. (2003). From cells to circuits: development of the zebrafish spinal cord. *Progress in Neurobiology* **69**, 419-449.

McLean, D. L., Fan, J., Higashijima, S., Hale, M. E. and Fetcho, J. R. (2007). A topographic map of recruitment in spinal cord. *Nature* **446**.

Megason, S. G. (2009). In toto imaging of embryogenesis with confocal time-lapse microscopy. *Methods in Molecular Biology* **546**, 317-332.

Megason, S. G. and Fraser, S. E. (2003). Digitizing Life at the Level of the Cell: High-performance Laser-scanning Microscopy and Image Analysis for in toto Imaging of Development. *Mechanisms of Development* **120**, 1407-1420.

Olivier, N., Luengo-Oroz, M., Duloquin, L., Faure, E., Savy, T., Veilleux, I., Solinas, X., Debarre, D., Bourgine, P., Santos, A. et al. (2010). Cell Lineage Reconstruction of Early Zebrafish Embryos Using Label-Free Nonlinear Microscopy. *Science* **329**, 976-971.

Park, H. C., Kim, C. H., Bae, Y. K., Yeo, S. Y., Kim, S. H., Hong, S. K., Shin, J., Yoo, K. W., Hibi, M., Hirano, T. et al. (2000). Analysis of upstream elements in the HuC promoter leads to the establishment of transgenic zebrafish with fluorescent neurons. *Developmental Biology* **227**, 279-293.

Rohon, J. V. (1884). Histogenese des Ruckenmarkes der Forelle. *Akad Wiss Math* **14**.

Sagasti, A., Guido, M. R., Raible, D. W. and Schier, A. F. (2005). Repulsive Interactions Shape the Morphologies and Functional Arrangements of Zebrafish Peripheral Sensory Arbors. *Current Biology* **15**, 804-814.

Saint-Amant, L. and Drapeau, P. (1998). Time Course of the Development of Motor Behaviors in the Zebrafish Embryo. *Journal of Neurobiology* **37**, 622-632.

Sapir, T., Geiman, E. J., Wang, Z., Velasquez, T., Mitsui, S., Yoshihara, Y., Frank, E., Alvarez, F. J. and Goulding, M. (2004). Pax6 and Engrailed 1 Regulate Two Distinct Aspects of Rental Cell Development. *The Journal of Neuroscience* **24**, 1255-1264.

Saueressig, H., Burrill, J. and Goulding, M. (1999). Engrailed-1 and Netrin-1 regulate axon pathfinding by association interneurons that project to motor neurons. *Development* **126**, 4201-4212.

Shcherbakov, D., Winklhofer, M., Petersen, N., Steidle, J., Hilbig, R. and Blum, M. (2005). Magnetosensation in zebrafish. *Current Biology* **15**, R162.

Shirasaki, R. and Pfaff, S. L. (2002). Transcriptional Codes and the Control of Neuronal Identity. *Annual Review of Neuroscience* **25**, 251-281.

Sipple, B. (1998). The Rohon-Beard Cell: The Formation, Function, and Fate of A Primary Sensory System in The Embryonic Zebrafish, Danio rerio. In *Biology*, vol. PhD. Philadelphia: Temple University.

Trinh, L. A., Hochgreb, T., Graham, M., Wu, D., Ruf, F., Jayasena, C., Saxena, A., Hawk, R., Gonzalez-Serrichchio, A., Dixson, A. et al. (2011). FlipTraps: fluorescent tagging and cre mediated mutagensis of proteins at their endogenous loci. *Genes & Development* **25**.

Williams, J. A., Barrios, A. Gatchalian, C., Rubin, L., Wilson, S.W., Holder, N. (2000). Programmed cell death in zebrafish Rohon Beard neurons is influenced by TrkC1/NT-3 signaling. *Developmental Biology* **226**, 220-230.

Zhou, Y., Yamamoto, M. and Engel, J. D. (2000). GATA2 is Required for the Generation of V2 Interneurons. *Development* **127**, 3829-3838.

CHAPTER II

In Toto Imaging and The FlipTrap: Tools to Understand Spinal Cord Development in Living Zebrafish

AUTHORS

Alana Dixson & Sean Megason

ABSTRACT

During embryogenesis and development, the central nervous system (CNS) transforms from what seems like an amorphous mass of cells to a rod-like structure, and then to a fully functional and complex system of tissues composed of multiple cell types. Using confocal laser scanning microscopy (CLSM), my goal was to demonstrate a modified version of *in toto* imaging microscopy methods that could track normal spinal cord organization in zebrafish from bud stage, ~ 11 hours post-fertilization (hpf), to 48 hpf. Additionally, I assisted in identifying several transgenic lines using a gene trap vector, the FlipTrap (FT), which is a Tol-2 based vector that randomly inserts a citrine fluorescent protein (YFP) cassette under the control of Cre-Lox into the genome. Insertion of YFP in frame creates a normally localized and functional fusion protein--a powerful tool for *in vivo* analysis of gene expression throughout development. Here I used two FT lines along with a modified version of *in toto* imaging to show that it is possible to use these tools to understand the gene expression and morphogenetic movements in the dorsal spinal cord.

INTRODUCTION

***In Toto* Imaging**

In the Fraser laboratory, Sean Megason developed *in toto* imaging, which allows 3D plus time (4D) capture of embryogenesis in the optically transparent zebrafish embryo (Megason, 2009). Figure 2 shows a sample image collected *in vivo* using confocal laser scanning microscopy (CLSM) in which each cell in this developing spinal cord is visible. A specially designed programming interface, MegaCapture, facilitates z-stack collection

over 72 hours continuously. This information is digitized and allows for single-cell resolution of the developmental process under study by using advances in microscopy with multiple live zebrafish, or other vertebrate embryos. Data are then segmented and analyzed using appropriate software packages such as Imaris or GoFigure. The power of *in toto* imaging is in its provision of segmentation and tracking of individual cells and cell lineages to create a digital embryonic and larval zebrafish spinal cord.

In toto imaging has several requirements, which I sought to meet on a basic level and began using in a modified version to observe development of neurons within the dorsal spinal cord. These requirements are: 1) cells must be individually recognizable; 2) components of cells must be tractable, that is a nucleus should be distinguishable as a nucleus and apart from the cell membrane or a protein produced within or around the cell; 3) the acquisition of time-lapse data must be within a period that will capture important cellular events such as cell division and migration; 4) the methods used to label individual cells should not disrupt normal gene function; 5) cell labels and imaging must not be cytotoxic or lead to the death of the organism under study.

In this project, each *in toto* imaging requirement above was met:

1) Labeling with mRNA or DNA developed by Sean Megason created red cell membranes and blue nuclei; these tools were injected at the one-cell stage, labeling each embryonic cell for up to 7 days (Figure 1).
2) The markers for individual cellular components consisted of spectrally distinct fluorescent proteins to make each component distinctive (Figure 2).

3) The initial goal of this project was to capture a z-stack of the entire dorsal-to-ventral thickness of the spinal cord with optical steps of 1 μm each within approximately 2 minutes. This proved to be challenging and could partially be achieved by reducing x and y dimensions, increasing the optical steps to 2 - 3 μm, using bidirectional scanning, decreasing the pixel dwell time, and collecting all fluorescent channels on one track instead of using multiple tracks (which provide cleaner images by avoiding any overlap in emission spectra).
4) To avoid disrupting normal gene function, mRNA injections were performed to produce fluorescent proteins that localize to nuclei or membranes in place of DNA, which upon integration into the genome may have unintended disruptive effects. The FlipTrap vector labels developmentally important genes while leaving normal gene function intact.
5) We minimized cellular damage by injecting the minimal concentration of both mRNA and the FlipTrap vector to achieve desired expression levels without gross abnormalities in embryonic morphology, behavior, or life span.

A method for mounting and immobilizing embryos was also designed to prevent movement out of frame during image capture, especially if long time-lapse sessions were planned, but would give animals the freedom to grow and develop at normal, or near normal, rates (Figure 3). This was achieved by using an embryo array, described previously (Megason, 2009), cast in a 1% agarose gel from a Lucite mold with the embryos placed inside the array and coverslipped. Alternatively, embryos could be embedded in 0.3 - 0.5% low-melting point agarose in a two-chamber tissue culture dish;

the LMP agarose allows movement of fluid and gases around the embryo, but holds the animal in place and tail extension proceeds uninhibited. I preferred to use the array submersed in embryo medium with a small percentage of anesthetic because it reduced body movements while permitting gas exchange but did not cause death or deformities to the animals. If I added fresh medium regularly, the embryos were healthy, though somewhat smaller than their non-imaged counterparts after longer time-lapse sessions.

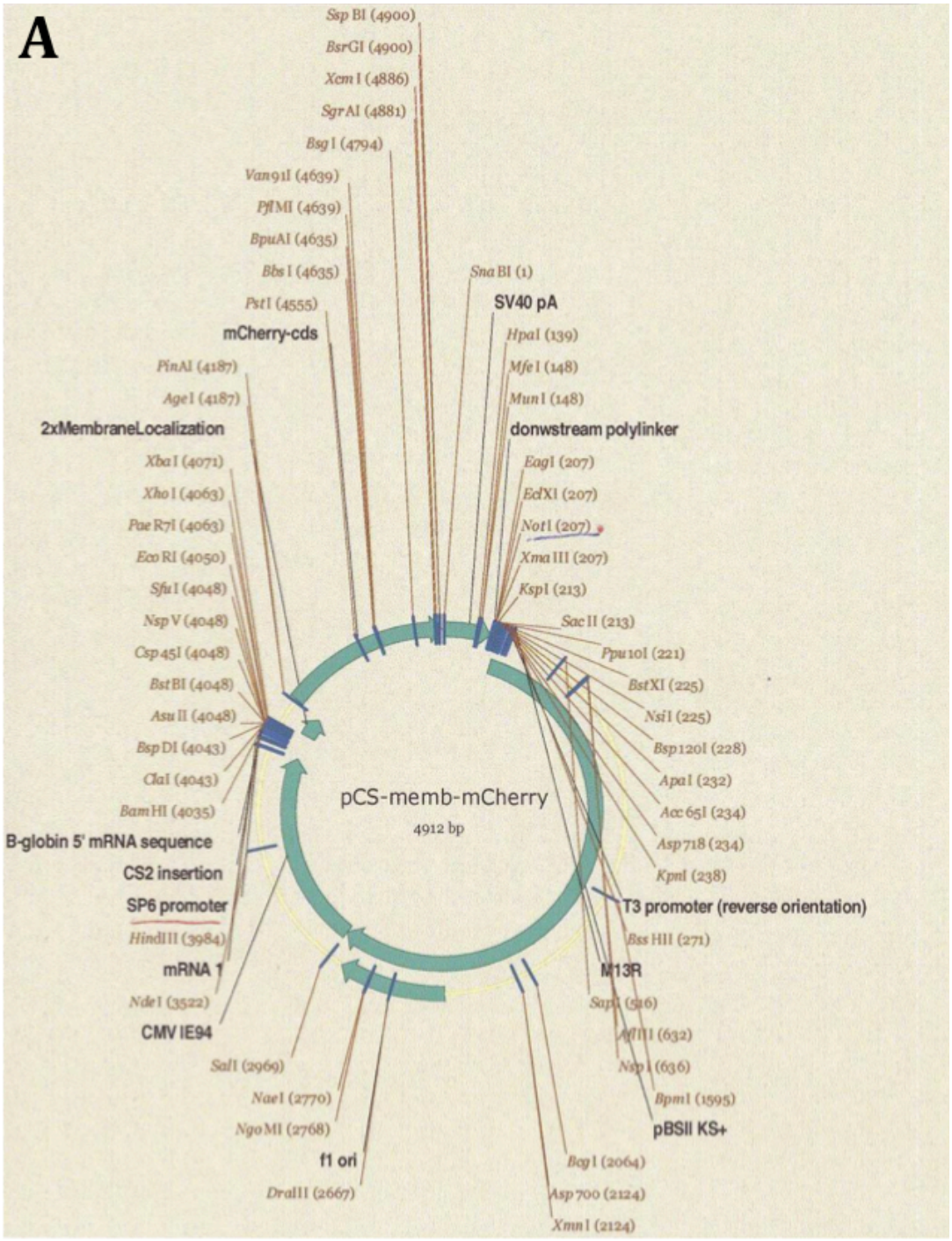

Figure 1A Plasmid Map of m-Cherry Membrane Label

A) The membrane label is m-cherry (RFP), a modified derivative of green fluorescent protein (GFP).

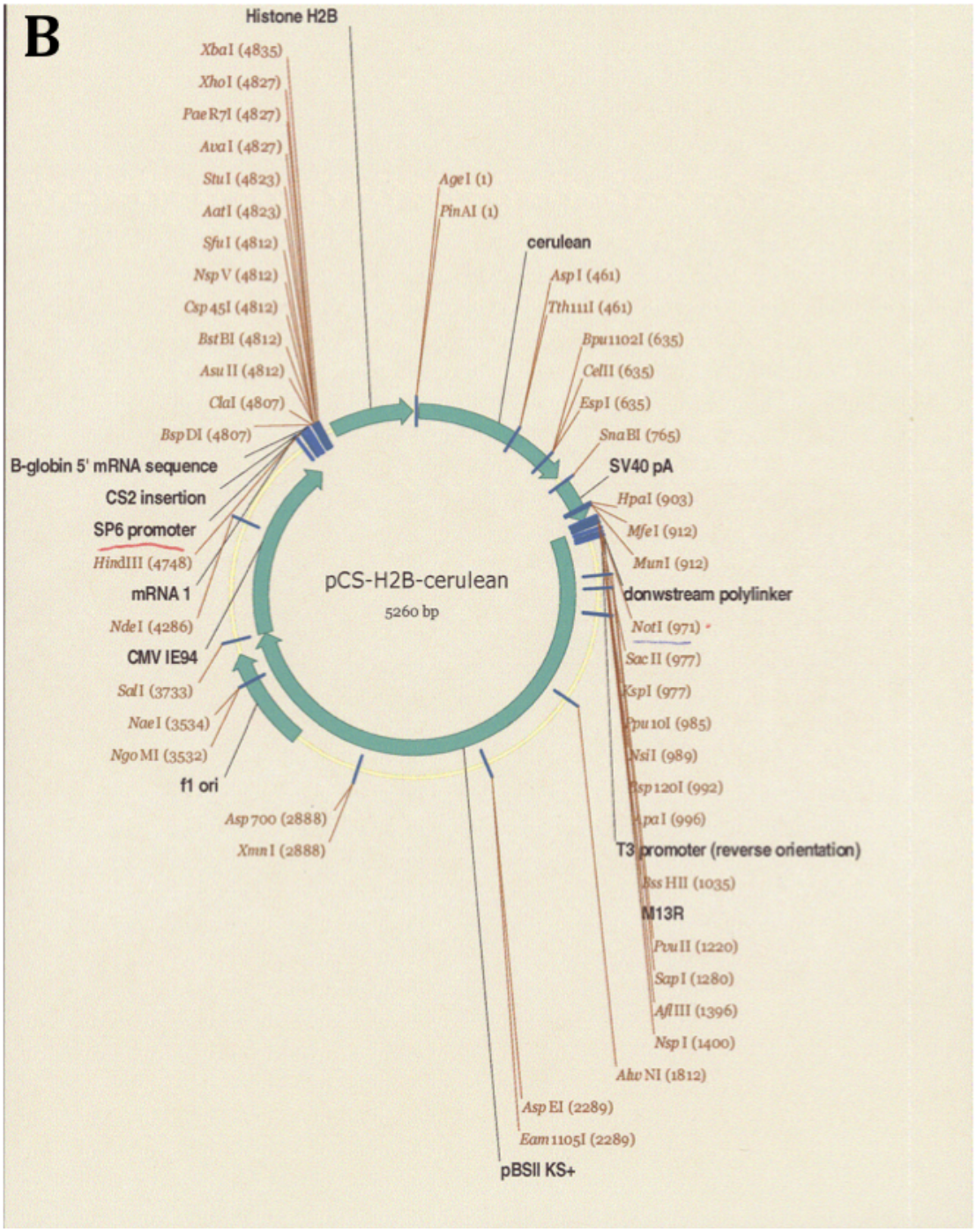

Figure 1B Plasmid Map of Cerulean Nuclear Label

B) The nuclear label is cerulean fluorescent protein, also a GFP derivative.

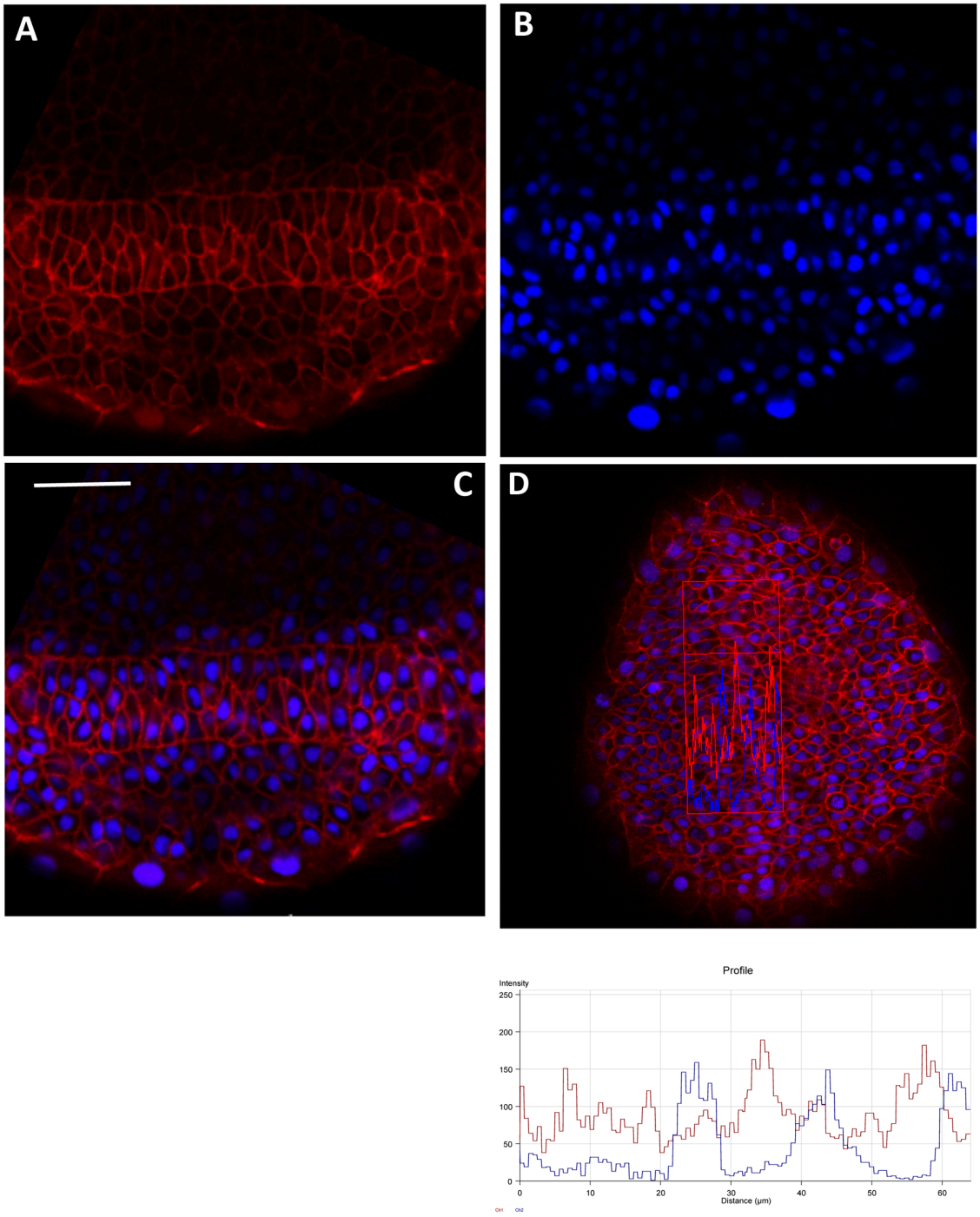

Fig. 2 Membrane and Nuclear Fluorescent Proteins Allow Automated or Manual Segmentation A-C) 12.5 hpf zebrafish embryonic neural keel; cells have been labeled with the segmentation markers m-cherry (RFP) localized to the membrane (A) and cerulean fluorescent protein (CFP) localized to the H2B protein of the nucleus (B). In

(C) the merged image shows clear cell out lines, which allow visualization of morphological changes, while the nuclear marker provides an easy target for tracking cell lineages and movements. D) In the intensity versus distance profile within the captured x-y area, we clearly see the outline of cell membranes and nuclei in these sharp images. Increasing the optical slice in z and reducing the pixel dwell time will change the resolution to generate much less crisp images. Nonetheless, these can still be segmented manually or automatically if their profile is similar to the one shown here. The C-Apochromat 1.2 NA water immersion objective by Zeiss was used on the Zeiss Pascal CLSM. RFP was excited using the 543 nm laser line at 90% power and long pass (LP) 560 filter for emission spectra was used; CFP was excited using the 458 nm laser line at 90% power, emission spectra were collected through a 475-525 bandpass filter. Scale bar = 50 μm.

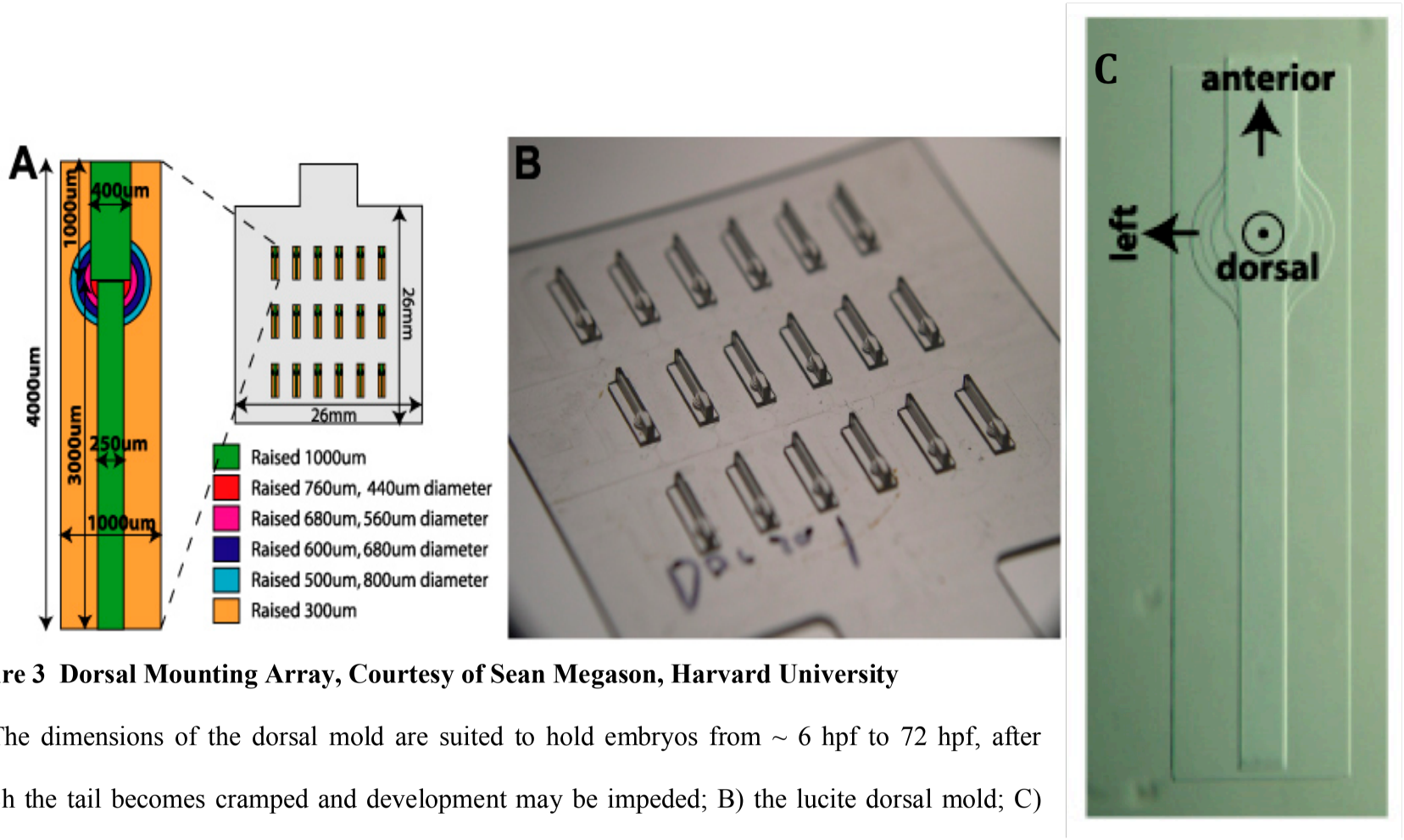

Figure 3 Dorsal Mounting Array, Courtesy of Sean Megason, Harvard University

A) The dimensions of the dorsal mold are suited to hold embryos from ~ 6 hpf to 72 hpf, after which the tail becomes cramped and development may be impeded; B) the lucite dorsal mold; C) image of dorsal mold cast in agarose. Animals mounted in this array develop normally and can be continuously imaged for up to 72 hpf given regular medium changes (Megason, 2009).

The FlipTrap

The FlipTrap vector was developed as one of the Specific Aims of the Center of Excellence in Genomic Science grant that was awarded to Marianne Bronner, Scott Fraser, Niles Peirce, and Sean Megason in 2006. Post-doctoral fellow Le Trinh, along with Sean Meagson, designed and injected the FlipTrap and its subsequent generations in zebrafish.

The FlipTrap vector (Figure 4) is a transposon-based gene trap that creates a genetically encoded citrine tag to track the endogenous temporal and spatial expression of developmentally important genes (Trinh, Hochgreb, Graham, Wu, Ruf, Jayasena, Saxena, Hawk, Gonzalez-Serrichchio, Dixson, Chow, Gonzalez, Leung, Solomon, Bronner-Fraser, Megason and Fraser, 2011b). When the vector randomly inserts into an intronic region, in frame citrine (Griesbeck, Baird, Campbell, Zacharias and Tsien, 2001), a variant of yellow fluorescent protein (YFP) and hereafter referred to as such for convenience, is transcribed along with the endogenous gene to create a fluorescent fusion protein under native control. The rationale for the FlipTrap vector design, and its construction and introduction via microinjection into one-cell stage zebrafish are thoroughly discussed by Trinh et al. in a forthcoming article (Trinh et al., 2011b).

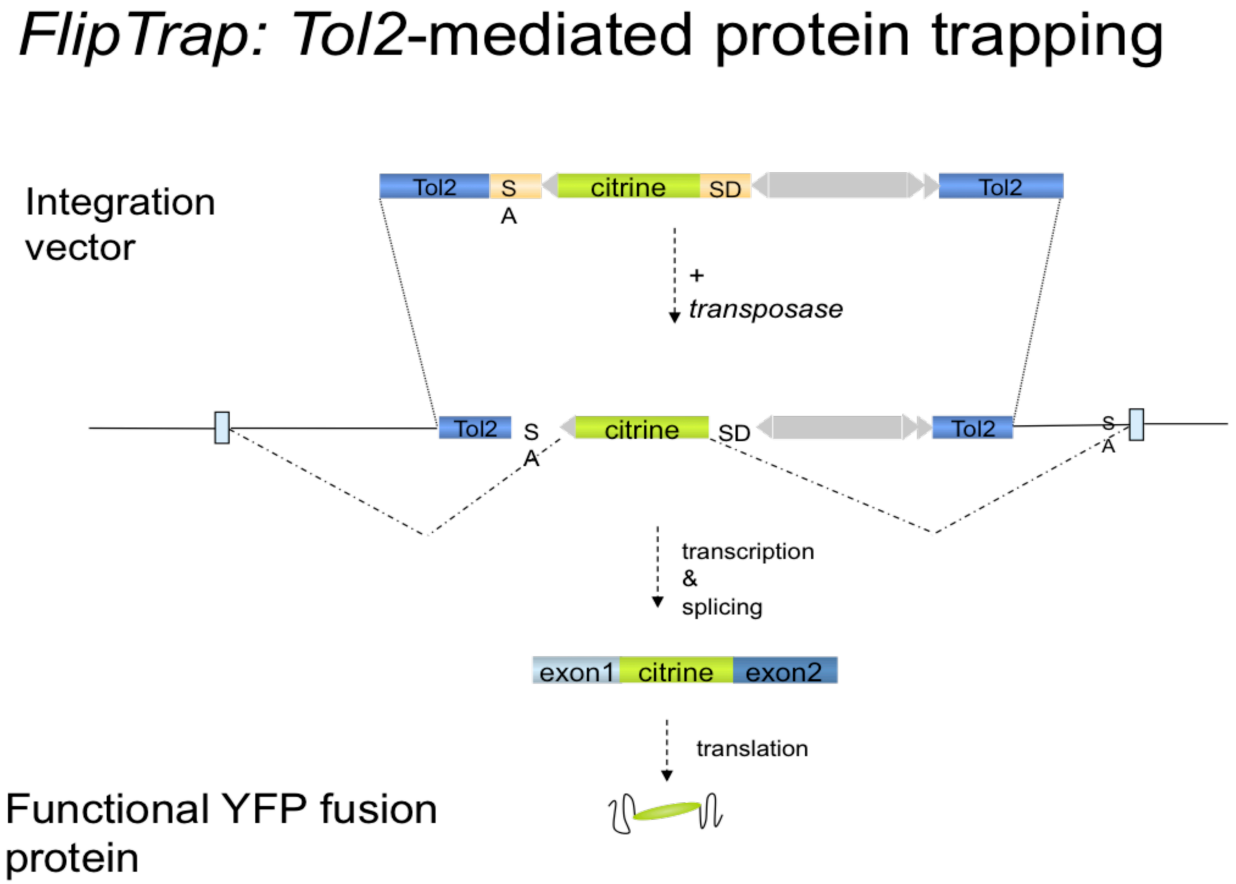

Figure 4 FlipTrap Vector and Protein Trapping The FlipTrap vector creates a gene trap with a cassette encoding the fluorescent protein citrine (YFP), and the resultant fusion protein trap functions normally.

METHODS

Embryo Preparation

Embryos were collected from adult Top Longfin or wild-type AB zebrafish (*Danio rerio*) bred three times a week from laboratory stock. Within 10 minutes of collection each embryo was co-injected with the two linearized, mRNA transcripts of the plasmids in Figure 1, transferred to a combination of 30% Danieaus embryo medium and 0.003% PTU (1-phenyl-2-thiourea), and incubated at 28°C until shield stage (~ 6 hours). After sorting embryos for a ubiquitous pattern of mRNA expression using an Olympus fluorescent microscope, embryos were dechorionated with watchmaker forceps and maintained in 30% Danieaus + PTU in a 1% agarose-coated petri dish until 90% epiboly or bud stage.

Imaging

An embryo array was cast in 1% agarose on top of a cover slip-bottom petri dish from the dorsal array, lucite mold described above. This array allows simultaneous imaging of up to 18 embryos. 30% Danieaus solution plus approximately 1.0-1.5 ml of 1X tricaine per 10 ml of medium were added to the petri dish with the solidified embryo array. Between 3 to 6 animals were then dorsally mounted in the array, directly in contact with the cover slip of the petri dish. Simultaneously, I pre-soaked a 25 mm x 25 mm glass cover slip in the same petri dish for approximately 5-10 minutes to minimize hydrophobic interactions that would inhibit properly overlaying the cover slip onto the embryos. The cover slip was then moved into place over the array by gently tapping the corners of it with a fine tip forceps or hair loop, carefully avoiding turning the embryos or pushing them out of

their wells. Once the array was in position over the depression around the embryo wells where the edges of the lucite mold were, it was pushed into the far corner of the depression and slowly lowered into the other corners by the tip of the watch maker forceps.

After mounting, animals were imaged on a Zeiss LSM 510 or Pascal microscope. The AIM software by Zeiss time series function was used to capture approximately 50–150 μm z-sections along the dorsal to ventral axis with the spinal cord area apposed to the cover slip. Optical slices of 1 μm were collected in single-track mode for two-color images from animals with just the mRNA-based segmentation markers, or in multi-track mode for transgenic animals that also had one or more expression markers. To get improved image quality, I used 5-7 scan speeds, and captured whole z-stacks in 7-13 minute acquisition intervals, depending on the thickness of the z-section and the scan speed used. I did not initiate bidirectional scanning in favor of reducing interlacing artifacts; this also increased the scan time and led to greater bleaching or embryo death, depending on the laser power.

For single z-stacks, I used 90% laser power, while for longer time-lapse movies I adjusted the laser power depending on the health of the embryo, but typically it was about 12% for the 543 nm laser line that excites the RFP and 20% to 30% for the 458 nm line that excites CFP. Emission spectra were collected through a long-pass (LP) 560 filter for RFP, and for CFP, emission spectra were collected through a 475-525 band-pass (BP) filter. For FT expression markers, I used 20-70% laser power depending on the

brightness of the fusion protein fluorescence, a 488 or 514 nm laser for excitation, and emission spectra were collected through a 505-525 BP filter. In all cases the Zeiss C-Apochromat 1.2 NA water-immersion lens was used with either water or Immersol immersion fluid on the objective.

FlipTrap Screen

Briefly, the FT vector was microinjected using a Nanoject II Auto-nanoliter Injector (Drummond Scientific) in plasmid form at 2-3 pg/μl at the one-cell stage by one operator (either Le Trinh or Sean Megason) to ensure consistency (Figure 5). We raised the surviving embryos as the F_0 generation and individually outcrossed both males and females with a wild-type mate from lab stocks of AB, Top Longfin (TL), or AB/TL adult zebrafish. We then screened the F_1 generation over 5 dpf on low-magnification fluorescent microscopes for YFP expression throughout the body. Positive embryos and young larvae, pooled per day and by pattern of newly observed fluorescence, were given an allele number and raised or genotyped to determine the trapped gene.

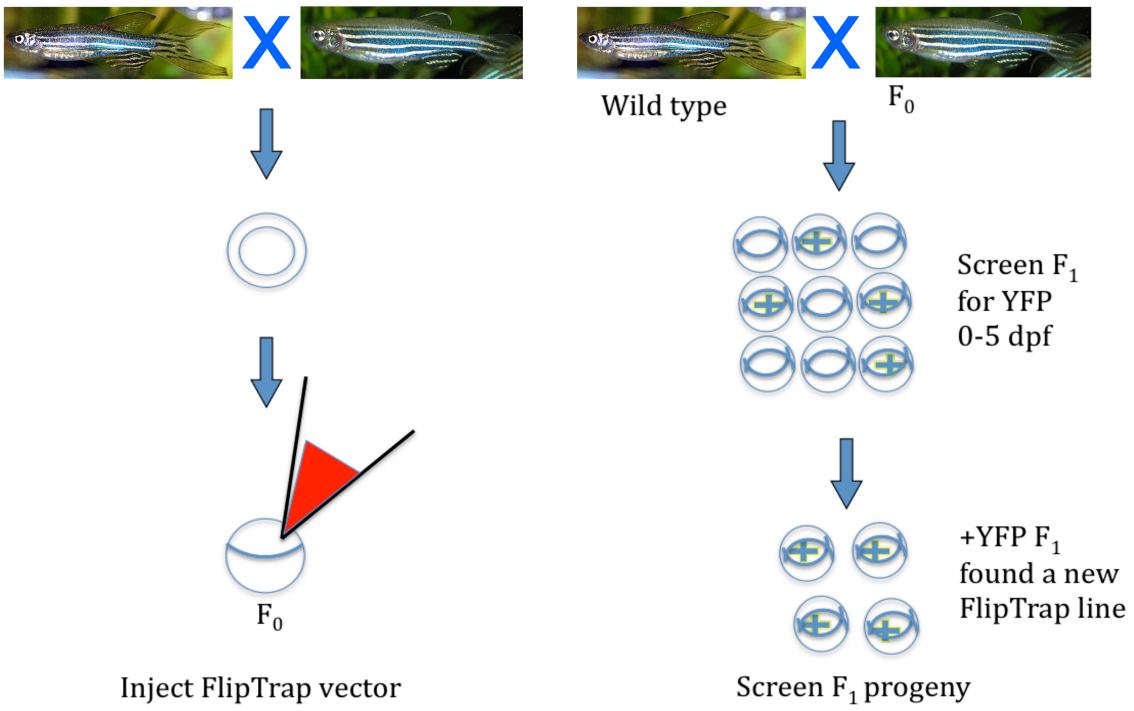

Figure 5 FlipTrap Screen Schematic

FlipTrap founders were identified in a typical F_1 screen. Each fluorescent pattern was given an allele number; one F_1 animal could produce several founders. Fish images are open source.

Ablations

I used a tunable Coherent Chameleon two-photon laser on the Zeiss LSM 510 NLO microscope to individually ablate individual RB neurons. First, neurons were selected using the region of interest (ROI) function on the LSM 510 software by drawing a circle or ellipse around the cells of interest; I imaged these neurons prior to initiation of killing in the confocal mode, Figure 8C. Next, the microscope was converted to the two-photon mode by opening the pinhole, and the appropriate laser was used at 80% power and 800 nm wavelengths to maximize destruction of individual neurons without damaging

surrounding, non-target tissue. The laser was focused on the ROIs for approximately 15 seconds to achieve full killing of cells, Figure 8D. Following ablations at 36 hpf I tracked recovery in the ablated regions, observing non-targeted RB cells and non-ablated, neighboring spinal cord neurons by traditional CLSM. In order to more effectively follow cell movements specifically, I crossed the FT fish with a transgenic line containing neurogenin 1 driving RFP (ngn1::RFP, courtesy Alvaro Sagasti, UCLA). To have healthy embryos for these studies, I did not inject animals with the mRNA used for the *in toto* imaging described previously.

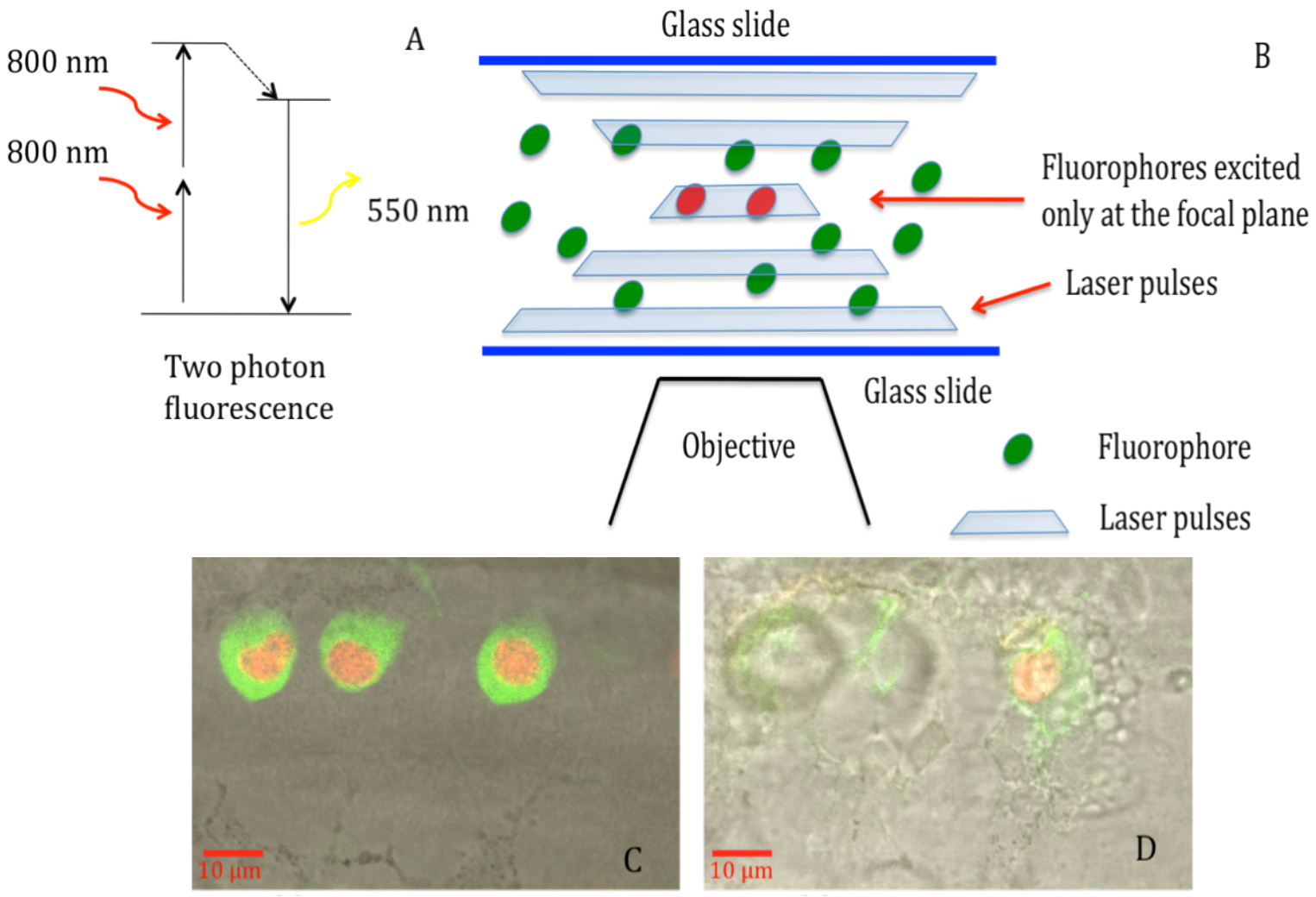

Figure 6 Two Photon Microscopy Basics and Ablated RB Neurons in Live Zebrafish

Figure 6 Two Photon Microscopy Basics and Ablated RB Neurons in Live Zebrafish

A) Jablonski energy diagram of two-photon emission and absorption; B) Schematic of fluorophores excited only at the focal plane; C-D) RB neurons in 36 hpf zebrafish double-transgenic embryos pre- and post-ablation as labeled. ct 7a x ngn1::RFP double transgenic line, trunk spinal cord RB neurons in live embryo. Red = ngn1, Green = YFP-PKCα. Microscope: Zeiss 510 Meta Confocal LSM. Mounting: Lateral side toward objective. Ablation: 800 nm laser; 80% power; scan speed 5; 10 continuous cycles.

RESULTS

I used two colors to outline cell membranes and nuclei in a series of images focused on the 1st through 5th somites and hindbrain region of embryonic Top Longfin (TL) or AB wild-type zebrafish from the Center of Excellence in Genomic Science (CEGS) lab stock. I injected mRNA that encoded fluorescent proteins that label histone 2B proteins (H2B) in the nucleus cerulean (CFP) and cell membranes m-cherry, which here I abbreviate the same as red fluorescent protein (RFP) for convenience. Because I introduced mRNA at the one-cell stage, embryos display ubiquitous fluorescence, starting at the mid-blastula stage (~ 4 hpf), and lasting throughout the first week post-fertilization, though after 72 hpf I have found the expression to be variable in brightness.

The trapped gene in two FT lines, ct 7a and ct 54a, was protein kinase C alpha (PKCα), which I pseudo-colored green. Green fluorescent protein (GFP) variants such as that used in the FT lines are functionally folded and became visible quickly, maturing in a few hours post-translation. I followed changes in PKCα expression for several hours

continuously and observed that the fusion protein becomes fluorescent in rostral neurons such as the trigeminal ganglion (TG) before caudal cells such as Rohon-Beard neurons (RBs) (see Chapter 3, Figure 2).

FT Cells Are a Subset of Both Peripheral and Central Sensory Systems

We used a transgenic line with the neurogenin 1 promoter driving RFP (ngn1::RFP) and Islet-1 immunological staining in the TG, where both markers are expected in TG neurons ubiquitously, and in RB neurons. I consistently found strong TG and RB staining with both molecular markers at every stage assayed (Chapter 3, Figure 2). I did not inject mRNA into animals reserved for immunohistological processing to avoid unnecessary spectral overlap of fluorescent proteins from fluorescent secondary antibodies and the ngn1 expression in the transgenic line; also the trapped protein in ct 7a and ct 54a outlined FT cells, providing a permanent segmentation marker along with the nuclear expression of the other two labels. FT cells were evident in the target location, the dorsal spinal cord, and extra-spinal cord ganglia; in the peripheral ganglia and RB neurons the fusion protein was visible in only a subset of cells (Chapter 3, Figure 3). FT animals show mRNA segmentation markers and gene expression clearly (Figure 7).

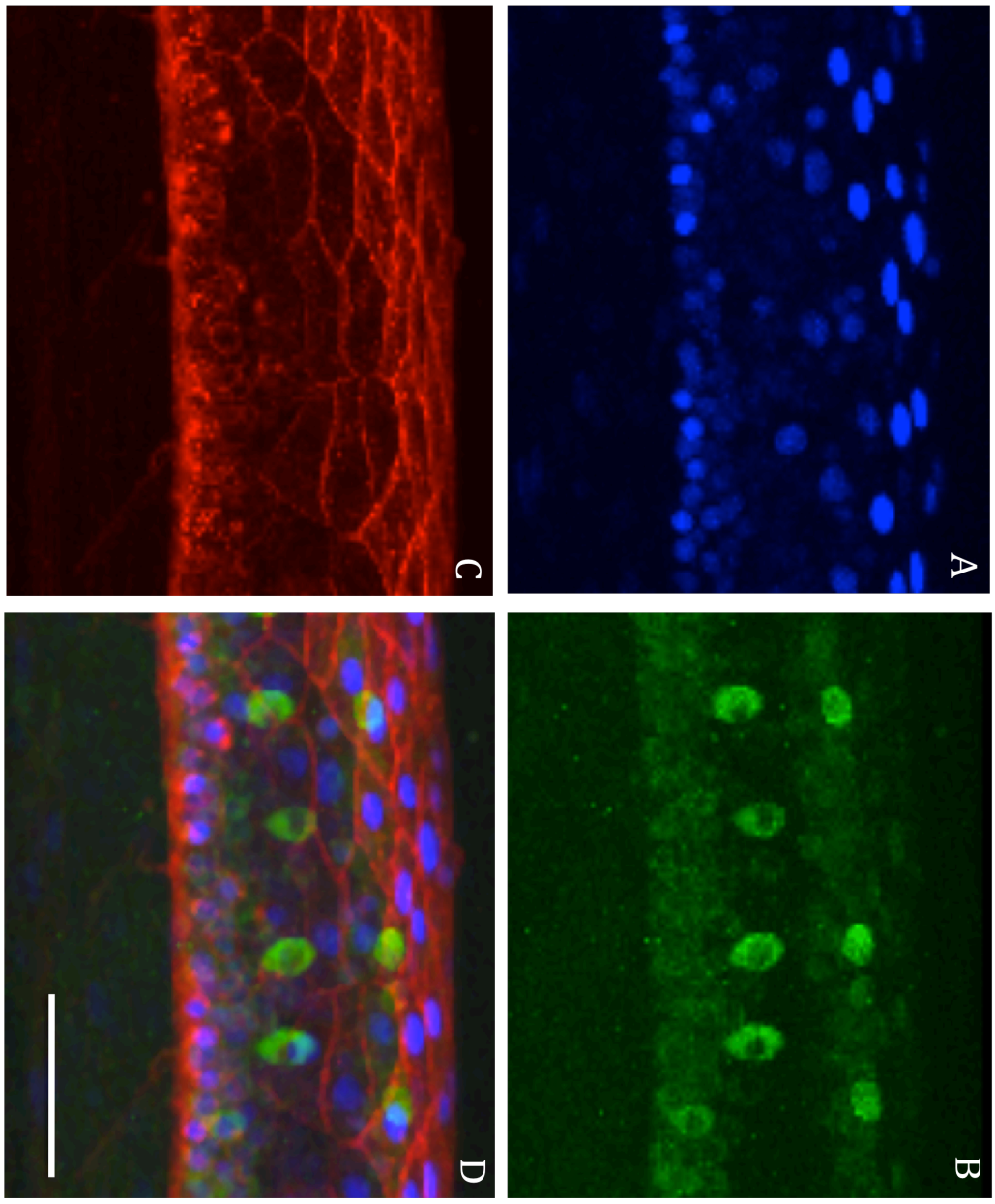

Figure 7 FT Embryo Labeled for *In Toto* Imaging

Figure 7 FT Embryo Labeled for *In Toto* Imaging

A-D) 31.5 hpf FT embryo labeled with *in toto* imaging segmentation markers: nuclei CFP (A), FT gene (B), membrane RFP fluorescence (C), and composite image (D). Captured on the Zeiss Pascal CLSM. The scale bar = 50 μm.

I used a separate color for trapped gene or transgene expression, and the differential interference contrast settings on the confocal microscope to capture a bright-field image of overall morphogenetic movements over the course of imaging. The segmentation markers were effective and allowed cell divisions to be visualized.

RB neurons are expected to begin disappearing during the first 48 hpf via programmed cell death (PCD). I used time lapse and static imaging during this period to see the removal of this population to determine if there were some autophagocytotic events along with PCD. Surprisingly, I found that instead of fragmenting their DNA, most RBs appeared healthy and normal, and as spinal cord tissues elongated and matured, the FT RBs became a single row with overlapping somata and bilaterally apposed central axons.

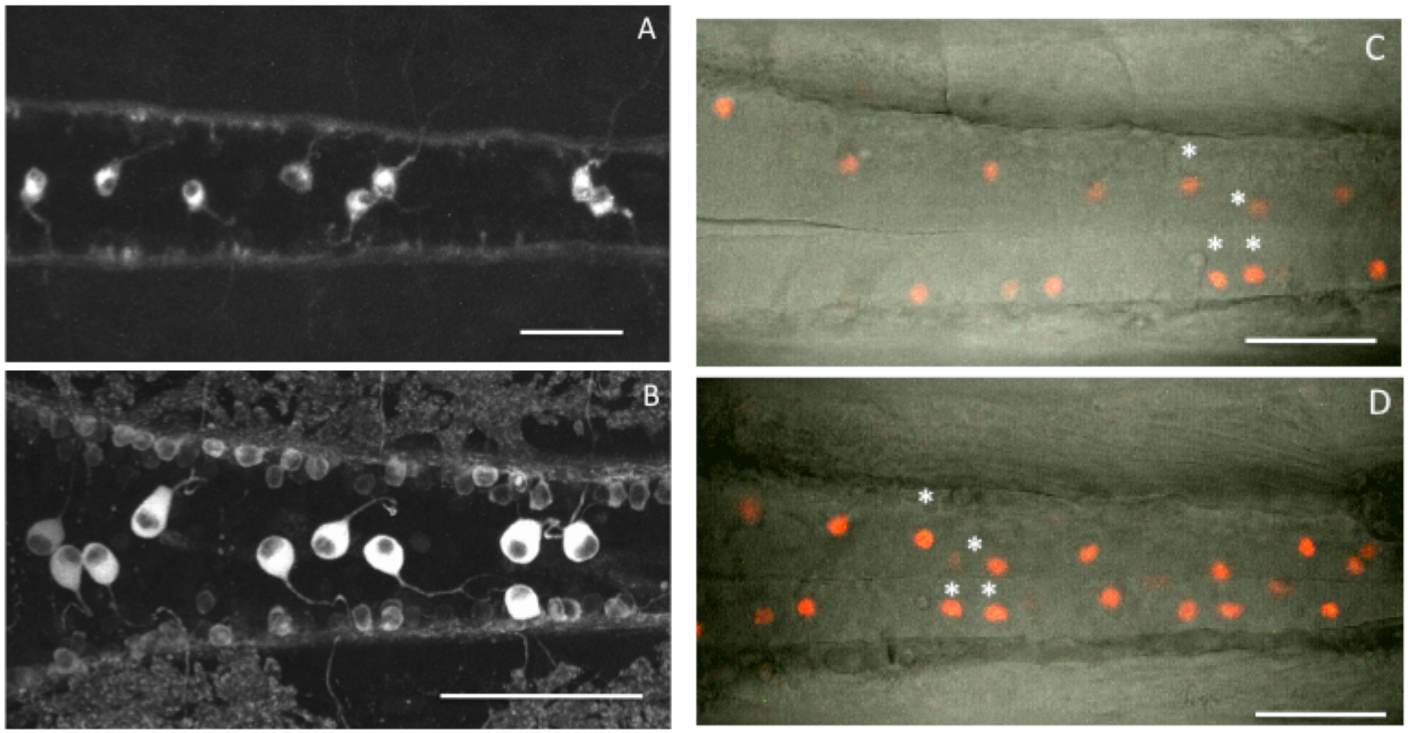

Figure 8 Between 32 - 42 hpf Rohon-Beard Neurons Do Not Die, but by 3 dpf Merge to Form a Single Row

RBs merging to form a single row: A) 48 hpf ct 7a spinal cord; B) 76 hpf ct 54 captured on the Zeiss LSM Exciter microscope each image is a 3D projection of a subset of the z-stack originally collected. They show the midline position of the RB somata within the spinal cord. A time-lapse movie of the spinal cord in a ngn1::RFP embryo 32-42 hpf showed that RB neurons (indicated by white *) did not undergo PCD and the same cells that were present at 32 hpf (C) were still there at 42 hpf (D). Scale bar in A to D is 50 μm; in B scale bar is 100 μm.

Ablated RB Neurons are Not Replaced

Given that the TG axonal arbors can be replaced by axons of RB neurons when the ganglion is missing bilaterally (Sagasti et al., 2005), I wanted to find out if upon ablation the somata of persistent RB neurons would be replaced by neighboring cells of the same or different classes either through inward migration or cell division. I ablated RB cells at different time points from 36 hpf to 4 dpf and time lapse imaged the recovery of the affected regions. I looked for cell divisions and changes in nearby RB position and found that, although the damaged tissues recovered, no other RB neurons moved into the position of their killed neighbors (Figure 9), which was expected. Adding nuclear markers that are ubiquitously expressed would show the movement of other cells in the region. Ablations were performed in embryos of the ngn1::RFP x ct 7a double transgenic line because the FT and ngn1 transgenes were similar to the segmentation markers that I used previously. Double transgenic animals could be bred for imaging instead of injecting through the chorion. This reduced preparation time and produced longer-lasting fluorescence compared to mRNA injections; however, the segmentation markers are not ubiquitous, so only neurons bearing the markers are visible by fluorescent protein expression, and other non-neuronal cells are only visible in the DIC channel.

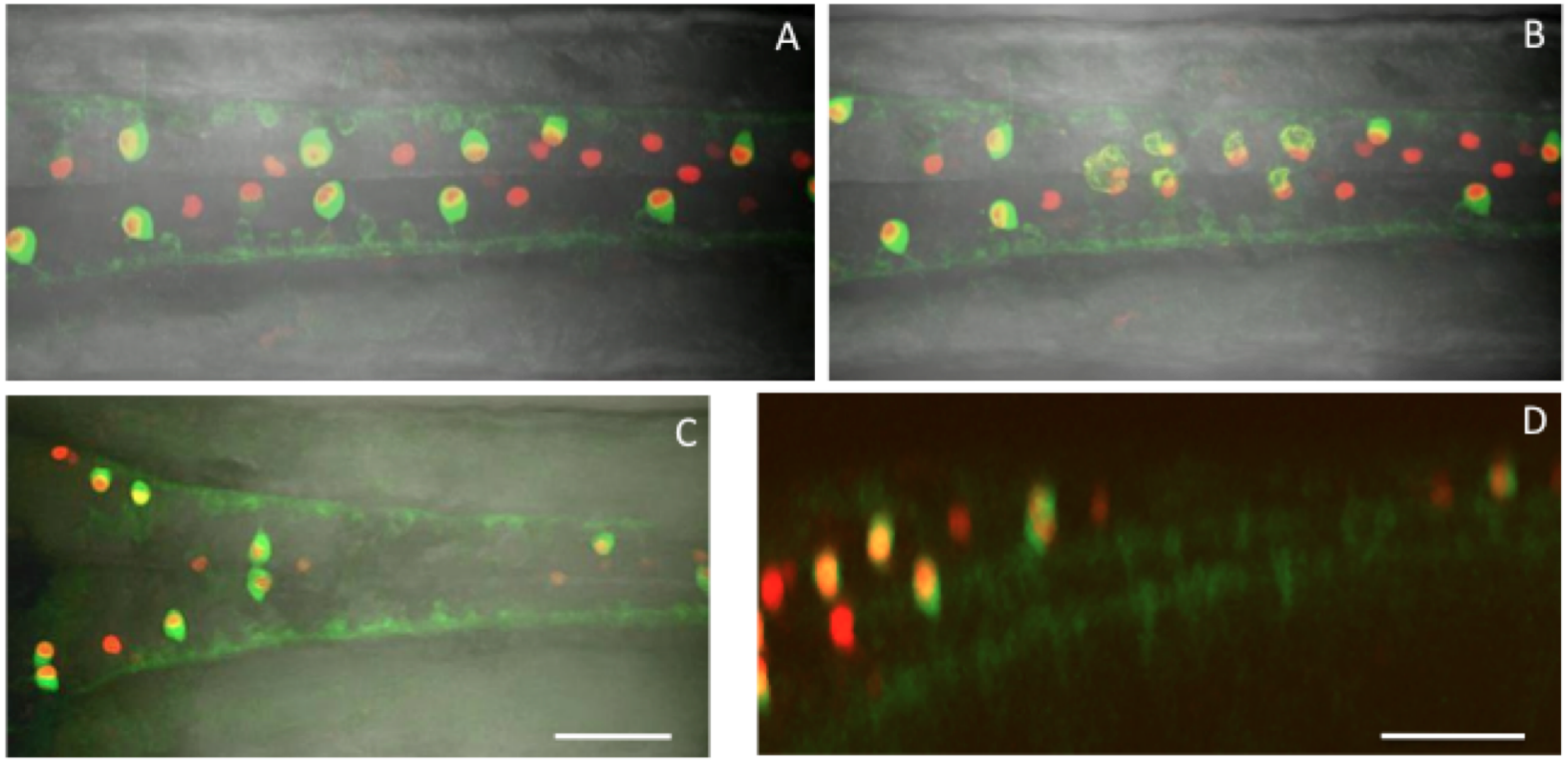

Figure 9 Ablated Tissue Contains No RBs and Recovers

A) Pre-ablation RB neurons at 36 hpf; B) Post-ablation RB neurons also at 36 hpf. C) At 52 hpf, RBs are still not present and the tissue appears to have recovered. D) A lateral view of the same embryo showing that RBs are missing entirely after ablation. Scale bar = 50 μm. The imaging parameters are the same as in Figure 6 above.

DISCUSSION

Interestingly, the DRG, RB, and TG cells that express PKCα are a subset of the total neurons in these populations. There are several waves of RB death, and of TG birth, migration, and death. DRG neurons also migrate into the ganglion at different times, populating it throughout the larval period. It is possible that, like the TG, RBs have some temporal staggering in birth date and that the cells that disappear among RBs first are the same that may die early in the TG, but early on neither population apparently possesses PKCα. The connection between PKCα cells in these sensory ganglia is still unknown, as well as the duration of their lifespan within the embryo.

The purpose of this project eventually was to modify the technical microscopy aims of *in toto* imaging to obtain high-resolution images, capturing even thin axons, and to generate a few examples of its use in studying neurons of the dorsal spinal cord. I have shown that it is possible to characterize spinal cord development anatomically and genetically as gene expression and cell migration occur simultaneously. For this I used injected mRNA fluorescent segmentation markers to label nuclei and cell membranes ubiquitously, DIC imaging to watch changes in tissue morphology without a separate dye, and a third fluorescent marker. In applying this modified technique to the preliminary study of two FT lines I found that RBs, which are believed to begin undergoing PCD during the first 48 hpf remain healthy. I was also interested in using *in toto* imaging to study the effects of loss of RB neurons through laser ablation on neighboring RBs. The ultimate aim of this project is to use laser ablation and *in toto* imaging to understand how RB neurons help to pattern the early spinal cord and affect embryonic and adult behaviors. Here I

have presented data to show that after killing some RB cells, neighboring RB neurons do not contribute to replacing the missing cells, during the first 52 hpf. Further investigations and analysis of time-lapse data collected during these studies will yield insights into how loss of RBs at different developmental time points may affect the anatomical organization of the early zebrafish spinal cord, especially interneurons and motoneurons near ablated regions, as well as how axonal arbor morphologies may change in response to early RB ablation.

ACKNOWLEDGEMENTS

I would like to thank: Drs. Scott Fraser and Marianne Bronner for training and financial support; Debbie Marshall for her hard work and diligence as a volunteer; Drs. Le Trinh, Sean Megason, and the CEGS screen team for technical support; Drs. Eduardo Rosa-Molinar, Alvaro Sagasti, Angeles Ribera, and David Koos for helpful zebrafish discussions; Dr. Thai Truong and the Fraser lab for imaging advice; Drs. Max Ezin, Rasheeda Hawk, and Aidyl Gonzalez-Serrichio for helpful discussions about this project. Funding was provided by the National Human Genome Research Institute (NHGRI) Center of Excellence in Genomic Science (CEGS) Grant: P50 HG004071, and the Achievement Rewards for College Scientists (ARCS) Foundation for fellowship support to ADD.

BIBLIOGRAPHY

Griesbeck, O., Baird, G. S., Campbell, R. E., Zacharias, D. A. and Tsien, R. Y. (2001). Reducing the Environmental Sensitivity of Yellow Fluorescent Protein. *The Journal of Biological Chemistry* **276**.

Megason, S. G. (2009). *In toto* imaging of embryogenesis with confocal time-lapse microscopy. *Methods in Molecular Biology* **546**, 317-332.

Sagasti, A., Guido, M. R., Raible, D. W. and Schier, A. F. (2005). Repulsive Interactions Shape the Morphologies and Functional Arrangements of Zebrafish Peripheral Sensory Arbors. *Current Biology* **15**, 804-814.

Trinh, L. A., Hochgreb, T., Graham, M., Wu, D., Ruf, F., Jayasena, C., Saxena, A., Hawk, R., Gonzalez-Serrichchio, A., Dixson, A. et al. (2011). FlipTraps: fluorescent tagging and cre mediated mutagensis of proteins at their endogenous loci. *Genes & Development* **25**.

CHAPTER III

Reversing The Dogma: New Evidence That Zebrafish Rohon–Beard Neurons Survive into Adulthood

AUTHOR

Alana D. Dixson

ABSTRACT

Rohon-Beard (RB) neurons are uniquely transient chemo- and mechano-sensory cells, which have been well characterized in the spinal chord of lower vertebrates. Here I report on a subset of zebrafish RB cells that perdure into the adult, contrasting with dogma suggesting that the entire population disappears during the early larval period. The coexistence of RB-like neurons with dorsal root ganglia (DRG) suggests that zebrafish have two post-embryonic sensory systems, challenging the previous notion that only peripheral sensory neurons survive.

INTRODUCTION

A dogma regarding vertebrate nervous system development states that the entire population of Rohon-Beard (RB) neurons, large mechano- and chemo-sensory cells in the dorsal spinal cord of anamniotes, undergoes complete elimination from the spinal cord within the embryonic and larval periods (Cole and Ross, 2001; Lamborghini, 1987). RB cells in the majority of species reportedly die in young larvae or earlier, but some survive into the adult. Xenopus RBs are functional until just before metamorphic climax (Lamborghini, 1987), while in human embryos, the presumed cognates of primary sensory neurons degenerate during the fetal period (Humphrey, 1944; Humphrey, 1950; Youngstrom, 1944). In contrast, newt and lamprey RB-like neurons never die (Nakao and Ishizawa, 1987).

In zebrafish, RBs reportedly disappear between 2 - 5 days post-fertilization (dpf) (Williams, 2000) with the early stages of apoptosis beginning at 24 hours post-

fertilization (hpf) (Reyes, Haendel, Grant, Melancon and Eisen, 2004; Sipple, 1998a), and by the end of the first week the entire population is removed (Cole and Ross, 2001; Reyes et al., 2004). Defined as primary neurons in zebrafish and other lower vertebrates because they are born first and establish their function during early embryogenesis (Kimmel, Hatta and Eisen, 1991; Kimmel and Westerfield, 1990), RB neurons provide the young animal with sensation throughout the head and trunk, along with trigeminal ganglion (TG) mechanosensory neurons (Clarke, Hayes, Hunt and Roberts, 1984; Kimmel et al., 1991; Kimmel and Westerfield, 1990; Sipple, 1998a). RBs are in part responsible for the embryonic escape reflex and detect noxious stimuli by 20 hpf, presumably maintaining this capacity until they are eliminated by some unknown mechanism upon establishment of the mature dorsal root ganglion (DRG) sensory system (Clarke et al., 1984; Cole and Ross, 2001; Lamborghini, 1987; Sipple, 1998a; Williams, 2000).

Despite reliable demonstrations of zebrafish RB apoptosis, more recent studies have shown that these cells may persist until 7-13 dpf (Reyes et al., 2004; Slatter, Kanji, Coutts and Ali, 2004). One subset of older RBs express protein kinase C alpha (PKCα) (Reyes et al., 2004; Slatter et al., 2004), while another possesses sodium channel defects (Nakano, Fujita, Ogino, Saint-Amant, Kinoshita, Oda and Hirata, 2010). In each case, the signs of cellular degeneration were consistent with programmed cell death (PCD). Most previous studies have relied heavily on immunohistochemistry, focusing on animals younger than 48 hpf, as tissue penetration issues in maturing larvae hamper longitudinal observation. It is unknown whether or not some embryonic zebrafish RBs survive to

unanticipated stages, maintaining their function as an adult RB, or give rise to a transdifferentiated derivative that escapes detection by typical methods

I identified several transgenic lines as part of the FlipTrap (FT) screen in the Center of Excellence in Genomic Science (CEGS) subgroup of the Fraser laboratory. The FT is a transposon based, gene-trapping vector containing a citrine cassette that is injected at the one-cell stage. Citrine co-expresses with trapped genes upon vector insertion into an intronic region, followed by in-frame transcription and normal translation of a bright citrine fusion protein, which is detected in a typical F_2 screen. Successful integration of the FT vector maintains endogenous control elements and the transgenic lines stably propagate.

I used two FT lines with citrine expression in RB and other sensory neurons to answer several questions testing the hypothesis that persistent RBs exist beyond 13 dpf: 1) Do FT RB neurons undergo PCD during the peak of RB death from 36-48 hours post-fertilization (hpf)? 2) Are FT RB cells present between 7 and 13 dpf? 3) Does an older, RB-like FT neuron exist beyond 14 dpf?

In this paper I characterize the FT citrine expression in RBs to show that these cells are a subset of total RBs, and that they survive the peak of apoptosis without further modification either genetically or with increased or decreased tactile stimulation. I further provide evidence of RB-like neurons past 14 dpf. Next, I show that persistent RBs contribute to the integrated escape response circuit at 36 and 48 hpf. Finally, I

demonstrate that older RBs coexist with the DRG well beyond its functional maturation and the dogmatic period of RB cell death. I observed RBs located in the rostral spinal cord slightly before and during their apoptotic peak at 30 - 34 hpf and 36 - 48 hpf, when one would expect to see a significant reduction in all but potentially long-lived subtypes. Here I look further at these results.

MATERIALS AND METHODS

FlipTrap Vector

The FlipTrap vector (Figure 4, Chapter 1) is a transposon-based gene trap that creates a genetically encoded citrine tag to track the endogenous temporal and spatial expression of developmentally important genes (Trinh, Hochgreb, Graham, Wu, Ruf, Jayasena, Saxena, Hawk, Gonzalez-Serricchio, Dixson, Chow, Gonzales, Leung, Solomon, Bronner-Fraser, Megason and Fraser, 2011a). When the vector randomly inserts into an intronic region in frame, citrine (Griesbeck et al., 2001), a variant of yellow fluorescent protein (YFP) and hereafter referred to as such for convenience, is transcribed along with the endogenous gene to create a fluorescent fusion protein under native control. The rationale for the FlipTrap vector design, its construction, and its introduction via microinjection into one-cell stage zebrafish are thoroughly discussed by Trinh et al. in a forthcoming article (Trinh et al., 2011a).

Briefly, the FT vector was microinjected using a Nanoject II Auto-nanoliter Injector (Drummond Scientific) in plasmid form at 2 - 3 pg/μl at the one-cell stage by one operator (either Le Trinh or Sean Megason) to ensure consistency (Figure 5, Chapter 1).

We raised the surviving embryos as the F_0 generation and individually out-crossed both males and females with a wild-type mate from lab stocks of AB, Top Longfin (TL), or AB/TL adult zebrafish. We then screened the F_1 generation over 5 dpf on low-magnification, fluorescent microscopes for YFP fluorescence throughout the body. Positive embryos and young larvae, pooled per day and by expression pattern of newly observed fluorescence, were given an allele number and raised or genotyped to determine the trapped gene.

Genotpying

We used 3 prime-end rapid amplification of cDNA ends (3′ RACE) to amplify the genomic region 3′ of the inserted citrine cassette (Trinh et al., 2011a). The 3′ RACE products were sequenced by Davis Sequencing.

Maintenance and Propagation of Zebrafish Adults and Embryos

Zebrafish (*Danio rerio*) were propagated and maintained at 28°C according to standard protocols (Westerfield, 1993). Briefly, adult fish were spawned at "dawn" when artificial lights turn on and eggs were collected at regular intervals of ~ 20 – 30 minutes. Embryos were grown in petri dishes containing methylene-blue treated egg water with 0.003% 1-phenyl-2-thiourea added between 18 – 20 hpf to suppress pigmentation. At 5 dpf larvae were transferred to fry tanks and placed on the fish maintenance system to receive food and flowing water. Animals selected for observations post-5 dpf were removed each day for imaging and either sacrificed according to IACUC approved procedures, or returned

to the fish facility for future use. I staged embryos and larvae by external features according to well established criteria (Kimmel and Westerfield, 1990).

Immunohistochemistry

Antibody Staining

In larvae > 3 dpf I identified RBs by location in the dorsal spinal cord, and morphological features consisting of a large, eccentric nucleus with granular cytoplasm, large soma, and both a central and peripheral axon (Kuwada et al., 1990); for animals younger than 3 dpf, expression of Islet-1 and neurogenin 1 (ngn1), along with the previous criteria, were used. Briefly, embryos were dechorionated with fine metal forceps and fixed in 2 - 4% paraformaldehyde (PFA) at 4°C overnight or for 4 hours at room temperature. Following fixation, animals were washed 6 x 5 minutes for 30 minutes in 1X phosphate-buffered saline (PBS) free of calcium and magnesium, washed overnight in PBS at 4°C, and then incubated for 12 - 16 hours at 4°C in blocking solution consisting of 5 - 10% heat inactivated goat serum, 1% DMSO, 1% BSA, and 0.1 (< 3 dpf) or 0.4% (> 3dpf) Triton X-100 in ddH_20. Next, samples were incubated for 24 hours at 4°C in the primary antibodies Zn-12 and Islet-1 at 1:50 and 1:100, respectively (Developmental Studies Hybridoma Bank), diluted in blocking solution. Embryos were washed in 1X PBS 6 x 5 minutes for 30 minutes and then 1X per hour for 7 hours and then placed in blocking solution overnight at 4°C. Blocked samples were incubated in goat anti-mouse secondary antibodies (Molecular Probes) Alexa 633 for Zn-12 and Alexa 594 for Islet-1 diluted 1:500 at room temperature for 4-6 hours for younger animals, or overnight at 4°C for those older than 3 dpf. Following secondary antibody staining, samples were washed at

room temperature for 4 hours with medium changes every 30 minutes and then equilibrated in a 1:1 glycerol-to-PBS mixture overnight.

Imaging

Depigmentation and Preservation

Animals not processed for IHC were collected at appropriate stages and preserved in 4% (wt/vol) paraformaldehyde in 1X PBS. To improve visualization of the fluorescent protein expression patterns, embryos and larvae were allowed to develop in 0.003% 1-phenyl-2-thiourea to inhibit formation of pigment (Westerfield 2000).

Whole-Mount Fluorescence Microscopy

Whole embryos and larvae were mounted in methylcellulose for fluorescence microscopy and image capture. Each animal was imaged live at 20X magnification on an Olympus MVX10 microscope for YFP expression with exciter filter BP460-480HQ, dichroic beam splitter DM485, and barrier filter BA495-540HQ. Images were collected digitally with an Axiocam HRc camera and further processed and labeled with ImageJ software.

Confocal and *In Vivo* Confocal Microscopy

I used the imaging the procedures outlined by Megason with several modifications (Megason, 2009). Embryos and larvae were mounted in 1 - 1.5% ultrapure, low-melting point agarose (LMP, Invitrogen catalog number 16520100) in egg water. For animals younger than 72 hpf, I created the dorsal embryo array, trimmed it to create a square patch of 3 - 5 embryo wells, and placed these cut squares into each chamber of a two-

chamber tissue culture dish (Thermo Scientific, LabTek Nunc Chamber Slide System, catalog number 177429). I mounted animals older than 72 hpf in LMP alone without arrays and with both older and younger specimens we used a hair loop tool to gain optical access to the dorsal spinal cord.

Larvae older than 5 dpf, which were not treated with PTU, were mounted at a 30° to 40° angle from normal with the dorso-lateral surface adjacent to the cover slip to visualize the region containing RB neurons ventral to the superficial, obstructing melanocytes. All embryos were imaged using the Zeiss C-Apochromat 1.2 NA water immersion objective on Zeiss CLSM microscopes in the Biological Imaging Center (BIC).

Cre-Mediated Mutagenesis

Upon injection of Cre recombinase, the YFP cassette is excised and the trapped gene shortened. This Cre-mediated mutagenesis flips an additional m-cherry (RFP) cassette, originally in the reverse orientation, forward. RFP replaces YFP, and wherever the gene was expressed we obtain a visual readout of the mutant RFP fusion protein. I injected approximately 40 ng/μl of Cer-Cre recombinase mRNA at the one-cell stage into FT animals as described above. Alternatively, a transgenic line expressing Cre-Cerulean recombinase under the control of a β-actin promoter (courtesy Tatiana Hochgreb) was crossed with the FT lines to produce mutagenized FT animals.

Behavioral Tests

The Touch Assay

To test the presence of a functional escape response mediated only by RB neurons, I used a modified touch assay as described by Wright et al. (Wright and Ribera, 2010). I stimulated the dorsolateral surface of the lower trunk at or below the level of the dorsal fin with the tip of a human hair affixed with super glue to the tip of a glass pasteur pipette once per trial and assigned a score as follows: 0 = no swimming, 0.5 = twitching only, 1 = swimming. Each animal underwent 10 trials and cumulative scores between 0 – 10 were calculated and assigned.

Morpholino Injections

The ngn1 morpholino (a gift from Alvaro Sagasti, University of California at Los Angeles) was prepared with phenol red and injected at the one-cell stage as above.

Data Analysis

For RB neuron counts I counted cells in spinal cord segments 1 - 5 for each animal, averaged these totals, and calculated a standard error of the mean (SEM) along with the average number of RBs per segment per day post-fertilization. For the touch assay, data from individual embryos were pooled per trial 1 – 11, per stage or time point, and averaged; finally an SEM was calculated. Comparisons between time points and fusion protein expression in Cre-treated animals were compared using the Kruskal-Wallis non-parametric test; a p-value of < 0.05 was assigned as statistically significant. The Kruskal-Wallis tests non-parametric data, assumes a normal distribution, and can give information

about the mean rank differences between groups. I chose this test following the methods of Wright et al., and assuming that, although individual group responses would have a normal distribution, response to stimuli is likely not a probability function.

RESULTS

The FlipTrap Labels a Subset of Sensory Neurons Throughout the PNS and CNS

The FlipTrap vector (Figure 1A) is a transposon-based gene trap that creates a genetically encoded citrine tag to track the endogenous temporal and spatial expression of developmentally important genes (Trinh et al., 2011a). When the vector randomly inserts into an intronic region in frame, citrine (YFP) is transcribed along with the endogenous gene to create a fluorescent fusion protein; control elements of the trapped gene remain intact. In two FT lines, ct 7a and 54a, the vector inserted between exons 3 and 4 of the Protein Kinase C alpha (PKCα) gene (Figure 1B), which we identified using 3 prime end rapid amplification of cDNA ends (3′ RACE). PKC isoforms are characterized by their activators, phorbol esters (PE) such as phosphatidylserine (PS), diacylglycerol (DAG), and calcium (Ca^{2+}) (Ohno and Nishizuka, 2002b). The "typical" PKCs use all three activators, the "novel" subgroup requires PS and DAG, and "atypical" are not activated by any of these molecules. An additional trap, ct 54b, also labels RB neurons, but genotyping efforts have been unsuccessful to date.

In ct 7a and 54a the YFP-PKCα fusion protein can be visualized with low magnification fluorescence microscopy beginning as early as ~ 20 - 24 hpf. Fusion protein expression was found consistently across clutches throughout the dorsal spinal cord. Most relevant

to the present study is the strong expression in the primary sensory neurons, RB cells. Several brain regions, the lens, trigeminal ganglion (TG), and a subset of DRG cells were also fluorescently labeled by 3 - 4 dpf (Figure 2).

The FlipTrap Fusion Protein is Expressed in a Subset of Rohon-Beard Neurons

During the first 5 dpf, I used anti-Islet-1 and anti-Zn-12 antibodies (n = 50 per stage each) along with a ngn1 x PKCα double transgenic line (n = 50 per stage), expressing the YFP-PKCα fusion protein and ngn1 driving red fluorescent protein (ngn1::RFP), to identify FT cells as RB neurons molecularly. In each FT line, both antibody and ngn1::RFP labeled more dorsal spinal cord neurons than the fusion protein and in the correct location for RB neurons (Figure 3A and B). From 6 dpf onward, obtaining reliable immunohistochemical phenotyping was difficult, but the double transgenic animals co-expressed each fluorescently tagged transgene up to 9 dpf, after which only YFP was observed.

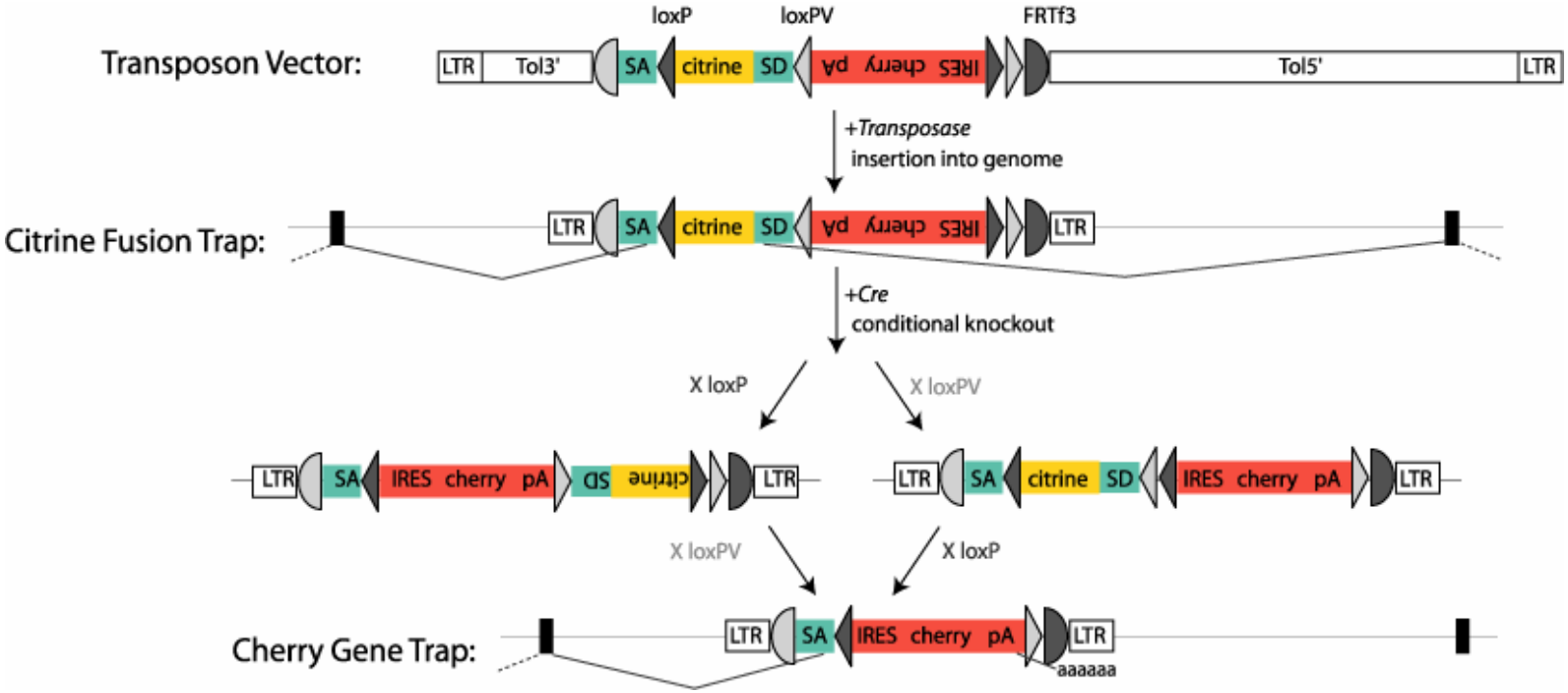

Figure 1A FlipTrap Gene Trapping Strategy

Schematic of the Tol2 mediated protein-trapping strategy and cre-mediated mutagenesis, courtesy of Le Trinh.

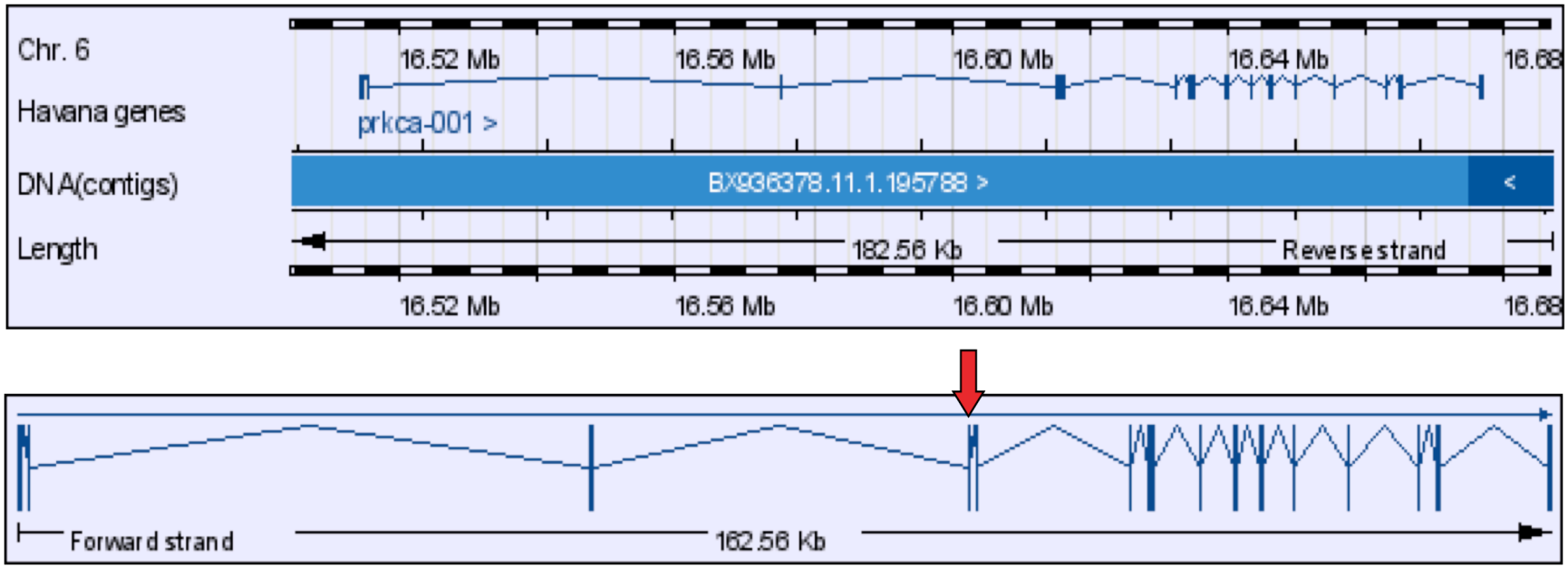

Figure 1B FlipTrap Insertion in Cts 54a and 7a

Chromosome map of PKCα and the insertion point of the FT vector in ct 7a and 54a.

(Source: http://vega.sanger.ac.uk/Danio_rerio/geneview?gene=OTTDARG00000027246;db=core)

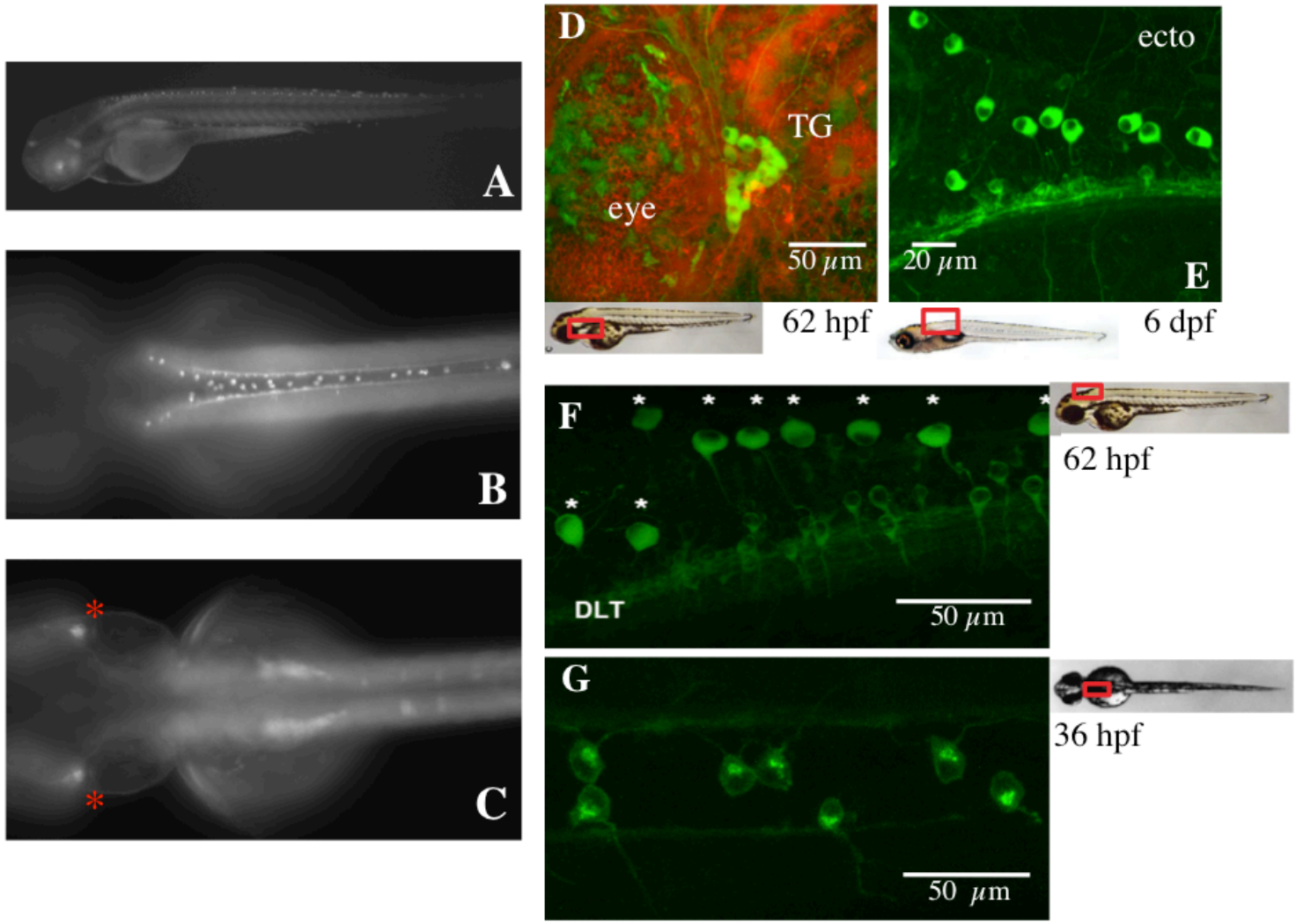

Figure 2 FlipTrap Fusion Protein Expression in Ct 7a

Figure 2 FlipTrap Fusion Protein Expression in Ct 7a

A-D) Using low-magnification, fluorescence microscopy beginning at ~ 20 hpf and over the ensuing 24 - 30 hours, we found YFP-PKCα fusion protein expression spreading from the Trigeminal Ganglion (TG, red * in (C)) and several brain regions to dorsal spinal cord neurons, including some RB cells, and the lens. By 3 - 4 dpf a small number of cells of the dorsal root ganglion (DRG) also contained the fusion protein. E-F) Characteristic of Rohon-Beard neurons, FT cells have dorsal spinal cord somata with peripheral axons extending outside of the spinal cord into the surrounding tissues, and a central axon that forms part of the dorsolatereral tract (DLT). G) FT labeled RB neurons have large, eccentric nuclei and are positioned in two bilateral rows along the spinal cord. In all images caudal is to the right and dorsal is up, except in A, D, and G in which animals are presented in a dorsal view. Green = YFP-PKCα fusion protein, red = Bodipy TMR, a lipophylic dye that labels muscle and cell membranes. Scale bar = 50 μm. * indicates RB neurons, DLT = Dorsolateral tract, DE = dorsal ectoderm, OV = otic vesicle. All CLSM images taken at 40X using the C-Apochromat 1.2 NA water immersion objective on the Zeiss Pascal or Exciter microscope. Bright field images of embryos borrowed from Parichy et al. (Parichy, Elizondo, Mills, Gordon and Engeszer, 2009) or the Kimmel staging atlas available for download from Zfin.org.

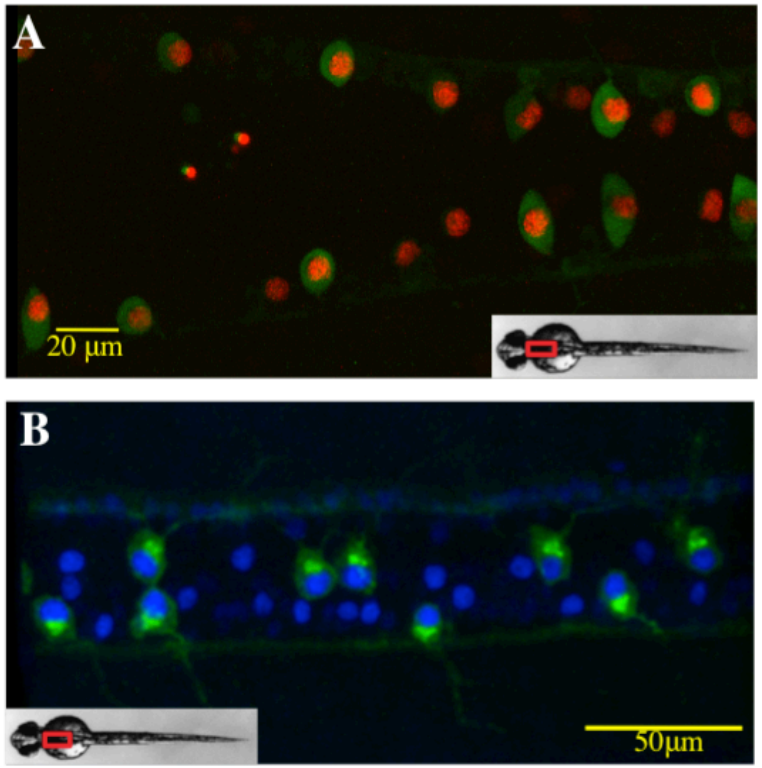

Table 1

Marker	Developmental period
Zn-12	10-14 to 48 hpf -- soma 48 hpf to ~ 6 dpf -- axons
Islet 1	10-14 hpf to ~ 5 dpf
ngn1	9 hpf to ~ 9 dpf

Figure 3 The FlipTrap Fusion Protein Co-Localizes with Other RB Neuron Markers

36 hpf ct 7a embryo, RB neurons labeled with ngn1::RFP (A) and Islet-1 antibody (B), alongside FT fusion protein expression. Green = FT fusion protein, blue = Islet-1 antibody staining, red = ngn1 transgene expression. Table 1 Immunohistochemical Markers Traditionally Used to Identify RB Neurons

FT Cells Are Reduced in ngn1 Morphants

To gain a preliminary understanding of how these FT cells fit in to the overall group of TG, DRG, and RB neurons, I used a neurogenin 1 morpholino to block mRNA translation. Morpholinos generated to block translation of ngn1 create a morphant phenotype in which neuronal populations within in the TG are temporarily reduced, while RB and DRG neurons are completely absent (Blader et al., 2003; Cornell and Eisen, 2002). Although another wave of neurogenesis leads to partial repopulation of the TG with later-born ngn1-specified sensory neurons, RB and DRG of all classes do not recover (Caron, Prober, Choy and Schier, 2008; Cornell and Eisen, 2002). If all FT-labeled cells were specified with ngn1, a reduction in the TG size and elimination of all RB and DRG neurons would be expected; this would also show that the FT-positive, dorsal spinal cord neurons with large somata are RB neurons. Analysis of morphants revealed the anticipated reduction and later repopulation of the FT labeled TG (data not shown) along with absent DRG and RB in single- and double-FT and ngn1::RFP transgenic lines (Figure 4A-D). Animals injected with ngn1 MO have no RB neurons at 36 hpf, and at 3 dpf both DRG and RB neurons are entirely missing compared to normal controls (compare with Figures 2 and 3).

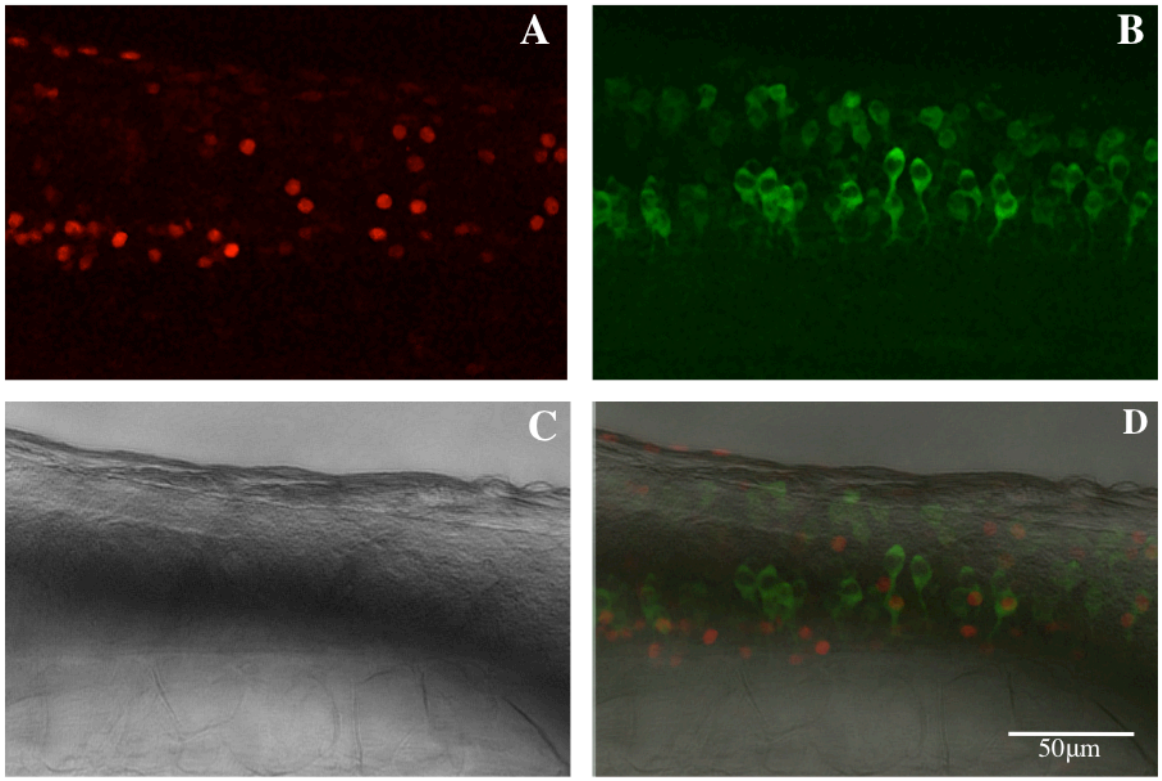

Figure 4 Ct7a x ngn1::RFP Animals Treated with ngn1 MO Injected animals show double expression of the fusion protein with ngn1::RFP (A), and FT-labeled interneurons (INs) (B) in the dorsal spinal cord. Brightfield image shows spinal section morphology (C); merge of A-C shows the altered location of INs (D). Green = FT fusion protein, red = ngn1 transgene expression. In all images green = YFP-PKCα fusion protein, caudal is to the right and embryos are viewed dorsal side facing objective lens. Scale bar = 50 μm. All images were taken on the Zeiss Pascal or 510 NLO microscopes.

Table 2

Hours (h) or days (d) post-fertilization	Number of YFP+, FlipTrap RB neurons in spinal cord segments (scs) 1-5, ± SEM		
~30 hpf	13 ± 1	~ 3/scs	N = 13
2 dpf	13 ± 2	~ 3/scs	N = 5
3 dpf	12 ± 1	~ 2/scs	N = 5
4 dpf	15 ± 1	~ 3/scs	N = 6
6 dpf	14 ± 1	~ 3/scs	N = 11
9 dpf	22 ± 1	~ 4/scs	N = 4
13 dpf	10 ± 1	~ 2/scs	N = 5

Table 3

Genotype	RB neurons in spinal cord segments (scs) 1-5, ± SEM significance P <0.05	
	36 hpf	48 hpf
FT P = 0.38	14 ± 1 ~ 3/scs N = 12	13 ± 1 ~ 3/scs N = 5

Figure 5 FlipTrap Rohon-Beard Neurons Do Not Undergo Significant Apoptosis

Each day a new set of FT fish were imaged to count the number of RB neurons to avoid altering the survival of the cells by use of a tricaine anesthetic.

In time-lapse movies of FT RB neurons (data shown for 32-42 hpf in Figure 8, Chapter 2), YFP positive neurons are present throughout the expanding neural tissue and they do not disappear during the peak period of RB cell death as reported previously by Cole et al. (Cole and Ross, 2001). The authors also showed that apoptotic debris from RBs were removed within one hour or less, but I have not seen evidence of massive PCD or cellular debris, despite having looked at hundreds of RBs, across several consecutive days, and at intervals of minutes to hours. This could be due to my use of a sodium channel-blocking anesthetic which reduces embryo movement, and that may alter RB lifespan (Ribera and Nüsslein-Volhard, 1998). Given that FT and ngn1-positive cells are evident even in animals that have received no prior anesthetic, and that apparently there is some heterogeneity of RB neurons, I believe that the results of the time-lapse may be explained by the presence of subsets of RB neurons that are variably sensitive to sodium channel alterations.

FlipTrap Rohon-Beard-Like Neurons Survive to 30 dpf and Coexist with the DRG

I further analyzed both lines (n = 50 embryos/line) via confocal laser scanning microscopy (CLSM) over the first 30 dpf to identify RB-like neurons by their characteristic morphology. These bipolar cells are the largest and most superficial neurons in the dorsal spinal cord with granular cytoplasm and large, eccentric nuclei. They are also easily identified by their central axons, which form part of the dorsolateral tract (DLT), and branching peripheral processes, that innervate surrounding ectodermal and muscle tissue. Although the peripheral axons have been shown to retract over time (Reyes et al., 2004), the dorsal position and morphology are still identifiably RB-like

(Reyes et al., 2004; Sipple, 1998a; Williams, 2000). The number of YFP-positive cells per DRG increased over time and both this expression and that of RB-like neurons persisted up to the last observed time point.

Both FlipTrap Rohon-Beard and DRG Neurons May Function in the Embryonic Escape Response

Sensitivity to mechanical stimuli is a characteristic of wild-type RB neurons that die early (Nakano et al., 2010; Ribera and Nüsslein-Volhard, 1998); only RBs can mediate this reflex up to 36 hpf. By 48 hpf the DRG has migrated into the spinal cord and begun to mature, but has not fully extended axons. At this point, previous workers have shown that the embryonic RB has undergone massive apoptosis, which suggests that these cells no longer function in the escape response (Cole and Ross, 2001).

Given that DRG and RB innervation overlaps and appear to subserve similar functions, I asked whether FT RBs and DRG were important to the escape response. Using the touch assay at 34 hpf, before the DRG has matured, and again at 49 hpf, after initial migration of individual DRG neurons, I tested the response of animals bearing FT RB in a double transgenic line that expresses RFP under control of the ngn1 promoter and the FT fusion protein. At 34 hpf, over 11 trials, double-transgenic animals initially responded vigorously to stimuli, over time habituated to it, and then markedly decreased their response. At 49 hpf, these same embryos were highly responsive throughout all 11 trials (Figure 7). These results were statistically significant and indicate that the escape response in zebrafish during the reported period of massive RB cell death actually

increases, before the DRG has had an opportunity to take over RB function, at least in these transgenic lines.

I did not test wild-type embryos in the same time periods, but to further understand how the FT fusion protein may affect RB performance, I tested the escape reflex at 38 hpf when RBs still mediate the response (Figure 8).

In Figure 7, the mean rank differences between the two time points 34 and 49 hpf were significantly different. I interpret the paired t-test results to show that the data are significantly different; therefore, we can reject the null hypothesis that the behavior of embryos is the same at 34 hpf versus 49 hpf. The embryos become more responsive over the period of reported RB apoptosis.

At 38 hpf, animals treated with Cre recombinase to create a mutant PKCα protein had altered escape responses. Compared to wild-type animals that were stimulated daily and those that were not, Cre-treated embryos were less responsive (Figure 8).

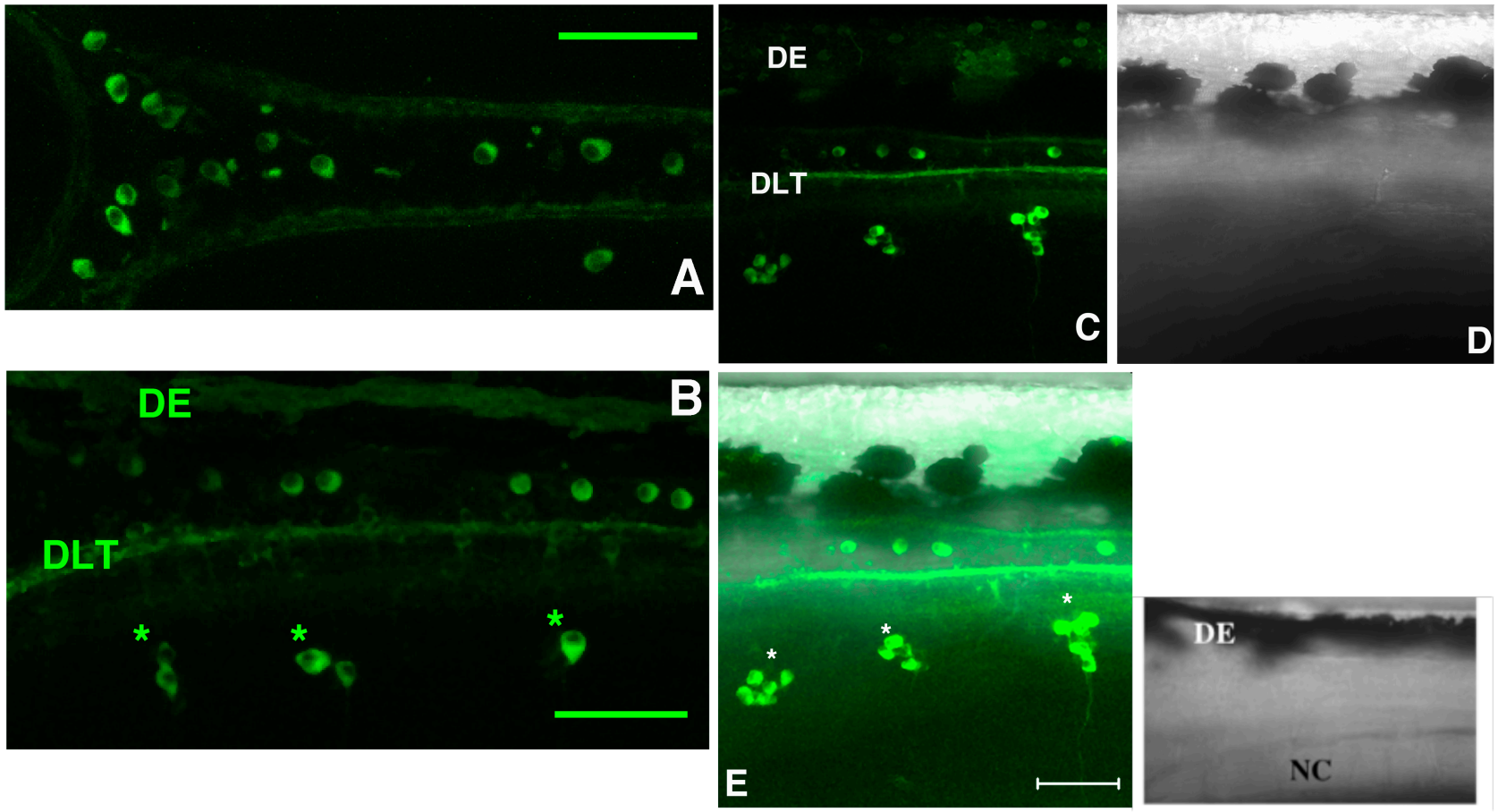

Figure 6 FT RBs Are Among Other Persistent RBs and Co-Exist with DRG Neuron

Figure 6 FT RBs Are Among Other Persistent RBs and Co-Exist with DRG Neurons

RB neurons at 9 dpf are among other persistent RBs (A). At 18 dpf (B) and 25 dpf (C), FT-labeled RBs are present in the rostral spinal cord; an *in vivo* image at 25 dpf shows that several FT DRG neurons are present at later stages along with fusion protein containing RBs. Interestingly, the ct 54b allele, which is co-expressed in a double ct 54a/b line, also labels RBs at later stages, and other neuron-like cells in the dorsal ectoderm (D). Offset is the brightfield image of (C) to show the orientation in which fish were mounted and the anatomy of the imaged section; here the obstructing melancocytes are evident. In all images green = YFP-PKCα fusion protein, dorsal is up, and caudal is to the right. Scale bars = 50 μm. * Indicates DRG, DLT = Dorsolateral tract, DE = dorsal ectoderm, OV = otic vesicle. All images captured with a 40X C-Apochromat 1.2 NA water immersion objective on the Zeiss Pascal microscope.

Paired t test:

t(9) = 2.85,

p value < 0.02, 95% confidence interval: -5.47 to -0.63

No response = 0

Twitching = 0.5

Swimming = 1

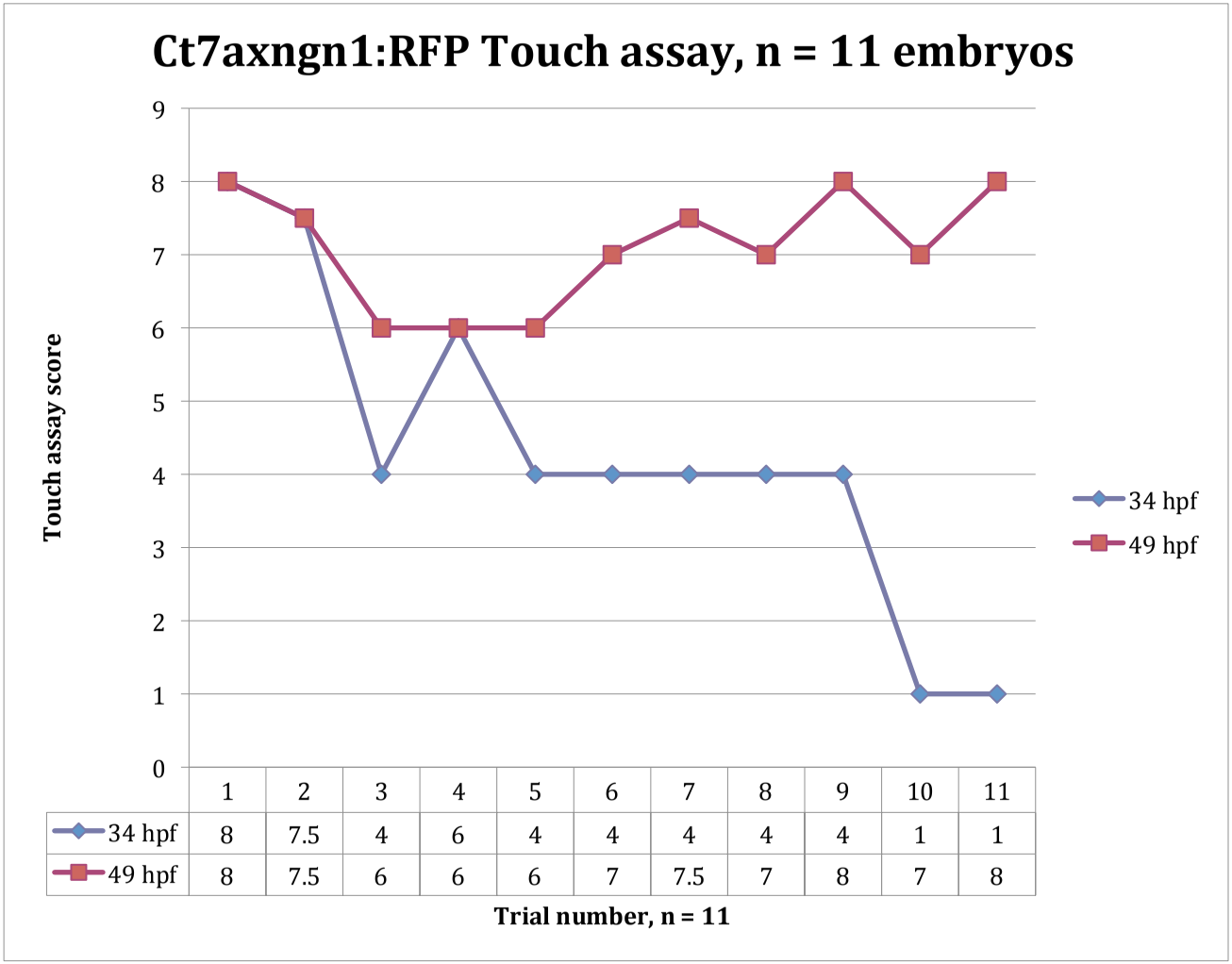

	1	2	3	4	5	6	7	8	9	10	11
34 hpf	8	7.5	4	6	4	4	4	4	4	1	1
49 hpf	8	7.5	6	6	6	7	7.5	7	8	7	8

Kruskal-Wallis test: adjusted H = 8.08, df = 1, P value < 0.005 x10^{-12}

Figure 7 Behavioral Assays Show That FT Embryos Have an Intact Embryonic Escape Response

No response = 0

Twitching = 0.5

Swimming = 1

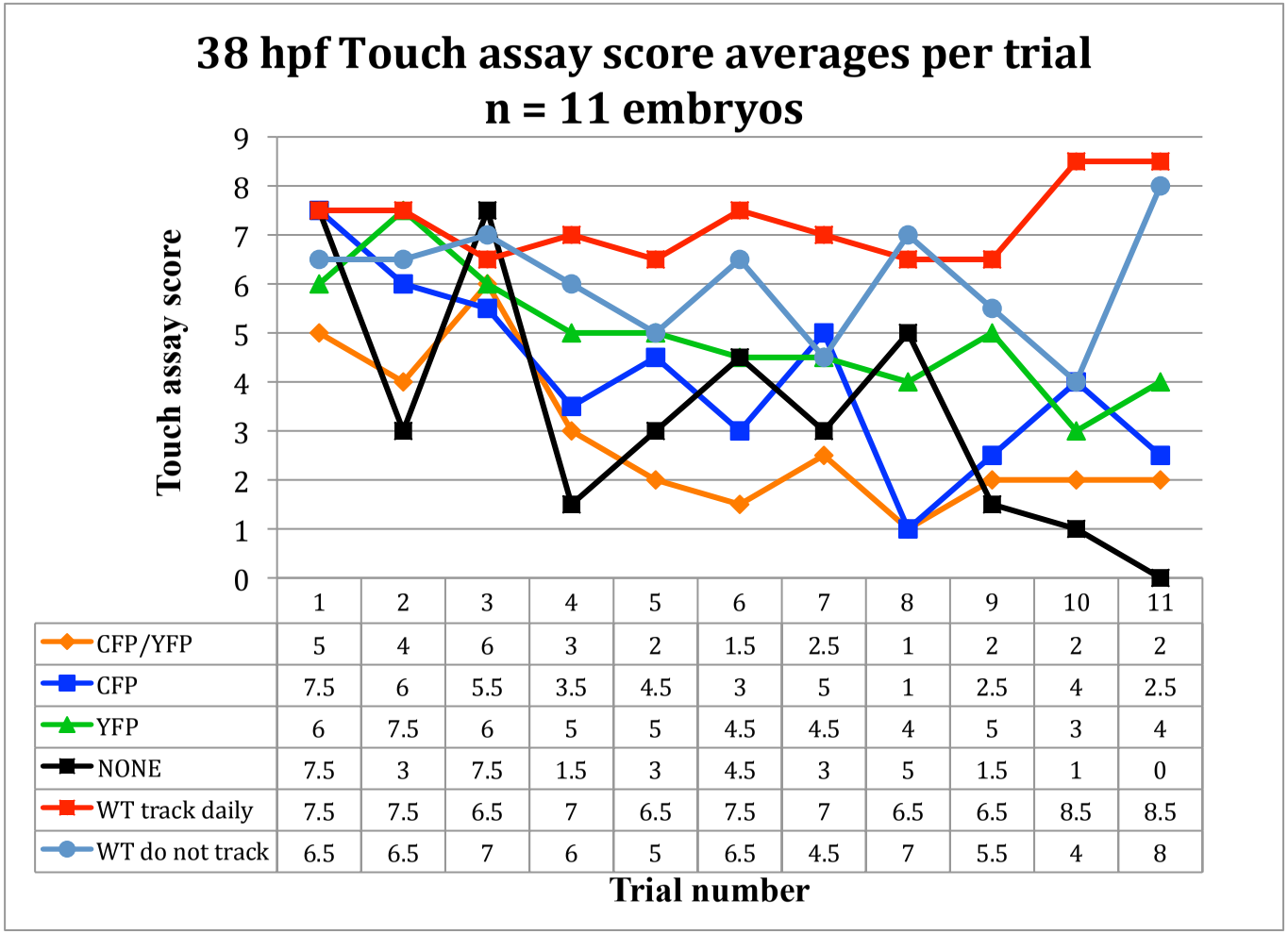

	1	2	3	4	5	6	7	8	9	10	11
CFP/YFP	5	4	6	3	2	1.5	2.5	1	2	2	2
CFP	7.5	6	5.5	3.5	4.5	3	5	1	2.5	4	2.5
YFP	6	7.5	6	5	5	4.5	4.5	4	5	3	4
NONE	7.5	3	7.5	1.5	3	4.5	3	5	1.5	1	0
WT track daily	7.5	7.5	6.5	7	6.5	7.5	7	6.5	6.5	8.5	8.5
WT do not track	6.5	6.5	7	6	5	6.5	4.5	7	5.5	4	8

Kruskal-Wallis test: adjusted H = 32.35, df = 5, P value = 5.06×10^{-6}

Figure 8 Cre-Treated FT Animals' Response to Touch is Altered Compared to Wild-Type

No response = 0

Twitching = 0.5

Swimming = 1

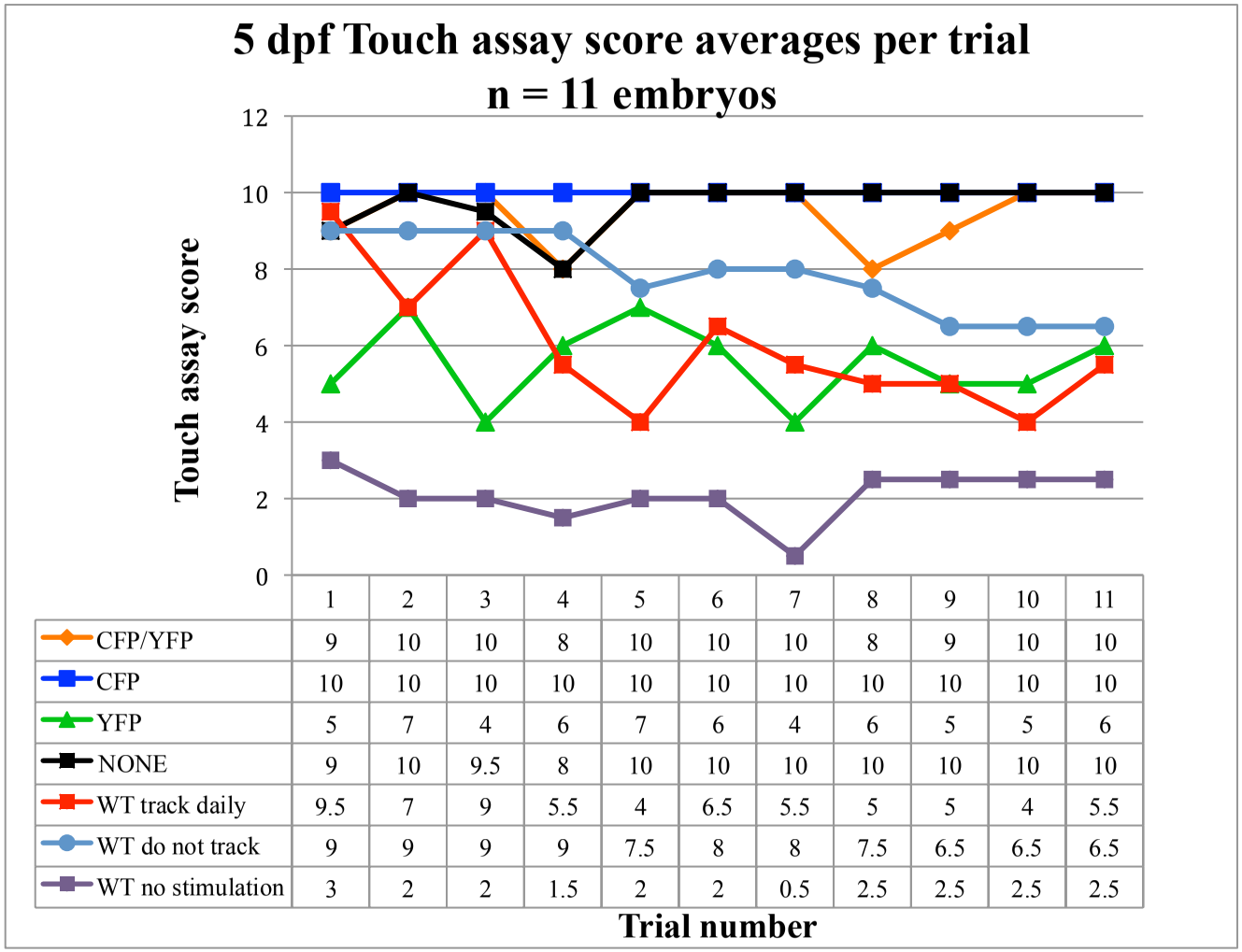

	1	2	3	4	5	6	7	8	9	10	11
CFP/YFP	9	10	10	8	10	10	10	8	9	10	10
CFP	10	10	10	10	10	10	10	10	10	10	10
YFP	5	7	4	6	7	6	4	6	5	5	6
NONE	9	10	9.5	8	10	10	10	10	10	10	10
WT track daily	9.5	7	9	5.5	4	6.5	5.5	5	5	4	5.5
WT do not track	9	9	9	9	7.5	8	8	7.5	6.5	6.5	6.5
WT no stimulation	3	2	2	1.5	2	2	0.5	2.5	2.5	2.5	2.5

Kruskal-Wallis test: adjusted H = 66.1, df = 6, P value = 2.60 x 10^{-12}

Figure 9 At 5 dpf Cre-Treated Animals are Hyper-Responsive Compared to Wild-Type Fish

No response = 0

Twitching = 0.5

Swimming = 1

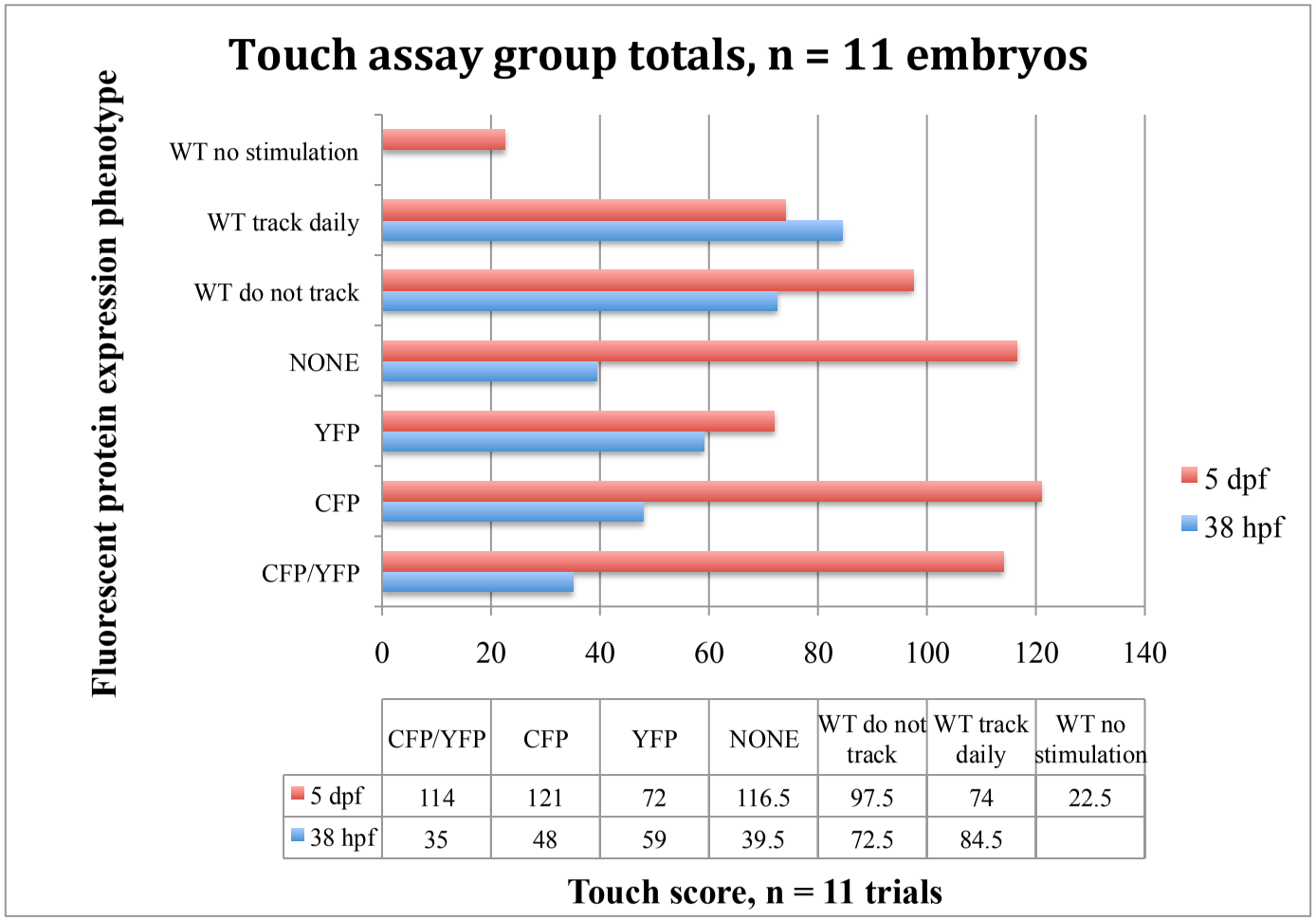

	CFP/YFP	CFP	YFP	NONE	WT do not track	WT track daily	WT no stimulation
5 dpf	114	121	72	116.5	97.5	74	22.5
38 hpf	35	48	59	39.5	72.5	84.5	

Kruskal-Wallis test: adjusted H = 2.94, df = 1, P value = 0.086

Figure 10 Cre-Treated Animals Increasingly Respond to Touch Over the First 5 dpf

Initially, I injected a cerulean-Cre mRNA transcript prior to using the cerulean-Cre transgenic line, but an RFP fusion protein was never visualized. Additionally, cerulean and YFP expression was variable, and at that time the screen team believed that this indicated that the recombination event did not occur. I discarded these embryos and later attempted to create the conditional mutants in both ct 54a and ct 7a using the cerulean-Cre transgenic line. This proved to be equally discouraging, as expression patterns included combinations of YFP and CFP, or one each, but never RFP. Later we discovered that Cre recombinase produced a mosaic pattern of RFP fluorescence in some FT lines and in others Cre expression itself was mosaic (Trinh et al., 2011a). The F_1 generation, however, may express the conditional allele with the RFP reporter. I decided to renew the effort to create a PKCα mutant with the two FT lines using the cerulean-Cre transgenics. Being aware that the dosage of Cre may not correspond with fluorescent protein read out, I decided to test all four phenotypes produced by crossing with the cre-producing line.

Mutagenized fish behaved spastically at 38 hpf (Figure 8), but by 5 dpf they had a hyper-responsiveness that never attenuated, compared to YFP expressing or wild-type embryos (Figure 9), showing that by 5 dpf the differences between each group of Cre-treated animals and wild types are evident. Interestingly, some animals also swam in odd patterns (data not shown), ranging from circular movements to staccato forward swimming, to a prolonged post-stimulus twitch that appeared to last longer than average in some animals and which was absent in wild-type fish. These assays also resulted in more Cre-treated animals compared to wild type that did not respond.

In Figure 10, the assay comparing responsiveness at 5 dpf of all animals, the CFP larvae were most responsive, whereas those wild-type fish that did not receive any stimulation post-fertilization were the least, and this difference was extremely statistically significant ($p < 0.0001$, $t(20) = 39.51$, 95% CI: 7.5 to 8.3). Pooled scores from each embryo, for each trial combined, are given per phenotype and these were plotted to see the strength of the response to stimulus. In comparing the CFP group to a more normal wild-type animal that had received stimulation every day, including medium changes, the CFP group were hyper-responsive, and this difference was also extremely statistically significant.

In intergroup comparisons I found that the animals with some CFP expression or no fluorescent protein expression were more similar than those with YFP only. Taking the animals with CFP only expression as a representative of the mRNA knockdown scenario and comparing it to both YFP-only and wild-type animals, CFP and YFP embryos' escape reflex was similar in a statistically significant way at 38 hpf, but by 5 dpf their responses were extremely different (Table 4).

Initially, I thought that the cerulean-Cre transgenic line would yield more clear-cut phenotypes when crossed with FT lines, and as the details of the mosaic expression in some lines had not been worked out at the time of these experiments (see Trinh et al., 2011 for explanation), I did not use untreated FT animals at each time point. Using CFP as a representative of the knockdown group, I observed that the difference in CFP and YFP expression is accompanied by a difference in reaction to stimulation at both 38 hpf and 5 dpf. Moreover, although there are some similarities between groups (see Table 4),

there are still enough intergroup differences in response rate to speculate that the mutagenesis of YFP-PKCα differs by group and underlies the observed behavioral outcomes.

In Table 4 below, I've compared each group and calculated the statistical significance of the difference in their responsiveness to the touch assay stimulus with a hair loop. Several comparisons stand out: 1) The none and YFP-only groups are not the same, indicating that the absence of YFP in these lines may not simply be due to the lack of fusion protein expression, but otherwise normal PKCα; 2) The YFP versus wild-type groups are always different in a statistically significant way, suggesting that this group does not represent a phenotype that is identical to wild-type, except for the fusion protein label; 3) The none versus wild-type groups are all different in a statistically significant way, also suggesting that this group does not represent the wild type PKCα expression. These results are preliminary and, until they can be validated with molecular and more specific behavioral or electrophysiological data, they are limited, serving as a guide for future studies on the role of PKCα in RB function.

DISCUSSION

Rohon-Beard (RB) neurons have dogmatically been defined as early-born, primary sensory neurons that die by the end of the embryonic or larval period in most vertebrates, including zebrafish. Their potential functional and molecular heterogeneity remains an open area of research and here we provide evidence for one category of RBs, namely, a persistent population.

Reyes et al. (2004), used an informative, Islet-1 transgene, immunohistochemistry, and *in vivo* backlabelling with DiI to show RBs at 7 dpf, raising the possibility that a longer-lived zebrafish RB subtype exists (Reyes et al., 2004). Given that transient, episomally derived islet-1 protein expression may not recapitulate the wild-type pattern with temporal fidelity or consistently appear in potentially long-lived RBs, these results do not preclude the possibility that a subset of islet-1-containing RBs persist. The FlipTrap vector overcomes the limitations of transient expression by creating endogenously controlled and permanent expression of PKC-α, a gene previously identified in RBs as late as 13 dpf (Slatter et al., 2004).

In the present study I show that PKCα-YFP positive RB neurons are a subset of the total population. I was not able to subcategorize them by the expression of typical RB markers zn-12, ngn1, and islet-1. This finding suggests that the molecular heterogeneity of RBs may reside in as-yet-unidentified signaling molecules that are not typically used to characterize these neurons, perhaps in ion channel diversity or responses to other stimuli.

It would be interesting to look for heterogeneity in the expression of these markers alone or correlated with other features of RBs.

Additionally, RBs expressing PKCα do not die during the peak period of RB cell death, 36–48 hpf, when caspases are involved in their PCD (Williams, 2000). Our time-lapse data show the same RBs bearing the FT fusion protein during and after this period. This suggests that at least the longer-lived RBs do not die by a caspase mechanism.

If there is an early wave of RB death, it is reasonable to divide the population into two classes: 1) early dying, and 2) persistent RBs that survive well into the larval period. In *Rana pipiens*, and *Ceratophrys ornata*, Kollros and Bovbjerg showed that the majority of RBs die prior to the larval period but a subset disappear after metamorphosis (Kollros and Bovbjerg, 1997). What causes differential PCD timing has not been demonstrated. Another explanation may be birth order and the function of early-born versus later-born primary neurons; the effects of the apoptotic machinery may be mediated through enzymes like protein kinases or their activators that are heterogeneously expressed in different RB populations.

Table 4 Intergroup Comparison of Touch Assay Responsiveness

Phenotype	Responsivity difference 38 hpf	Unpaired Student t test & 95% confidence interval (95% CI)	Responsivity difference 5dpf	Unpaired Student t test & 95% confidence interval (95% CI)
CFP vs YFP	No	P< 0.07, 95% CI: -1.8 to 0.9 Not quite statistically significant	Yes	P< 0.0001, 95% CI: 3.8 to 5.2 Extremely statistically significant
CFP vs None	No	P< 0.4, 95% CI: -0.9 to -2.2 Not statistically significant	No	P< 0.13, 95% CI: -0.1 to 0.8 Not statistically significant
CFP vs CFP/YFP	Yes	P< 0.003, 95% CI: -2.0 to -0.5 Very statistically significant	No	P< 0.05, 95% CI: -1.1 to 0.01 Not quite statistically significant
CFP vs WT no stimulation	N/A animal not assayed		Yes	P< 0.001, 95% CI: 7.5 to 8.3 Extremely statistically significant
CFP vs WT daily stimulation	Yes	P<0.0001, 95% CI: -4.4 to -1.9 Extremely statistically significant at 38 hpf	Yes	P< 0.0001, 95% CI: 2.8 to 5.1 Extremely statistically significant
CFP vs WT no daily stimulation	Yes	P<0.0081, 95% CI: -3.3 to -0.6 Very statistically significant at 38 hpf	Yes	P< 0.0001, 95% CI: 1.5 to 2.8 Extremely statistically significant
YFP vs None	Yes	P< 0.05, 95% CI: 0.04 to 3.1 Statistically significant	Yes	P< 0.0001, 95% CI: -4.9 to -3.3 Extremely statistically significant

Table 4 (continued)

Phenotype	Responsivity difference at 38 hpf	Unpaired Student t test & 95% confidence interval (95% CI)	Responsivity difference at 5dpf	Unpaired Student t test & 95% confidence interval (95% CI)
YFP vs CFP/YFP	Yes	P< 0.0001, 95% CI: -2.9 to -1.4 Extremely statistically significant	Yes	P< 0.0001, 95% CI: 3.0 to 4.8 Extremely statistically significant
YFP vs WT no stimulation	N/A animal not assayed		Yes	P< 0.0001, 95% CI: 2.7 to 4.2 Extremely statistically significant
YFP vs WT no daily stimulation	Yes	P< 0.05, 95% CI: -2.2 to -0.02 Statistically significant	Yes	P< 0.0001, 95% CI: -3.3 to -1.4 Extremely statistically significant
YFP vs WT daily stimulation	Yes	P< 0.0001, 95% CI: -3.2 to -1.4 Extremely statistically significant	Yes	P< 0.4, 95% CI: -1.8 to 0.8 Statistically significant
CFP/YFP vs None	No	P< 0.4, 95% CI: -1.9 to 0.7 Not statistically significant	No	P< 0.3, 95% CI: -0.7 to 0.2 Not statistically significant
CFP/YFP vs WT no stimulation	N/A animal not assayed		Yes	P< 0.0001, 95% CI: 6.7 to 8.0 Extremely statistically significant

Table 4 (continued)

Phenotype	Responsivity difference at 38 hpf	Unpaired Student t test & 95% confidence interval (95% CI)	Responsivity difference at 5dpf	Unpaired Student t test & 95% confidence interval (95% CI)
CFP/YFP vs WT daily stimulation	Yes	P < 0.001, 95% CI: -5.5 to -3.2 Extremely statistically significant	Yes	P< 0.0001, 95% CI: 2.2 to 4.7 Extremely statistically significant
CFP/YFP vs WT no daily stimulation	Yes	P< 0.0001, 95% CI: -4.5 to -2.0 Extremely statistically significant	Yes	P< 0.003, 95% CI: 0.6 to 2.4 Very statistically significant
None vs WT daily stimulation	Yes	P< 0.0001, 95% CI: -5.5 to -2.2 Extremely statistically significant	Yes	P< 0.0001, 95% CI: 2.4 to 4.9 Extremely statistically significant
None vs WT no stimulation	N/A animals not assayed		Yes	P< 0.0001, 95% CI: 7.0 to 8.2 Extremely statistically significant
None vs WT no daily stimulation	Yes	P< 0.005, 95% CI: -4.4 to -0.8 Very statistically significant	Yes	P< 0.0004, 95% CI: 0.9 to 2.6 Extremely statistically significant

In mammals and anamniotes, ngn2 is found in early-differentiating primary sensory neurons and ngn1 labels a later-differentiating population (Anderson, 1999). Zebrafish have one neurogenin gene that presumably executes the functions of both ngn1 and ngn2 and drives formation of RBs (Cornell and Eisen, 2002). Interestingly, the zebrafish TG is composed of two sets of ngn1-positive neurons that are born at different times, possess distinct ion channels, and perform different sensory functions (Caron et al., 2008). These findings lead one to speculate that ngn1 may also drive multiple waves of RB neuron specification, a difficult task in zebrafish considering the short time course over which two episodes of ngn1 expression would specify first RB and later DRG neurons in the lateral neural plate (Cornell and Eisen, 2002).

Given that RBs are all born by the end of gastrulation (Cornell and Eisen, 2000), our one-cell stage ngn1 morpholino injection, with its persistent effect for several days, would well cover the entire period of potential RB neurogenesis. Electroporating the morpholino into the neural plate throughout gastrulation would allow a more thorough dissection of the timing of ngn1 control over RB birth. This technique is coming into use in zebrafish more (Cerda, Thomas, Allende, Karlstrom and Palma, 2006) and has been shown to be effective in the neural plate. Perhaps early RBs persist as a permanent, adult derivative with multiple sensory modalities, while later-born cells perform a transient, embryonic function before dying via apoptosis, or vice versa. Such a system in the embryonic and larval spinal cord, which would overlap with the DRG, may underlie an expanded set of sensory functions that we have yet to determine. It will be interesting to

learn if RB birth order is significant and correlates with the timetable for death and persistence.

The finding that PKCα-expressing RBs are among other functional RBs suggests that insertion of the FT vector did not disrupt the mechanosensory capabilities of RBs expressing the fusion protein. At 34 hpf, when RBs bearing the fusion protein are present, the DRG lacks YFP expression, consistent with the observation that the DRG has not fully formed. FT embryos produced an escape response mediated only by RB neurons. At 49 hpf, when the DRG has begun to coalesce and contains one YFP-PKCα-positive DRG neuron, but does not have fully functional axonal arbors, the escape reflex was still functional in FT embryos.

The touch assay revealed a behavioral phenotype when I mutagenized PKCα by crossing ct 7a with a cerulean-Cre transgenic line, suggesting that this protein may be involved in RB responses to mechanical stimuli. This may be due to some downstream effect on signaling molecules or ion channels in RBs. Discovering the exact mechanism of action will parse out the role of PKCα in RB function.

The presence of PKCα may also contribute to negative feedback mechanisms that help the animal respond proportionally to stimuli and that reliably produce responses. An alternate explanation is that these effects are mediated somehow by the small amount of the truncated protein mosaically present throughout the animal, perhaps as a dominant negative mutant. The behaviors in the F_1 generation will have to be tested and correlated

to their expression patterns and genotype to get a full picture of how PKCα functions in zebrafish

Behavioral differences may indicate a variable reduction in PKCα in Cre-treated fish as a group, which should be tested in subsequent generations. Also, a morpholino against the fusion protein mRNA and the native sequence may elucidate the contribution of the FT itself to the behavioral differences and what may be purely due to reduction of PKCα.

Manipulation of sodium channels and alteration of touch stimuli appear to inhibit RB apoptosis, favoring a longer-living variant (Ribera and Nüsslein-Volhard, 1998). Sensory capabilities may be one functional distinction between RBs in the embryonic, larval, and adult stages, and characterizing their behavior in the immature and mature CNS will elucidate the fate of persistent RBs. Further molecular and physiological phenotyping are critical to understanding why some cells of this population are transient and others enduring, and how the developing embryo alters the lifespan of one subset of RBs over another.

It may be that at least three populations of zebrafish RBs may be present in the early embryo, namely: 1) RBs that die early, via a caspase-dependent mechanism; 2) RBs that die later, via a form of PCD that involves autophagy; and 3) RBs that do not die. The latter group may be inducible, deriving from groups 1 and 2 under certain conditions.

It is also plausible that voltage-gated sodium channel alterations are present in persistent cells in wild-type animals as well as in the cases of identified RB mutants that affect lifespan (Hirata, Nakano and Oda, 2009). This question requires further investigation to characterize potential electrophysiological heterogeneity among RBs correlated with molecular subtypes. Though the presence of RBs in newt and lamprey adults does not resolve this question, cross species comparisons of the genes that regulate RB survival would be instructive. Along with further characterization of the electrophysiological phenotype of persistent RBs in both mutant and wild-type strains, we may gain some understanding of the functional roles of RB subclasses, their connectivity, and lifespan.

Interestingly, at 36 hpf, neurons have begun to populate the DRG, and soon project peripheral processes whose arbors presumably will replace RB function in target tissues such as skin and myotomes (Cole and Ross, 2001; Sipple, 1998a; Wright and Ribera, 2010). From this evidence, it would appear that RB death is linked to DRG maturation, an example of phylogenetic apoptosis (Buss, Sun and Oppenheim, 2006). However, the early DNA fragmentation at 24 hpf in RBs and the existence of these cells in mutants lacking the normal complement of DRG along the body axis leads one to infer a cause other than competition with nascent DRG for peripheral targets or trophic factors (Cole and Ross, 2001; Reyes et al., 2004; Williams, 2000). The results presented here also suggest that DRG coalescence and axonogenesis are unrelated to RB lifespan.

RB neurons in the early embryo exert developmental control over the location of DRG neurons, as shown in a recent study in which non-cell-autonomous control of RB-derived

BDNF induced transdifferentiation and differential migration of DRG neurons (Wright and Ribera, 2010). Interestingly, when the TG is bilaterally killed via laser irradiation, RB axons innervate TG domains (Sagasti et al., 2005). The TG may exert similar control over RB neurons, possibly mediated by BDNF or other developmentally important factors. Even in the case of massive injury, why would an impermanent neuronal subtype affect or functionally replace a permanent one? Perhaps the transient cell population persists under certain conditions, harbors progenitor properties, or contains a subpopulation that is not transient.

Most reports regarding RB death rely on the terminal deoxynucleotidyl transferase-mediated dUTP nick end-labeling (TUNEL) assay to understand the temporally and spatially dynamic process of PCD, an essentially living, developmental program. TUNEL may miss cells that are not dying and those that have died between fixations (Furutani-Seiki, Jiang, Brand, Heisenberg, Houart, Beuchle, van Eeden, Granato, Haffter, Hammerschmidt, Kane, Kelsh, Mullins, Odenthal and Nusslein-Volhard, 1996). Moreover, using this assay, investigators cannot distinguish Type I from Type II cell death, i.e., apoptosis vs autophagy (Penaloza, Lin, Lockshin and Zakeri, 2006), both of which have been postulated to operate simultaneously among RBs (Lamborghini, 1987). This discrepancy invites an *in vivo* study of RB death along with reliable electron micrographic data of apoptotic RBs to shed more light on the cause and timing of the population's demise (Lamborghini, 1987; Reyes et al., 2004; Williams, 2000).

The trapped gene highlighted in the present work, PKCα, may support RB neuron survival. One mechanism for enhanced survival may be mediated through the affect of PKCα on other signaling molecules, including its activators Ca^{2+}, phosphatidyl serine (PS), and diacylglycerol (DAG), and other proteins known to be involved in RB lifespan (such as CDK5). Given the importance of sodium channels to RB longevity, a comparison of the involvement of sodium and calcium channels, intracellular Ca^{2+} concentrations, ionic flux, and tissue gradients in RB survival would also elucidate how different ions acting in the same organ and circuits affect neuronal function and maturation, and CNS development generally.

In the rat spinal cord, blocking PKCα with antisense oligonucleotides has been shown to have an ameliorating effect on morphine tolerance, prolonging effective analgesia for surgically treated animals compared to controls (Hua, Moore, Malkmus, Murray, Dean, Yaksh and Butler, 2002). These and other results suggest that the presence of PKCα in vertebrate sensory neurons plays an important role in nociception as well as mechanoreception. Understanding how PKCα-positive RB neurons, which may also be present in amniotes, including humans, develop may give us a greater understanding of how opiates affect the developing nervous system and fetal perceptions of pain.

In summary, YFP-PKCα positive neurons of ct 7a and ct 54a appear to be a subset of the larger population of both Islet-1 and ngn1 expressing RB cells and are present along with other persistent RBs, containing ngn1 post-7dpf. The YFP-PKCα-positive RBs are among those that function in the escape response at 36 and 48 hpf, before the DRG

reaches functional maturity. Further, the FT subset coexists with YFP-PKCα cells of the DRG as early as 2 - 3 dpf and as late as 30 dpf, providing further evidence that the appearance and maturation of this ganglion does not coincide with the complete disappearance of all RB neurons. The central dogma established after Rohon and Beard (Beard, 1889; Rohon, 1884) discovered these primary sensory cells may have reached its full maturity--and surpassed its utility. Studies regarding the function and characteristics of the persistent RB neuron will provide a new look at an old cell type.

ACKNOWLEDGEMENTS

I would like to thank: Drs. Scott Fraser and Marianne Bronner for training and financial support; Debbie Marshall for her hard work and diligence as a volunteer; Drs. Le Trinh, Sean Megason, and the CEGS screen team for technical support; Drs. Eduardo Rosa-Molinar, Alvaro Sagasti, Angeles Ribera, and David Koos for helpful zebrafish discussions; Dr. Thai Truong and the Fraser lab for imaging advice; Drs. Max Ezin, Rasheeda Hawk, and Aidyl Gonzalez-Serrichio for helpful discussions about this project. Funding was provided by the National Human Genome Research Institute (NHGRI) Center of Excellence in Genomic Science (CEGS) Grant: P50 HG004071, and the Achievement Rewards for College Scientists (ARCS) Foundation for fellowship support to ADD.

BIBLIOGRAPHY

Anderson, D. J. (1999). Lineages and transcription factors in the specification of vertebrate primary sensory neurons. *Current Opinion in Neurobiology* **9**, 517-524.
Beard, J. (1889). On the early development of Lepidosteus osseous. *Proceedings of the Royal Society of London* **46**, 1108-1118.
Blader, P., Plessy, C. and Stra¨hle, U. (2003). Multiple regulatory elements with spatially and temporally distinct activities control *neurogenin1* expression in primary neurons of the zebrafish embryo. *Mechanisms of Development* **120**, 211-218.
Buss, R. R., Sun, W. and Oppenheim, R. W. (2006). Adaptive Roles of Programmed Cell Death During Nervous System Development. *Annual Reviews of Neuroscience* **29**, 1-35.
Caron, S. J. C., Prober, D., Choy, M. and Schier, A. F. (2008). In vivo birthdating by BAPTISM reveals that trigeminal sensory neuron diversity depends on early neurogenesis. *Development* **135**, 3259-3269.
Cerda, G. A., Thomas, J. E., Allende, M. L., Karlstrom, R. O. and Palma, V. (2006). Electroporation of DNA, RNA, and morpholinos into zebrafish embryos. *Methods* **39**, 207-211.
Clarke, J. D. W., Hayes, B. P., Hunt, S. P. and Roberts, A. (1984). Sensory Physiology, Anatomy and Immunohistochemistry of Rohon-Beard Neurones in Embryos Of *Xenopus Laevis*. *Journal of Physiology* **348**, 511-525.
Cole, L. K. and Ross, L. S. (2001). Apoptosis in the Developing Zebrafish Embryo. *Developmental Biology* **240**, 123-142.
Cornell, R. A. and Eisen, J. S. (2000). Delta signaling mediates segregation of neural crest and spinal sensory neurons from zebrafish lateral neural plate. *Development* **127**, 2873-2882.
Cornell, R. A. and Eisen, J. S. (2002). Delta/Notch signaling promotes formation of zebrafish neural crest by repressing Neurogenin 1 function. *Development* **129**, 2639-2648.
Furutani-Seiki, M., Jiang, Y.-J., Brand, M., Heisenberg, C.-P., Houart, C., Beuchle, D., van Eeden, F. J. M., Granato, M., Haffter, P., Hammerschmidt, M. et al. (1996). Neural degeneration mutants in the zebrafish, *Danio rerio*. *Development* **123**, 229-239.
Griesbeck, O., Baird, G. S., Campbell, R. E., Zacharias, D. A. and Tsien, R. Y. (2001). Reducing the Environmental Sensitivity of Yellow Fluorescent Protein. *the Journal of Biological Chemistry* **276**.
Hirata, H., Nakano, Y. and Oda, Y. (2009). Phenotypic analysis of a new fish mutant harboring Rohon-Beard neuron defects. *Neuroscience Research* **65**, S135.
Hua, X. Y., Moore, A., Malkmus, S., Murray, S. F., Dean, N., Yaksh, T. L. and Butler, M. (2002). Inhibition of spinal protein kinase C alpha expression by an antisense oligonucleotide attenuates morphine infusion-induced tolerance. *Neuroscience* **113**, 99-107.
Humphrey, T. (1944). Primitive neurons in the embryonic human central nervous system. *Journal of Comparative Neurology* **81**, 1-45.
Humphrey, T. (1950). Intramedullary sensory ganglion cells in the roof plate area of the embryonic human spinal cord. *Journal of Comparative Neurology* **92**, 333-399.

Kimmel, C. B., Hatta, K. and Eisen, J. S. (1991). Genetic control of primary neuronal development in zebrafish. *Development* **Supplemental**, 46-57.
Kimmel, C. B. and Westerfield, M. (1990). Primary neurons of the zebrafish. In *Signals and Sense*, (ed. G. M. Edelman W. E. Gall and M. W. Cowan), pp. 561-588. New York: Wiley-Liss.
Kollros, J. J. and Bovbjerg, A. M. (1997). Growth and Death of Rohon-Beard Cells in *Rana pipiens* and *Ceratophrys ornata*. *Journal of Morphology* **232**, 67-78.
Kuwada, J. Y., Bernhardt, R. R. and Nguyen, N. (1990). Development of Spinal Neurons and Tracts in The Zebrafish Embryo. *The Journal of Comparative Neurology* **302**, 617-628.
Lamborghini, J. E. (1987). Disappearance of Rohon-Beard Neurons From the Spinal Cord of Larval *Xenopus laevis*. *The Journal of Comparative Neurology* **264**, 47-55.
Megason, S. G. (2009). In toto imaging of embryogenesis with confocal time-lapse microscopy. *Methods in Molecular Biology* **546**, 317-332.
Nakano, Y., Fujita, M., Ogino, K., Saint-Amant, L., Kinoshita, T., Oda, Y. and Hirata, H. (2010). Biogensis of GPI-anchored proteins is essential for surface expression of sodium channels in zebrafish Rohon-Beard neurons to respond to mechanosensory stimulation. *Development* **137**, 1689-1698.
Nakao, T. and Ishizawa, A. (1987). Development of the spinal nerves in the lamprey: I. Rohon-Beard cells and interneurons. *Journal of Comparative Neurology* **256**, 342-355.
Ohno, S.-g. and Nishizuka, Y. (2002). Protein Kinase C Isotypes and Their Specific Functions: Prologue. *Journal of Biochemistry* **132**, 509-511.
Parichy, D. M., Elizondo, M. R., Mills, M. G., Gordon, T. N. and Engeszer, R. E. (2009). Normal Table of Postembryonic Zebrafish Development: Staging by Externally Visible Anatomy of the Living Fish. *Developmental Dynamics* **238**, 2975-3015.
Penaloza, C., Lin, L., Lockshin, R. A. and Zakeri, Z. (2006). Cell death in development: shaping the embryo. *Histochemical Cell Biology* **126**, 149-158.
Reyes, R., Haendel, M., Grant, D., Melancon, E. and Eisen, J. S. (2004). Slow Degeneration of Zebrafish Rohon-Beard Neurons During Programmed Cell Death. *Developmental Dynamics* **229**, 30-41.
Ribera, A. B. and Nüsslein-Volhard, C. (1998). Zebrafish Touch-Insensitive Mutants Reveal an Essential Role for the Developmental Regulation of Sodium Current. *The Journal of Neuroscience* **18**, 9181-9191.
Rohon, J. V. (1884). Histogenese des Ruckenmarkes der Forelle. *Akad Wiss Math* **14**.
Sagasti, A., Guido, M. R., Raible, D. W. and Schier, A. F. (2005). Repulsive Interactions Shape the Morphologies and Functional Arrangements of Zebrafish Peripheral Sensory Arbors. *Current Biology* **15**, 804-814.
Sipple, B. A. (1998). The Rohon-Beard Cell: The Formation, Function, and Fate of a Primary Sensory System in the Embryonic Zebrafish, *Danio rerio*, vol. PhD (ed., pp. 47: Temple University.
Slatter, C. A. B., Kanji, H., Coutts, C. A. and Ali, D. W. (2004). Expession of PKC in the Developing Zebrafish, *Danio rerio*. *Journal of Neurobiology* **62**, 425-438.
Trinh, L. A., Hochgreb, T., Graham, M., Wu, D., Ruf, F., Jayasena, C., Saxena, A., Hawk, R., Gonzalez-Serricchio, A., Dixson, A. et al. (2011). A versatile gene trap to visualize and interrogate the function of the vertebrate proteome., (ed., pp. 53. Pasadena: California Institute of Technology.

Westerfield, M. (1993). The Zebrafish Book. Eugene: University of Oregon Press.
Williams, J. A., Barrios, A. Gatchalian, C., Rubin, L., Wilson, S.W., Holder, N. (2000). Programmed cell death in zebrafish Rohon Beard neurons is influenced by TrkC1/NT-3 signaling. *Developmental Biology* **226**, 220-230.
Wright, M. A. and Ribera, A. B. (2010). Brain-Derived Neurotrophic Factor Mediates Non-Cell-Autonomous Regulation of Sensory Neuron Position and Identity. *The Journal of Neuroscience* **30**, 14513-14521.
Youngstrom, K. A. (1944). Intramedullary sensory type ganglion cells in the spinal cord of human embryos. *Journal of Comparative Neurology* **81**, 47-53.

CHAPTER IV

Sensing Magnetic Fields from Cradle to Grave? Biogenic Magnetite in Zebrafish Across The Lifespan

AUTHORS

Alana D. Dixson, Timothy D. Raub, Joseph L. Kirschvink

ABSTRACT

Biogenic magnetite has been detected in a broad range of organisms, including magnetotactic bacteria, migratory fish and birds, invertebrates, and humans and has been shown to mediate magnetosensation in many species through the effects of pulse-remagnetization on behavior. The mechanisms of magnetite biomineralization are well characterized in several species of bacteria; however, the story in higher organisms is far from complete. Previous studies have shown deposits of magnetite in projections of the trigeminal nerve alongside behavioral evidence suggesting that both optical pumping and magnetite-based mechanisms may operate simultaneously. Subsequent efforts to identify the anatomical seat of magnetoreceptors have focused on the same locations in new organisms, excluding other areas. We report the unexpected presence of biogenic magnetite in the lateral line region of the genetically and physiologically tractable vertebrate model organism, *Danio rerio*. Zebrafish, as they are commonly known, possess a magnetic sense and lend themselves to further imaging and behavioral studies which may uncover one type of vertebrate magnetoreceptor and supporting nervous tissue.

INTRODUCTION

A magnetic sense has been reported in organisms as diverse as honeybees, elasmobranchs, and birds (Kirschvink, Jones and MacFadden, 1985). Three main hypotheses (Johnsen and Lohmann, 2005; Walker, Diebel and Kirschvink, 2003; Wiltschko and Wiltschko, 2005) propose radically different mechanisms for deriving an internal neurophysiologic response to external magnetic fields: 1) electrical induction

mediated via electro-receptors (Kalmijn, 1978); 2) magnetite-based magnetoreceptors (Kirschvink and Gould, 1981); and 3) chemical magnetoreception transmitted via pigments in cells of the visual system (Ritz, Adem and Schulten, 2000). Here we will not review the first mechanism in zebrafish, which are a fresh-water species that neither possess the structures, nor live in the marine environment required for electrical induction. Birds, however, and possibly other vertebrates, may use both magnetite-based magnetoreceptors and chemical or optical pumping mechanisms (Wiltschko and Wiltschko, 2005); these two hypotheses are discussed below in the context of our present study.

Magnetite is an inverse spinel with an end-member composition of Fe_3O_4, which is spontaneously ferromagnetic at room temperature. It is the only known ferromagnetic material to be formed under biochemical control in eukaryotes, and has a wide phyletic distribution (Gould, 1979; Kirschvink and Gould, 1981; Kirschvink et al., 1985; Lowenstam, 1962; Walcott, Gould and Kirschvink, 1979; Walker et al., 2003). Biogenic magnetite crystals are readily identified in the fossil record and in living magnetotactic bacteria by their narrow particle size distribution (generally ranging between 30-120 nm), single-domain magnetic stability, chemical purity, particle elongation, and arrangement in chains (Kopp, Weiss, Maloof, Vali, Nash and Kirschvink, 2006; Walker, Kirschvink, Perry and Dizon, 1985b). As these physical characteristics in magnetite are precisely those known to yield magnetic single domains, they have long been thought to reflect natural selection for maximizing cellular magnetic moments (Kirschvink and Lowenstam, 1979). As a variety of rock-magnetic techniques have been developed to identify single-

domain particles, these can be applied to characterize trace levels of biogenic magnetite in tissues.

Magnetoreception and magnetite biomineralization are commonly, though somewhat controversially linked (Kirschvink et al., 1985). Theoretical models predict that mechanical torque on magnetite crystals arranged in chains or clumps transduces magnetic stimuli to as yet unidentified magnetoreceptors coupled to neural cells (Kirschvink, Kuwajima, Ueno, Kirschvink, Diaz-Ricci, Morales, Barwig and Quinn, 1992b; Winklhofer and Kirschvink, 2010). Several authors have suggested that other minerals, such as maghemite and magnetite of different domain states, are necessary for adequate magnetoreception (Solov'yov and Greiner, 2007), but these are actually based on initial studies that have proven to be histological artifacts, as well as the mis-identification of the minerals involved by the use of demonstrably incorrect techniques (Winklhofer and Kirschvink, 2010).

Several non-conservative methods have been developed to extract magnetite from solid blocks of tissue but yield identifiable grains (Kirschvink et al., 1985; Kirschvink, Kobayashi-Kirschvink and Woodford, 1992a; Kirschvink et al., 1992b), and combined with high-resolution transmission electron microscopy (TEM) identify the structural diversity of individual crystals (Walker et al., 1985b). Paleomagnetic experimental techniques have generated *in situ* assays for the presence of biogenic magnetite such as the Moskowitz test, which exploits special cryogenic magnetic properties of single-domain, stoichiometric magnetite crystals with shape anisotropy or arranged in chains

(Moskowitz, Frankel and Bazylinski, 1993); and room-temperature remanence magnetometry using ultra-sensitive magnetometers which detect magnetite crystals at part-per-trillion sensitivity (at lower concentrations than magnetometers employed by the Moskowitz test) (Walker et al., 1985b). Ferromagnetic resonance (FMR) spectroscopy distinguishes crystal arrangements in chains versus clumps, identifies single-domain (SD) versus multi-domain (MD) magnetic states (Kopp et al., 2006; Weiss, Kim, Kirschvink, Koppe, Sankaran, Kobayashi and Komeili, 2004), and is insensitive to slight sample oxidation, which in practice tends to limit application of the Moskowitz test (Kopp, Raub, Schumann, Vali, Smirnov and Kirschvink, 2007; Lippert and Zachos, 2007). Taken as a whole, this suite of laboratory methods is foundational in demonstrating the presence of biogenic magnetite.

In the "optical pumping" or "radical-pair" mechanism a photon of light is hypothesized to induce radical pairs in visual pigments. Weak magnetic fields promote the conversion of singlet spin pairs to triplets (Ritz et al., 2000), lengthening their duration and allowing alternative biochemical reactions to occur. For this mechanism to operate, animals must have access to photons of light (Ritz et al., 2000; Ritz, Ahmad, Mouritsen, Wiltschko and Wiltschko, 2010), sufficient quantities of visual pigments in appropriate neuroanatomical structures (Wiltschko and Wiltschko, 2005), and no magnetic oscillations that interfere with the singlet-to-triplet interconversion (Ritz et al., 2010; Wiltschko and Wiltschko, 2005). The pineal gland in some amphibians and the eye in most other organisms provide the necessary light aperture, while other locations would have to combine suitable chemicals with access to light or equivalent energy (Wiltschko and Wiltschko,

2005). However, all of the behavioral evidence could be explained reasonably by the modulation of a magnetite-based receptor system by visual cues (Winklhofer and Kirschvink, 2010). Kirschvink and Winklhofer (2010) also noted that none of these experiments were run using fully double-blind protocols, despite simple and inexpensive methods to do so. As the Rf field levels interpreted to influence the behavioral assays are many orders of magnitude below any that have ever been implicated as ever having had a biological effect –of any sort– it stands out as an extraordinary claim that requires at least a minimum of robust, double-blind control.

Magnetite therefore, remains the simplest and most elegant candidate for transmitting magnetic field stimuli to the nervous system due to its presence in known magnetotactic bacteria and its demonstrated role in both "compass" and "map" senses of many higher organisms (Johnsen and Lohmann, 2005; Wiltschko and Wiltschko, 2005). The compass sense relies on the direction of magnetic field lines, allowing animals to recognize north-south as a fiduciary axis for migrations or other purposes (Johnsen and Lohmann, 2005; Lohmann, Lohmann and Putnam, 2007; Wiltschko and Wiltschko, 1995). The map sense employs several geomagnetic field parameters, especially inclination, intensity, and possibly gradients thereof (for instance local magnetic anomalies), to navigate immediate topography (Johnsen and Lohmann, 2005; Lohmann and Johnsen, 2000; Walker, Kirschvink and Dizon, 1985a; Wiltschko and Wiltschko, 2005).

Use of the term "map" has been the subject of some debate (Bennett, 1996; Lohmann et al., 2007), because it may invoke misleading comparisons with human maps. How

animals perceive the positional information they derive from the Earth's geomagnetic field may markedly differ from our concept of a map, but function in a similar way (Lohmann et al., 2007). This finer-scale ability combined with compass orientation could explain how animals consistently navigate to the same geographical locations, migrating over long and short distances where visual and other sensory cues might change seasonally.

Single-domain magnetite has the energetic stability and crystalline structure to function in both map and compass senses (Kirschvink and Walker, 1985), and some very simple models show that it could also function as an inclination-only receptor (Winklhofer and Kirschvink, 2010).

Criticism of the single-domain magnetite model for magnetic sensation has come from theoretical evaluations of the ability of various mechanisms to respond to oscillating magnetic fields on the order of 50/60 Hz (Vanderstraeten and Gillis, 2010). As it is well known that the motion of magnetite-based structures are damped viscously in cytoplasm at frequencies above 10 Hz (Kirschvink et al., 1992b; Kirschvink, Padmanabha, Boyce and Oglesby, 1997) and oscillating magnetic fields in the 50/60 Hz band are not present in the natural environment, there is no reason to suspect that sensory systems in animals would have been driven to detect them (Kirschvink et al., 1997).

Our goal was to test for ferromagnetic materials like magnetite in zebrafish, *Danio rerio,* which could function in the magnetic sense demonstrated phenomenologically by

Scherbakov et al. (Shcherbakov et al., 2005). If such material were present, we wanted to determine its anatomical location, find out if it was single-domain magnetite, and to understand its crystal arrangement. Here we provide evidence for the presence of biogenic magnetite throughout the life cycle of zebrafish, similar to stores in other aquatic vertebrates. We also show that zebrafish possess sufficient magnetite quantities to function in magnetoreception, likely in lateral line organs, outside of and in addition to the more expected trigeminal-innervated locations. The degree to which our findings apply to other non-migratory teleosts and terrestrial animals remains a question; nevertheless, we demonstrate that zebrafish possess magnetite suitable for use in magnetoreception.

METHODS

Rock Magnetometry

Sample Preparation

Adult zebrafish from the Center of Excellence in Genomic Science (CEGS) zebrafish facility were unfed for 3 days before capture and sacrifice according to Institutional Animal Care and Use Committee (IACUC) approved procedures. Animals were then washed in ultrapure, reverse-osmosis filtered water, and immediately stored on ice or in a -20°C freezer until starting rock magnetism experiments.

Larval zebrafish who had not begun feeding were prepared as above, transferred whole with an acid-washed pipette to an acid-washed NMR tube and stored in a solution of 100% methanol at -20°C until magnetometry measurements were taken.

Powdered adult fish samples were prepared by the same procedures outlined above and subsequently cut into head, trunk, and tail sections with an acid-washed Kyocera™ ceramic knife. The sections were placed in acid-washed glassware with tin foil covering the top opening and stored at -80°C for 1-2 hours prior to placing in a Virtis™ freeze dryer housed in the Sessions Lab at Caltech. Samples were freeze dried for 24-48 hours until all tissues appeared to be completely desiccated (courtesy of Alex Sessions at in the Division of Geological and Planetary Sciences at the California Institute of Technology) and then pulverized using an acid-washed glass mortar and pestle until a fine powder of small grain size was produced. The powder was transferred to an acid-washed NMR tube with a sheet of paper. The capped tubes were then placed in a -20°C freezer until magnetometry experiments were begun.

Clean Lab Techniques

Samples for SQUID magnetometry were prepared on a HEPA-filtered clean bench using acid-washed, non-magnetic tools and ultra-pure water, following techniques developed extensively for this purpose (Kirschvink et al., 1992a; Walker et al., 1985b). The suite of rock magnetic analyses was done on frozen tissue samples suspended on acid-washed quartz-glass fibers (flame-pulled from standard 3 mm NMR tubes). A stream of clean, dry N2 gas was fed into the base of the superconducting rock magnetometer, after being chilled by passing through a coiled copper tube bathed in liquid nitrogen, then passed through a 0.2 μm particulate filter. Samples were allowed to equilibrate to sub-zero temperatures before measurement to inhibit mechanical rotation of the ferromagnetic particles. Rock-magnetic experiments generally followed the methods outlined in

Kirschvink et al., (Kirschvink, Kopp, Raub, Baumgartner and Holt, 2008), including the progressive acquisition of anhysteretic remanent magnetization (ARM) in a 100 mT peak, 830 Hz, alternating-field (Af) with a 0-1 mT DC bias, the Af demagnetization of this peak ARM, the acquisition of isothermal remanent magnetization (IRM) up to peak fields of 1000 mT, the progressive Af demagnetization of this IRM, and the back-field demagnetization of the peak IRM.

Controls

A blank NMR tube was used as the negative control. The measurements were compared to standard chiton tooth positive control moments, which are derived from well-characterized biogenic magnetite.

FMR Spectroscopy

Sample Preparation

Powdered adult fish samples described above were subjected to FMR spectroscopic analysis prior to SQUID-based rock magnetometry experiments to allow the samples to have a uniform magnetization. NMR tubes containing powdered fish were wiped clean with 100% ethanol and tube caps were wrapped in clean paraffin film prior to analysis. We used a Bruker™ ESP 300 E EPR Spectrometer at Caltech to measure magnetic anisotropy in samples at a 9.3 GHz (X-band) frequency; samples were assayed at room temperature, at 20 K with the sample chamber under a constant flow of liquid-helium-chilled gaseous helium, and at 77 K after freezing in liquid nitrogen. Due to instability of the signal from the 77 K samples, only the room temperature and 20K data are reported.

Controls

For positive controls we filled acid-washed NMR tubes with less than 1 mm height of synthetic magnetite and stored these at -20°C until FMR assays were performed. Negative controls consisted of a blank, acid-washed NMR tube that was sealed and stored as previously described.

SQuID Microscopy

Sample Preparation

Zebrafish adults were prepared as above for magnetometry experiments, but following sacrifice an acid-washed wooden tooth pick was placed through the mouth and gill arch of each animal (n = 8) to keep the mouth open, samples were placed in clean Mylar film and stored in a - 20°C freezer. On the day of SQuID imaging two fresh adult fish were sacrificed and both these and n = 2 of the above frozen samples were sectioned using a Kyocera, acid-washed ceramic knife as follows: Section 1 animals were bisected through the mouth and abdomen and hemisectioned to retain the neural arches and spinal cord in one side. Additionally, in n = 1 fresh animal Section 2 was prepared from a whole block of tissues taken from between the gill arch to the anal opening in the anterior to posterior axis and from 1 mm below the neural arches to the middle of the abdomen in the dorsal to ventral direction. The latter section included all of the lateral musculature and overlying skin, but excluded all internal organs, which were removed with non-magnetic forceps.

Image Acquisition

Biological samples for magnetic (SQUID) microscopy were mounted between two sheets of clean-lab grade, 15-μm-thick Mylar film that is known from previous experiments to be essentially free of ferromagnetic contaminants. They were then exposed briefly to the strong (> 200 mT) static magnetic field of an NdFeB magnet to give them an isothermal remanent magnetization (IRM) capable of saturating all known biogenic magnetites. These were then mounted snugly on the compression stage of the ultra-high resolution scanning SQuID microscope so that the upper surface of the Mylar film would contact smoothly with the overlying sapphire window, bringing the magnetized tissue materials in close proximity (~ 200 μm) to the superconducting sensor. Small fragments of broken chiton teeth were located within the scan area, but away from the sample, to aid in the co-localization of the magnetic and optical images. Each sample was then rastered back and forth in a grid (of variable step size), while the vertical component of the magnetic field at each point was stored in a digital array (voltage readings converted to units of nanotesla, nT), along the lines used by Fong et al. (Fong, Holzer, McBride, Lima and Baudenbacher, 2005). Due to the thickness of the sample, and unknown depth from the surface to the magnetic sources, these data are most useful in estimating the number of discrete dipole sources, rather than for quantitative estimates of the dipole moments per cell.

RESULTS

Zebrafish Contain Ferromagnetic Materials of Probable Biological Origin

The magnetic properties of trace levels of magnetite can be revealed using several rock magnetometric techniques; among the most useful of these are acquisition of isothermal remanent magnetization (IRM) and anhysteretic remanent magnetization (ARM). When a sample is magnetized and demagnetized in alternating (Af) or pulsed magnetic fields, the gain and loss of magnetization yields a spectrum of particle coercivities that constrains the mineralogy, composition, particle size, and microscopic arrangement of the individual magnetic particles. An ARM is created when a direct current (DC) biasing field is applied along with a large alternating demagnetizing field to a magnetic sample, and is highly sensitive to interparticle interactions (Cisowski, 1981).

We adapted a standard rock magnetometry protocol in a DC-semiconducting quantum interference device (SQUID) magnetometer to impart IRM to whole frozen or room-temperature adult zebrafish. We discovered considerable ferromagnetic materials that gave stronger IRM closer to the head than the tail. Compared to the negative control blank EPR tube, adult zebrafish acquired a strong IRM both when fish were initially at room temperature or frozen.

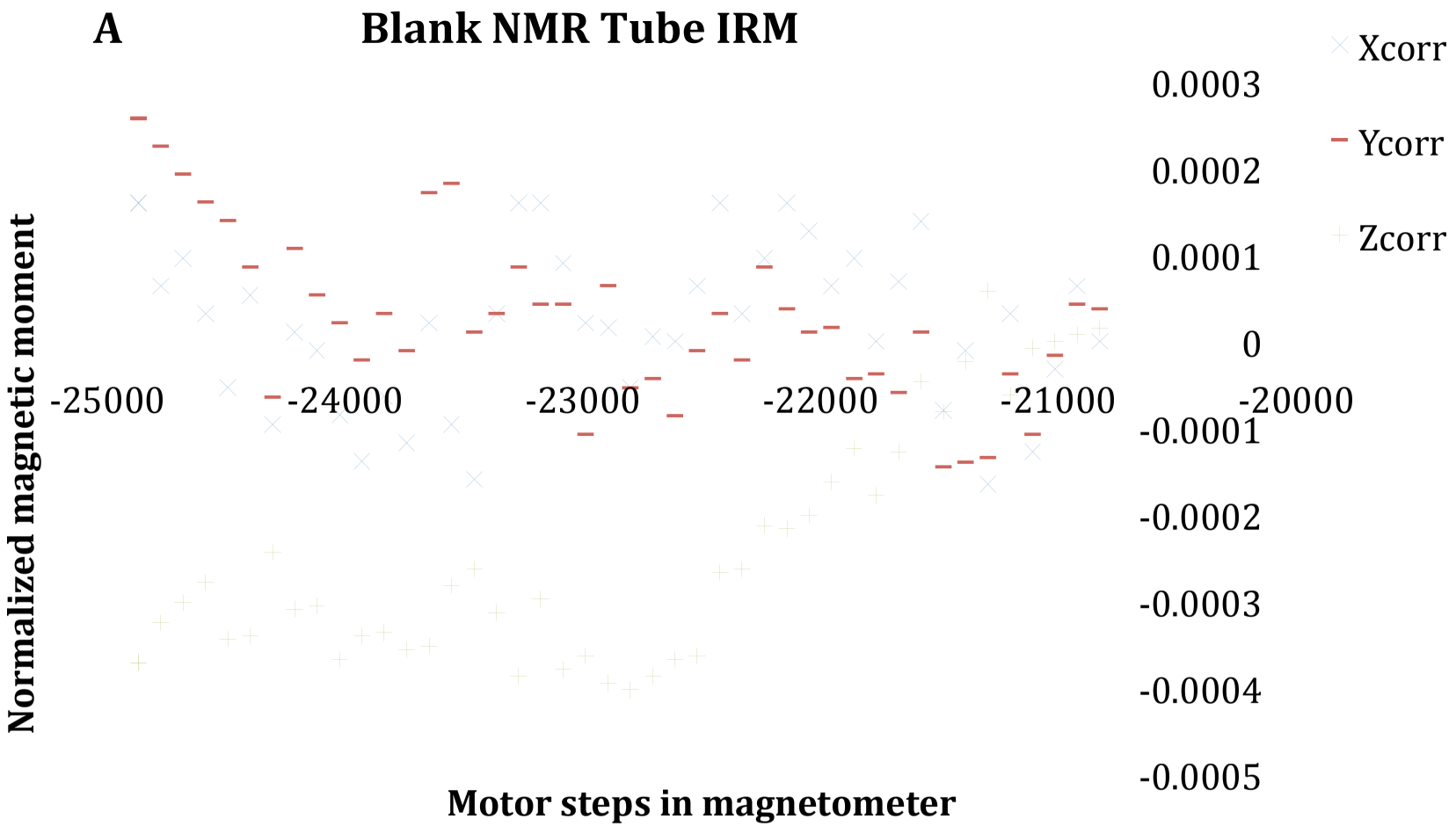
A
Blank NMR Tube IRM
Xcorr
Ycorr
Zcorr
0.0003
0.0002
0.0001
0
-0.0001
-0.0002
-0.0003
-0.0004
-0.0005
-25000
-24000
-23000
-22000
-21000
-20000
Normalized magnetic moment
Motor steps in magnetometer

B Wild-Type Adult Female RT IRM

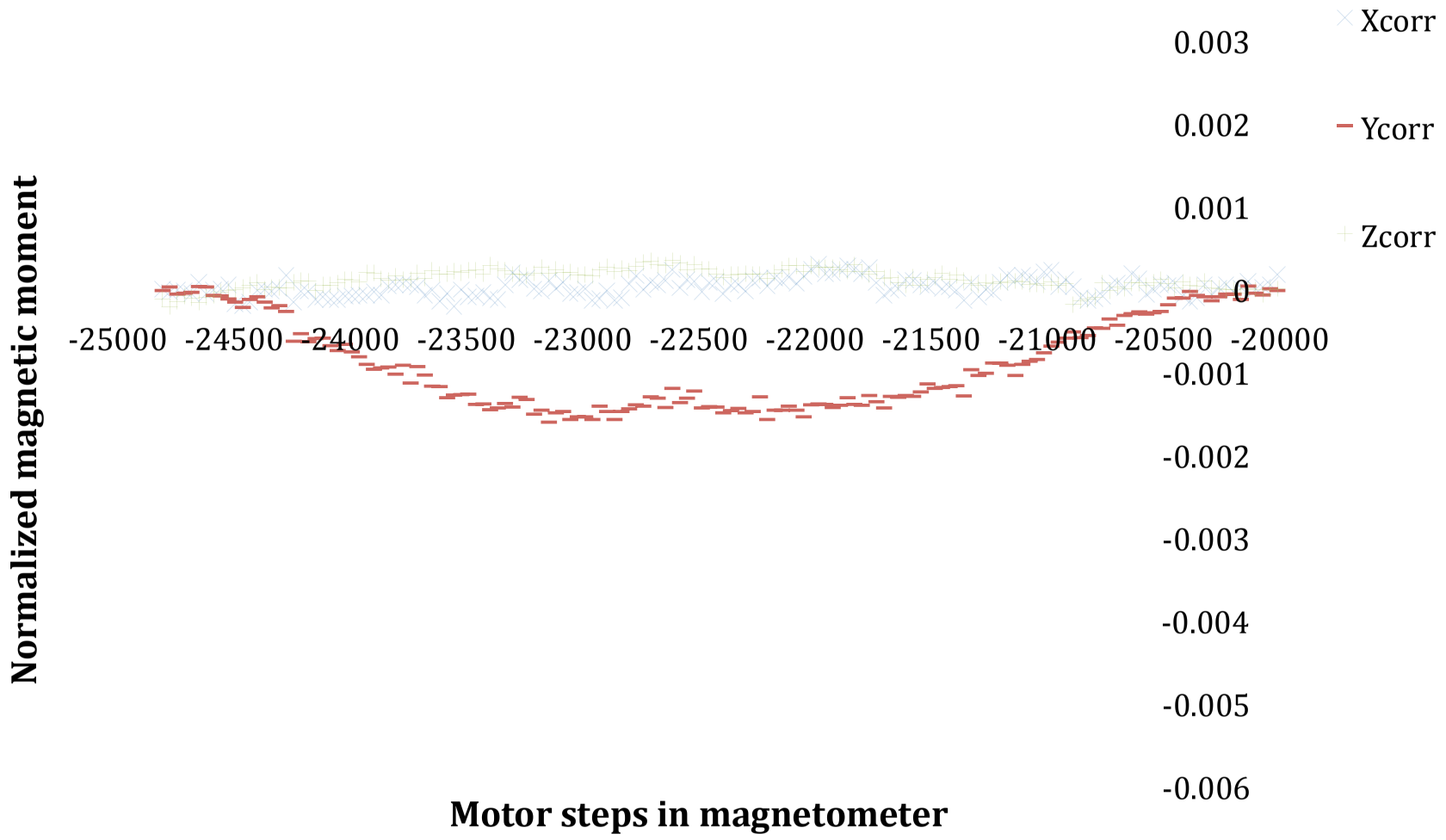

C **Wild-Type Adult Female Frozen IRM**

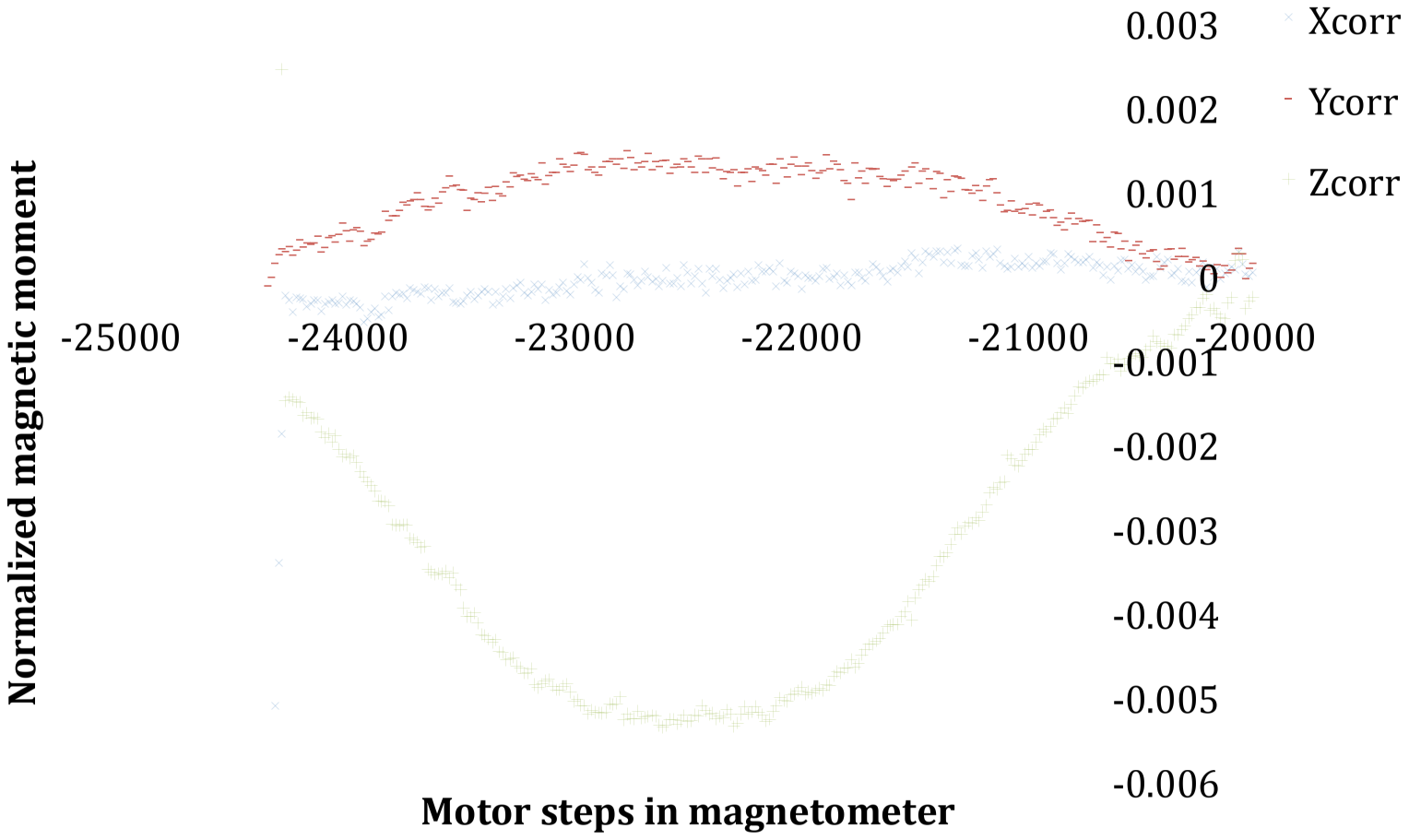

Figure 1. Full-Body Zebrafish Scan(s) and Whole-Zebrafish Rockmag

A) Blank NMR tube negative control. B) Room-temperature adult zebrafish sample. C) - 20°C frozen adult zebrafish sample. Am^2

Adult fish show changes in IRM that are characteristic for the presence of ferromagnetic iron oxides like magnetite. The normalized fish moments are not disordered as in the blank EPR tube. Also note that the z values are much more displaced in the frozen animal compared to the room-temperature fish. Freezing helps maintain the magnetite in a fixed position and prevents changes in orientation that would limit the crystal's ability to respond to the induced magnetic field. The room-temperature sample is much more subject to thermal agitation and produces correspondingly less IRM signal.

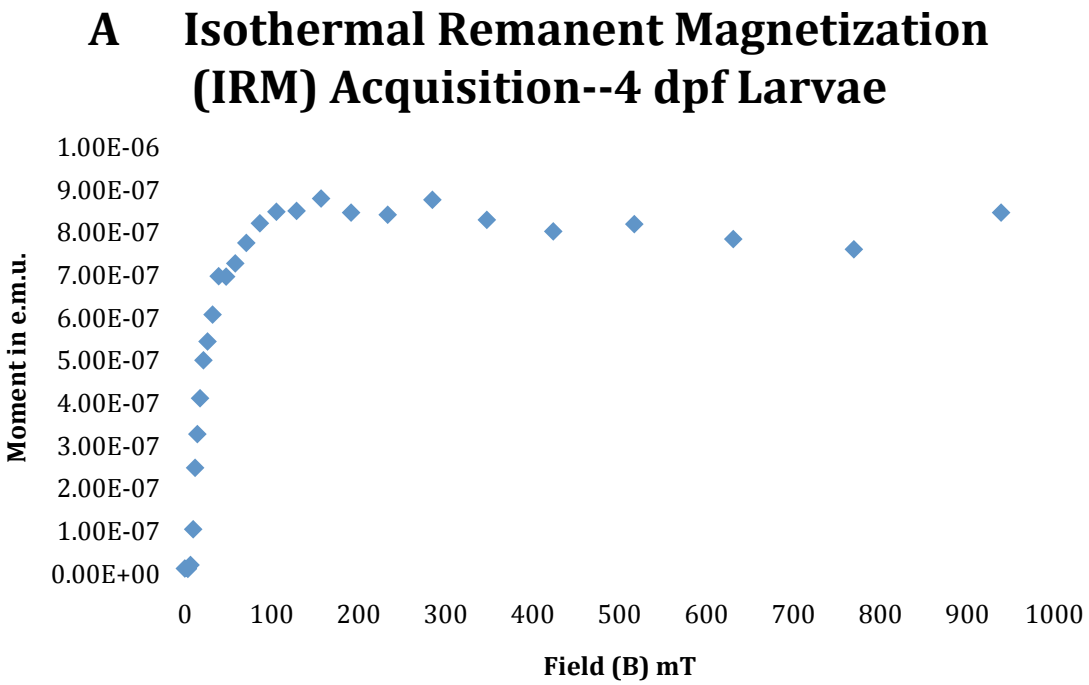

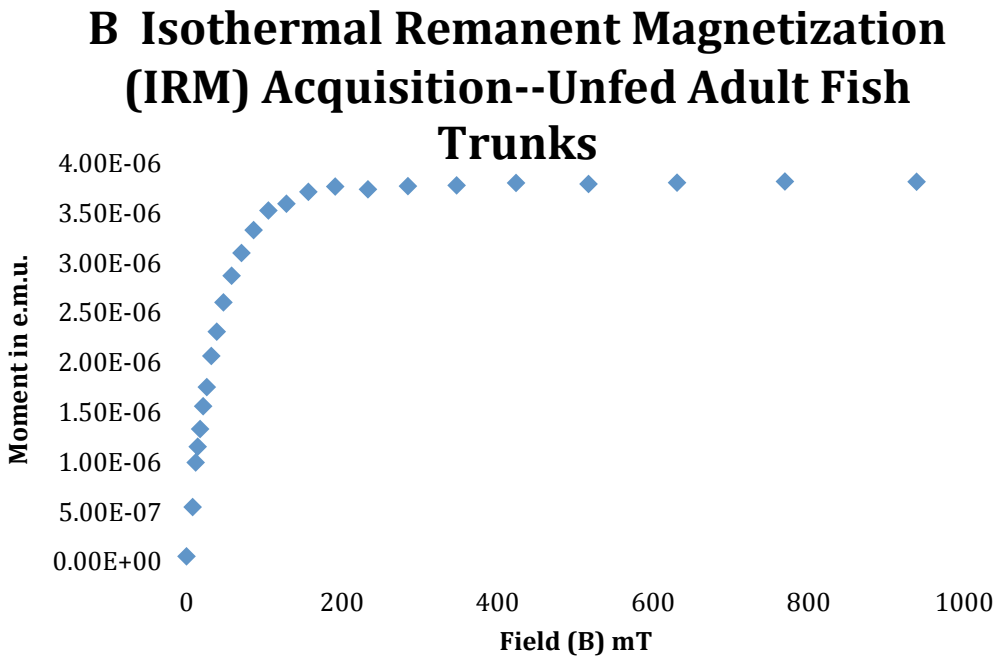

Figure 2. Larval and Adult Zebrafish Scan

Rock magnetometry on whole (larval) or freeze-dried samples revealed a measurable magnetic moments and curves characteristic of ferromagnetic material. A) Larval

zebrafish rock magnetometer scan. B) Adult zebrafish.

IRM acquisitions by both adult and larval zebrafish were characteristic of magnetite. We found IRM saturation = 8.28 x 10^{-7} emu for 4 dpf larvae (stdev = 3.54 x 10^{-08}, error 0.043), or ~ 9.20 x 10^{-10} emu/g magnetite/fish. If we assume 1.79 x 10^{-10} cc magnetite/fish of single-domain, 80-nm-sized cubes each at 5.12 x 10^{-16} cc, and 90 emu/g saturation magnetization for magnetite with a density of 5.15 g/cc of the crystal, we would have approximately n = 348,767 crystals of 80 nm magnetite per fish, or n = 178,569 crystals of 100 nm per fish. If larval fish have 5000 crystals per 2 μm cell, larvae at 4 dpf would have roughly 36–70 magnetocytes in total.

Section of adult fish body N = 8	Grams magnetite	80 nm magnetite crystals/fish	100 nm magnetite crystals/fish	IRMsat	Min # ~2 μm xal-aggregate magnetocytes	# Trout-equivalent magnetocytes by e.m.u./observed
Head	4.15 E-10	157,268	80,521	3.73 E-07 Stdev: 2.03 E-08	20 – 100,000	~73,000 - 140,000
Trunk	5.17 E-09	1,961,643	1,004,361	3.72 E-06 Stdev: 9.21 E-08	250 – 1,250,000	~800,000 – 1,300,000
Tail	5.61 E-10	212,686	108,895	4.09 E-07 Stdev: 2.14 E-08	28 – 140,000	~85,000 – 150,000

Figure 3. Rockmag of Heads versus Trunks versus Tails. Adult Zebrafish Magnetite is Concentrated in The Trunk

Varying crystal aggregate shape, un-close packing, and smaller crystal size all can increase the number of idealized magnetocytes by up to ~ 5,000x from the "min" theoretical estimate. Zebrafish and trout magnetocytes are easiest reconciled by approximately spherical aggregates of 20% close-packed or else prismatic aggregates of

~ 10% close-packed SD magnetite. Moments are in electromagnetic units (emu; 1 emu = 10^{-3} Am^2)

Zebrafish Contain Biogenic, Single-Domain Magnetite Arranged in Clumps: FMR Spectroscopy Detects Biogenic Magnetite

Electron paramagnetic resonance (EPR) spectroscopy, also called ferromagnetic resonance (FMR), is a useful screening tool for identifying magneto-fossils containing biogenic magnetite (Kopp et al., 2006). It has also been used to investigate the ferromagnetic content of biological samples with minimal extracellular structure, such as magnetotactic bacteria; here, we applied FMR to tissues of the more complex zebrafish.

The basis of FMR is the Zeeman effect in which electrons whose magnetic moments are aligned with an externally generated magnetic field have a lower energy than electrons with spins aligned against the field. This splitting causes a characteristic signature spectrum for each molecule at different microwave frequencies and detects the magnetic anisotropy of ferromagnetic compounds (Weiss et al., 2004). Previous work in our lab used FMR to distinguish magnetite crystal morphology and chain structure in whole and lysed magnetotactic bacteria (Kopp et al., 2006) and to establish criteria to identify biogenic magnetite through FMR. The values of g_{eff}, A, ΔB_{FWHM} (mT), and α can be used to distinguish some biologically precipitated ferromagnetic minerals from inorganically crystallized materials. We captured spectra of the ferromagnetic content of the freeze-dried powders of food-restricted adult zebrafish.

Section of adult fish body N = 8	g_{eff}	A	ΔB_{FWHM} (mT)	α
Head	2.0849	0.72178	384.7507	0.49976
Trunk	2.1064	0.60248	151.3197	0.25072
Tail	2.0772	0.60573	262.7566	0.36048

Biogenic magnetite	g_{eff}	A	ΔB_{FWHM} (mT)	α
Fe_3O_4	< 2.12	< 1.0	< 250	0.25

Table 1. FMR Heads versus Trunks versus Tails Unfed Adult Fish

FMR spectra confirmed relatively narrow size distributions of anisotropic particles, similar to spectra produced by biogenic magnetofossils. The material appeared to be concentrated more in the trunk than in the head, consistent with the direct measurements with the SQUID magnetometry.

In control experiments we scanned blank EPR tubes, which carry almost non-existent magnetic content and produce background resonances far below that of assayable ferromagnetic compounds. Fish food was individually prepared by type of feeding the fish received, i.e., bloodworms, fish flakes, and brine shrimp embryos or pre-hatching cysts. These controls gave potential ferromagnetic contamination spectral signatures from predigested food remaining in the alimentary canal or attached to fish tissues.

Assays on fully fed animals characterized the ferromagnetic content of digested food sources versus biogenic magnetite, which we assumed would produce spectra similar to bacterially produced magnetite.

Magnetite in Zebrafish is Single-Domain and Highly Interacting

Lowrie and Fuller compared thermoremanent magnetization (TRM) to IRM in naturally occurring magnetite samples ranging from high to low purity (Johnson, Lowrie and Kent, 1975; Lowrie and Fuller, 1971) which also carried multi- and single-domain states. They drew upon the key distinction that in single- compared to multi-domain grains at lower induced fields the TRM is more stable than IRM to alternating field (Af) demagnetization, in which saturation remanence is removed in an AC field. This test became a classic means to assay the domain status of magnetic grains. Anhysteretic remanent magnetization (ARM) can accurately assess grain size and domain status, replacing TRM if heating will destroy the sample (Johnson et al., 1975; King, Banerjee, Marvin and Ozdemir, 1982; Lowrie and Fuller, 1971). We used this method in zebrafish because our group had previously used it in magnetic tests on sockeye salmon tissue (Walker, Quinn, Kirschvink and Groot, 1988).

When assaying for biogenic magnetite, the hardness of the ARM compared to IRM in Lowrie-Fuller curves points to the presence of single-domain magnetite. In fish with empty alimentary canals, the magnetic material, which we presume to be magnetite, has a lower IRM than ARM. Compared to the strong interparticle interaction of chiton tooth samples and highly interacting, intact magnetite-containing magnetosomes, our fish

magnetic material is highly interacting. We interpret these results to show that zebrafish adult magnetite exists in clumps or aggregates.

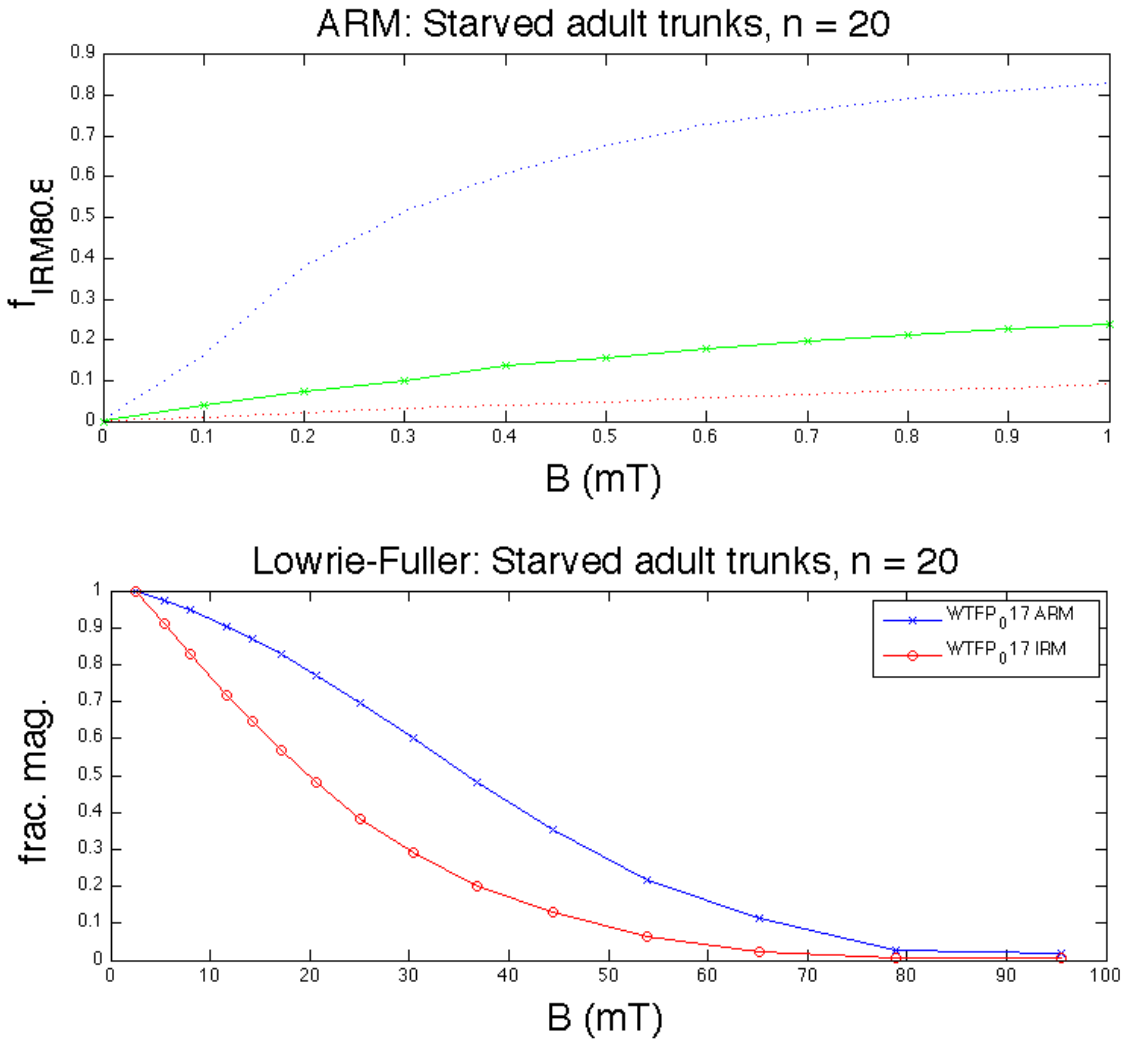

Figure 4. ARM Acquisition and Lowrie-Fuller Test of Magnetic Material Presumed to Be Magnetite

Figure 4. ARM Acquisition and Lowrie-Fuller Test of Magnetic Material Presumed to Be Magnetite

Top: ARM acquisition shows the presence of interacting, possibly clumped zebrafish magnetite. Red and blue curves are standard control samples; the red are data from non-interacting magnetite crystals present in mutant single-crystal magnetotactic bacterial cells (Kopp et al., 2008), and the blue are data from the strongly interacting magnetic particles present in the magnetite capping layers of chiton teeth (Kirschvink & Lowenstam, 1979). The green curve is our freeze-dried zebrafish sample. Bottom: Results for the ARM-modification of the Lowrie-Fuller test (Johnson et al., 1975). In the zebra fish, the demagnetization of the ARM requires stronger peak Af magnetic fields than does the saturation IRM for the same samples, indicating that the remanent magnetization of the sample is dominated by strongly interacting single-domain magnetic material.

Although the magnetic techniques described above cannot definitively identify magnetite of biogenic origin in the fashion of diffraction analysis (Moskowitz et al., 1993), it does narrow the range of possible ferromagnetic materials to essentially single-domain magnetite. Given the known range of metals used by living organisms, iron-based ferrites are the only plausible candidates for producing ferromagnetic crystals. And among the possible iron oxides and sulfides, only the Magnetite/Magnetite system has the coercivity and interaction properties consistent with these data. Taken together with the lack of other plausible contaminants in zebrafish, for which we controlled, and given their ability to orient in magnetic fields (Shcherbakov et al., 2005), we suggest that the

magnetic moments evident in zebrafish tissue samples are due to biogenic magnetite and not inorganic iron sulfides.

SQuID Magnetometry Reveals Several Magnetic Dipoles in the Zebrafish Trunk

We wanted to visualize zebrafish magnetite aggregates *in situ*, especially given the unanticipated result that the trunk contains appreciably more magnetite than the head. The scanning SQuID microscope images the magnetic moments produced by ferromagnetic materials. In SQuID images of adult zebrafish flank sections we observed several dozen discrete dipoles that were not localized in areas of pigmentation, the spinal cord, or neural arches. Instead, dipoles were scattered throughout the trunk and head of zebrafish and appeared to have varying levels of intensity.

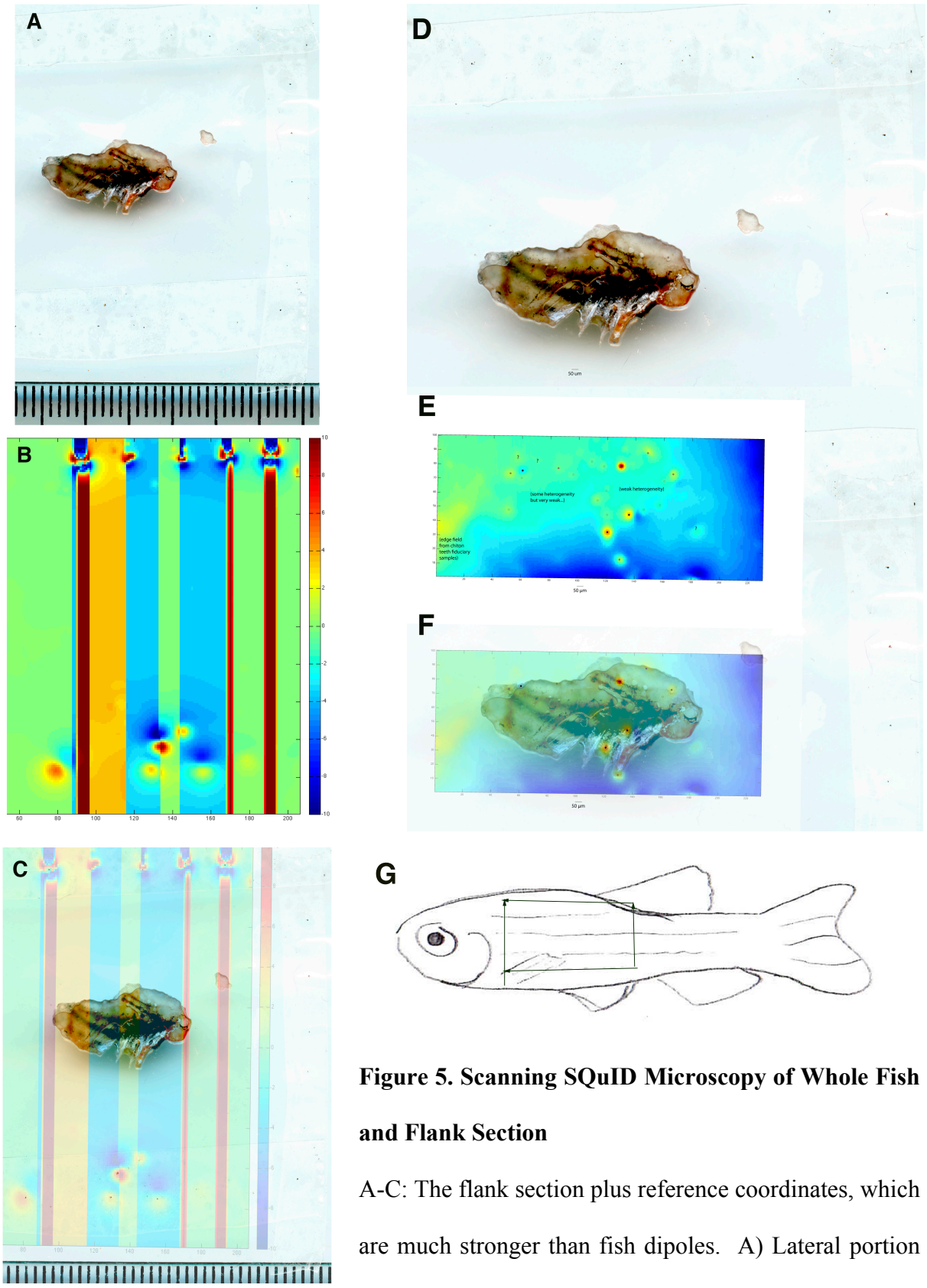

Figure 5. Scanning SQuID Microscopy of Whole Fish and Flank Section

A-C: The flank section plus reference coordinates, which are much stronger than fish dipoles. A) Lateral portion of adult zebrafish flank; this sample encompasses the entire left half of the fish between

the gill arch and anal opening and was excised immediately post-sacrifice with a pair of fine, non-ferromagnetic ceramic tweezers. All internal organs were discarded, but underlying musculature remained intact. The image was taken from the cut side inward. On the top, bottom, and right side of the image the reference strip of chiton tooth chips under non-magnetic Scotch tape is shown. B) SQuID microscope image of chiton tooth chips reference strip creates magnetic coordinates. D-F: Flank section imaged alone without chiton teeth reveals fish dipoles. D) Flank section alone with magnetic map as in A. E) SQuID image, showing magnetic dipoles. F) Overlay of D and E, showing location of magnetic dipoles on fish flank section. G) Schematic of adult zebrafish with square denoting location of section. Scale 1 mm per tick mark.

We crushed chiton teeth to produce magnetite chips as a control and to create a magnetic map adjacent to the zebrafish. The chiton tooth chips were applied to double-sided Scotch tape, which was then taped to the Mylar film on top of which the flank sample was laid. The individual chips of magnetite were very small, probably around $1/20^{th}$ the size of a chiton tooth, yet they produced a dipole moment that produced far more signal than the zebrafish magnetite. For this reason, we scanned interior to the Scotch tape magnetic map and just captured the dipoles in the fish section.

DISCUSSION

Zebrafish Produce Magnetite Early and Throughout Life

Magnetite in zebrafish across the lifespan is unusually abundant and appears to be mostly clumped. We also performed magnetic field discrimination tests on small larvae (< 4 dpf), which did not yield any discernible behavioral outputs (data not shown). These experiments may be worth repeating if we can correlate the size, shape, and concentration of magnetite crystals in these young animals with a developmental time-series of behavioral output. It is possible that the magnetite in young animals is not linked with sensory structures and that responses to magnetic field changes will only be evident over time as the magnetoreceptors mature.

Although we did not demonstrate that larval magnetite crystals are used in magnetotactic behaviors, future studies in larval and adult animals should test for compass orientation after pulse remagnetization, or experimentally changing the direction of the magnetic field. Previous workers have shown that these manipulations will cause a reversal of behavior such as swimming into a positively reinforced magnetic field if animals possess single-domain, magnetite-based magnetoreceptors (Kirschvink, 1989).

The presence of magnetite at different life stages is not new, in fact we have detected concentrations of magnetite in both bees and salmon before adulthood (Gould and Kirschvink, 1978; Walker et al., 1988); butterflies also produce magnetite during development (Jones and MacFadden, 1982).

Trigeminal and Lateral Line Organs in Zebrafish Magnetosensation

Proponents of the optical pumping hypothesis assert that a light-dependent mechanism predominates in some organisms and that magnetite will exist only in areas where the trigeminal projections innervate candidate structures, such as the beak in birds, or the olfactory epithelium and trigeminal ganglion in fish. This overlooks other anatomical regions, which they do not believe contain magnetosensory structures.

Evidence for this view comes from light experiments designed to test for the presence of a radical-pair mechanism in European robins, *Erithacus rubecula*. Wiltschko et al. (Wiltschko, Stapput, Ritz, Thalau and Wiltschko, 2007) found that under conditions of an oscillating broadband field in the range hypothesized to disrupt singlet-to-triplet interconversion, a so-called fixed-direction, magnetite-based compass operated in turquoise and yellow light (502 nm and 590 nm respectively) when the radical-pair compass identified at 564 nm, did not (Ritz et al., 2000; Wiltschko et al., 2007). The magnetite device did not seem to orient birds in a direction required for migration. The authors speculated that the magnetite compass may be an evolutionary relic that never disappeared after light-dependent magnetic sensors appeared in the eye (Wiltschko et al., 2007).

Proponents of maghemite/superparamagnetic magnetoreceptors also support the importance of trigeminal nerve projections based on evidence in birds (Falkenberg, Fleissner, Schuchardt, Kuehbacher, Thalau, Mouritsen, Heyers, Wellenreuther and Fleissner, 2010). The dendritic system has been suggested as an ideal site for

magnetoreception because it is capable of providing the anatomical arrangement to detect multiple components of the magnetic field simultaneously (Falkenberg et al., 2010; Fleissner, Stahl, Thalau, Falkenberg and Fleissner, 2007).

Unexpectedly, we identified the trunk, bilaterally along the flank as a large magnetite repository in zebrafish. Projections of the dorsal root ganglion (DRG), mature Rohon-Beard (RB) neurons, and the posterior lateral line innervate this region; RB neurons are the first to send axons throughout the trunk, followed by lateral line projections, and finally the DRG. The timing of the respective migration of these central and peripheral nervous system components into the trunk is controlled by molecular cues and genetic programs, these are in turn influenced by a variety of endogenous and exogenous factors.

One candidate structure for the location of zebrafish magnetic stores is the lateral line, which has been found in other teleosts. Several salmonid species possess magnetite in the lateral line (Moore, Freake and Thomas, 1990; Ogura, Kato, Arai, Sasada and Sakaki, 1992). Moore and Riley reported the presence of single-domain, highly interacting magnetite in an organic matrix associated with the lateral line of the Atlantic salmon (Moore et al., 1990); the remanences were high enough to indicate that the magneto-receptor system would be capable of sensing geomagnetic field direction. Moore and Riley also found magnetite in the mandibular canal of the lateral line of the European eel, *Anguilla anguilla* (Moore and Riley, 2009); though both the migratory (silver) and non-migratory (yellow) stages showed measurable magnetite content, migratory eels had more than 5 times the SIRM per gram of tissue compared to their non-migratory

counterparts. Each of these species is known for extensive oceanic migrations that are required for normal spawning behaviors.

The early embryonic and larval lateral line in zebrafish is comprised of the anterior and posterior segments, with distinct ganglia and neuromasts, both of which appear to be highly conserved among teleosts (Ghysen and Dambly-Chaudiere, 2004). Individual posterior lateral line (PLL) neurons innervate different target organs, creating a somatotopy that can be visualized by gene expression in subsets of sensory neurons. Adult lateral line patterns vary widely (Ghysen and Dambly-Chaudiere, 2004) as new primordia are added in maturing zebrafish and resultant neuromasts migrate dorso-ventrally (Ghysen and Dambly-Chaudiere, 2004).

The neuromasts of the lateral line and their innervation are well structured to encounter magnetic stimuli from several directions even in young embryos. It has previously been noted that the most likely candidate for a magnetoreceptor is a hair-cell like structure (Kirschvink and Gould, 1981; Kirschvink et al., 1992b). Its external location makes the lateral line easily visualized via several microscopy methods.

The association of increased magnetite with silver eel lateral lines prompted Moore and Riley (Moore and Riley, 2009) to suggest that an “ontogenic shift” had occurred in which lateral line magnetite was enlisted for migratory behavior. Indeed this sensory structure may have been the initial site of teleost magnetite production or storage. Alternatively, magnetite stores may have been close enough to lateral line nerve terminals that an

incidental association with these tiny permanent magnets would allow the development of rudimentary magnetosensation as the magnetic fields or movements of the magnetite crystals caused changes in firing that could be transduced along with other sensory information to the fish CNS. The earliest iteration of the magnetosensory apparatus may have detected local geomagnetic anomalies during short distance movements. It is plausible that in animals such as zebrafish that do not participate in extensive migrations, magnetite-based magnetoreceptors remained unchanged, while in migratory species such as eel and salmon the magnetoreceptive capacity of the lateral line was co-opted for a specialized role in sensing large geomagnetic field differences.

CONCLUSIONS AND FUTURE RESEARCH

Biogenic magnetite in vertebrates has mostly been found in areas containing trigeminal ganglion projections; here we have reported its presence in lateral-line-innervated anatomy in a model organism, the zebrafish, a small, non-migratory teleost. In teleosts such as the European eel and several species of salmon, the lateral line canal also contained magnetite (Hanson, Karlsson and Westerberg, 1984; Moore et al., 1990; Moore and Riley, 2009; Ogura et al., 1992). In homing pigeons and other birds large magnetic deposits identified as magnetite were found in musculature and the authors hypothesized that the muscle spindle might mediate signal transduction of magnetic stimuli detected by magnetoreceptors (Presti and Pettigrew, 1980). Given the diverse distribution of biogenic magnetite, it is possible that magnetite biomineralization developed from a common pathway that takes places in different anatomical locations associated with nervous structures whose extensive dendritic trees were in contact with individual crystals. These

suitable sensory structures could then adapt to assess magnetic information.

The next step in this research is to characterize zebrafish magnetic crystals via typical methods, such as TEM-based electron diffraction, X-ray dispersive imaging, and electron microprobe analysis or Mossbauer spectroscopy, to confirm the identity of magnetite. Additionally, reflectance mode confocal laser scanning microscopy (CLSM) will be a useful tool to see individual magnetosomes as they lie in tissues. This will allow us to view the subcellular localization of magnetite crystals and hopefully extract magnetoreceptor cells and individual magnetoreceptors.

Zebrafish are an ideal candidate organism for studying magnetosensation in all its forms, from the neurophysiology and anatomy of magnetosensory structures to the genetics of magnetite biomineralization and the behavioral manifestations of the magnetic sense in vertebrates.

ACKNOWLEDGEMENTS

The authors would like to thank Isaac Hilburn for his technical assistance with software and hardware issues, LeighAnn Fletcher for zebrafish husbandry, Dr. Scott Bogue for use of his magnetometer, and Dr. Theresa Raub for SQuID microscope assistance. This work was supported by grants from the National Science Foundation (NSF) Human Frontiers Science Program (HFSP) Grant: RGP0028 to JLK for the paleomagnetic and FMR work, and the National Human Genome Research Institute (NGHRI) for the Center of Excellence in Genomic Science (CEGS) Grant: P50 HG004071 to Drs. Marianne Bronner and Scott Fraser, in whose laboratories the zebrafish for this study were housed. Additionally, ADD would like to thank Scott Fraser for use of the Biological Imaging Center (BIC) at Caltech and Dr. Marianne Bronner for continued laboratory support throughout this project.

BIBLIOGRAPHY

Bennett, A. T. D. (1996). Do Animals Have Cognitive Maps? *The Journal of Experimental Biology* **199**, 219-224.

Falkenberg, G., Fleissner, G., Schuchardt, K., Kuehbacher, M., Thalau, P., Mouritsen, H., Heyers, D., Wellenreuther, G. and Fleissner, G. (2010). Avian Magnetoreception: Elaborate Iron Mineral Containing Dendrites in the Upper Beak Seem to Be a Common Feature of Birds. *PLOS ONE* **5**.

Fleissner, G., Stahl, B., Thalau, P., Falkenberg, G. and Fleissner, G. (2007). A novel concept of Fe-mineral-based magnetoreception: histological and physicochemical data from the upper beak of homing pigeons. *Naturwissenschaften* **94**, 631-642.

Fong, L. E., Holzer, J. R., McBride, K. K., Lima, E. A. and Baudenbacher, F. (2005). High-resolution room-temperature sample scanning superconducting quantum interference device microscope configurable for geological and biomagnetic applications. *Review of Scientific Instruments* **76**, 9.

Ghysen, A. and Dambly-Chaudiere. (2004). Development of the zebrafish lateral line. *Current Opinion in Neurobiology* **14**, 67-73.

Gould, J. L. (1979). Do Honeybees Know What They Are Doing. *Natural History* **88**, 66-75.

Gould, J. L. and Kirschvink, J. L. (1978). Bees Have Magnetic Remanence. *Science* **201**, 1026-1028.

Hanson, M., Karlsson, L. and Westerberg, H. (1984). Magnetic Material In European Eel (Anguilla Anguilla L.). *Comparative Biochemistry and Physiology* **77A**, 221-224.

Johnsen, S. and Lohmann, K. J. (2005). The Physics and Neurobiology of Magnetoreception. *Nature Reviews: Neuroscience* **6**, 703-712.

Johnson, H. P., Lowrie, W. and Kent, D. V. (1975). Stability of Anhysteretic Remanent Magnetization in Fine and Coarse Magnetite and Maghemite Particles. *Geophysical Journal of the Royal Astronomical Society* **41**, 10.

Jones, D. S. and MacFadden, B. J. (1982). Induced Magnetization in The Monarch Butterfly, Danaus-Plexippus (Insecta, Lepidoptera). *Journal of Experimental Biology* **96**, 1-9.

Kalmijn, A. J. (1978). Electric and magnetic sensory world of sharks, skates and rays. In *Sensory Biology of Sharks, Skates and Rays*, (ed. F. S. Hodgson and R. F. Mathewson), pp. 507-528. Arlington, VA: Office of Naval Research.

King, J., Banerjee, S. K., Marvin, J. and Ozdemir, O. (1982). A comparison of different magnetic methods for determining the relative grain size of magnetite in natural materials: some results from lake sediments. *Earth and Planetary Science Letters* **59**, 404-419.

Kirschvink, J. L. (1989). Magnetite Biomineralization and Geomagnetic Sensitivity in Higher Animals: An Update and Recommendations for Future Study. *Bioelectromagnetics* **10**, 239-259.

Kirschvink, J. L. and Gould, J. L. (1981). Biogenic Magnetite As A Basis For Magnetic Field Detection in Animals. *BioSystems* **13**, 181-201.

Kirschvink, J. L., Jones, D. S. and MacFadden, B. J. (1985). Magnetite Biomineralization and Magnetoreception in Organisms. In *Topics in Geobiology*, vol. 5 (ed. New York and London: Plenum Press.

Kirschvink, J. L., Kobayashi-Kirschvink, A. and Woodford, B. J. (1992a). Magnetite biomineralization in the human brain. *Proceedings of the National Academy of Science* **89**, 7683-7687.

Kirschvink, J. L., Kopp, R. E., Raub, T. D., Baumgartner, C. T. and Holt, J. W. (2008). Rapid, Precise, and High-Sensitivity Acquisition of Paleomagnetic and Rock-Magnetic Data: Development of a Low-Noise Automatic Sample Changing System for Superconducting Rock Magnetometers. *Geochemistry Geophysics Geosystems* **9**, 1-18.

Kirschvink, J. L., Kuwajima, T., Ueno, S., Kirschvink, S. J., Diaz-Ricci, J. C., Morales, A., Barwig, S. and Quinn, K. (1992b). Discrimination of low-frequency magnetic fields by honeybees: Biophysics and experimental tests. In *Sensory Transduction*, (ed. D. P. Corey and S. D. Roper), pp. 225-240. New York: Rockefeller University Press.

Kirschvink, J. L. and Lowenstam, H. A. (1979). Mineralization and Magnetization of Chiton Teeth-Paleomagnetic, Sedimentologic, and Biologic Implications of Organic Magnetite. *Earth and Planetary Science Letters* **44**, 193-204.

Kirschvink, J. L., Padmanabha, S., Boyce, C. K. and Oglesby, J. (1997). Measurement of the threshold sensitivity of honeybees to weak, extremely low-frequency magnetic fields. *The Journal of Experimental Biology* **200**, 1363-1368.

Kirschvink, J. L. and Walker, M. M. (1985). Particle-size considerations for magnetite-based magnetoreceptors. In *Magnetite Biomineralization and Magnetoreception in Organisms*, vol. 5 (ed. J. L. Kirschvink D. S. Jones and B. J. MacFadden), pp. 243-254. New York and London: Plenum Press.

Kopp, R. E., Raub, T. D., Schumann, D., Vali, H., Smirnov, A. V. and Kirschvink, J. L. (2007). Magnetofossil spike during the Paleocene-Eocene thermal maximum: Ferromagnetic resonance, rock magnetic, and electron microscopy evidence from Ancora, New Jersey, United States. *Paleoceanography* **22**, 1-7.

Kopp, R. E., Weiss, B. P., Maloof, A. C., Vali, H., Nash, C. Z. and Kirschvink, J. L. (2006). Chains, clumps, and strings: Magnetofossil taphonomy with ferromagnetic resonance spectroscopy. *Earth and Planetary Science Letters* **247**, 10 - 25.

Lippert, P. C. and Zachos, J. C. (2007). A biogenic origin for anomalous fine-grained magnetic material at the Paleocene-Eocene boundary at Wilson Lake, New Jersey. *Paleoceanography* **22**, 1-8.

Lohmann, K. J. and Johnsen, S. (2000). The neurobiology of magnetoreception in vertebrate animals. *Trends in Neuroscience* **23**, 153-159.

Lohmann, K. J., Lohmann, C. M. F. and Putnam, N. F. (2007). Magnetic maps in animals: nature's GPS. *The Journal of Experimental Biology* **210**, 3697-3705.

Lowenstam, H. A. (1962). Magnetite in denticle capping in recent chitons (*Polyplacophora*). *Geological Society of America Bulletin* **73**, 435.

Lowrie, W. and Fuller, M. (1971). On the Alternating Field Demagnetization Characteristics of Multidomain Thermoremanent Magnetization in Magnetite. *Journal of Geophyiscal Research* **76**, 6339-6349.

Moore, A., Freake, S. M. and Thomas, I. M. (1990). Magnetic Particles in the Lateral Line of the Atlantic Salmon (*Salmo salar L.*). *Philosophical Transactions: Biological Sciences* **329**, 11-15.

Moore, A. and Riley, W. D. (2009). Magnetic particles associated with the lateral line of the European eel Anguilla anguilla. *Journal of Fish Biology* **74**, 1629-1634.

Moskowitz, B. M., Frankel, R. B. and Bazylinski, D. A. (1993). Rock magnetic criteria for the detection of biogenic magnetite. *Earth and Planetary Science Letters* **120**, 283-300.

Ogura, M., Kato, M., Arai, N., Sasada, T. and Sakaki, Y. (1992). Magnetic particles in chum salmon (*Oncorhynchus keta*): extraction and transmission electron microscopy. *Canadian Journal of Zoology* **70** 874-877.

Presti, D. and Pettigrew, J. D. (1980). Ferromagnetic coupling to muscle receptors as a basis for geomagnetic field sensitivity in animals. *Nature* **285**, 99-101.

Ritz, T., Adem, S. and Schulten, K. (2000). A model for photoreceptor-based magnetoreception in birds. *Biophysical Journal* **78**, 707-718.

Ritz, T., Ahmad, M., Mouritsen, H., Wiltschko, R. and Wiltschko, W. (2010). Photoreceptor-based magnetoreception: optimal design of receptor molecules, cells, and neuronal processing. *Journal of the Royal Soceity Interface* **7**, S135-S146.

Shcherbakov, D., Winklhofer, M., Petersen, N., Steidle, J., Hilbig, R. and Blum, M. (2005). Magnetosensation in zebrafish. *Current Biology* **15**, R162.

Solov'yov, I. A. and Greiner, W. (2007). Theoretical Analysis of an Iron Mineral-Based Magnetoreceptor Model in Birds. *Biophysical Journal* **93**, 1493-1509.

Vanderstraeten, J. and Gillis, P. (2010). Theoretical Evaluation of Magnetoreception of Power-Frequency Fields. *Bioelectromagnetics* **31**, 371-379.

Walcott, C., Gould, J. L. and Kirschvink, J. L. (1979). Pigeons Have Magnets. *Science* **205**, 1027-1029.

Walker, M. M., Diebel, C. E. and Kirschvink, J. L. (2003). Detection and Use of the Earth's Magnetic Field by Aquatic Vertebrates. In *Sensory Processing in Aquatic Environments*, (ed. S. P. Collins and N. J. Marshall), pp. 53-74. New York: Springer-Verlag.

Walker, M. M., Kirschvink, J. L. and Dizon, A. E. (1985a). Magnetoreception and Biomineralization of Magnetite: Fish. In *Magnetite Biomineralization and Magnetoreception in Organisms*, vol. 5 (ed. J. L. Kirschvink D. S. Jones and B. J. MacFadden), pp. 417-437. New York and London: Plenum Press.

Walker, M. M., Kirschvink, J. L., Perry, A. and Dizon, A. E. (1985b). Detection, Extraction, and Characterization of Biogenic Magnetite. In *Magnetite Biomineralization and Magnetoreception in Organisms*, vol. 5 (ed. J. L. Kirschvink D. S. Jones and B. J. MacFadden), pp. 155-166. New York and London: Plenum Press.

Walker, M. M., Quinn, T. P., Kirschvink, J. L. and Groot, C. (1988). Production of Single-Domain Magnetite Throughout Life By Sockeye Salmon, *Oncorhynchus nerka*. *Journal of Experimental Biology* **140**, 51-63.

Weiss, B. P., Kim, S. S., Kirschvink, J. L., Koppe, R. E., Sankaran, M., Kobayashi, A. and Komeili, A. (2004). Ferromagnetic resonance and low-temperature magnetic tests for biogenic magnetite. *Earth and Planetary Science Letters* **224**, 73-89.

Wiltschko, R., Stapput, K., Ritz, T., Thalau, P. and Wiltschko, W. (2007). Magnetoreception in birds: different physical processes for two types of directional responses. *HFSP Journal* **1**, 41-48.

Wiltschko, R. and Wiltschko, W. (1995). Magnetic Orientation in Animals. Berlin, Heidelberg, New York: Springer Verlag.

Wiltschko, W. and Wiltschko, R. (2005). Magnetic orientation and magnetoreception in birds and other vertebrates. *Journal of Comparative Physiology A* **191**, 675-693.

Winklhofer, M. and Kirschvink, J. L. (2010). A quantitative assessment of torque-transducer models for magnetoreception. *Journal of the Royal Soceity Interface*.

CHAPTER V

Conclusion

AUTHOR

Alana Dixson

Zebrafish As A Model for Health and Disease in the Central Nervous System

The original goal of my doctoral work was to devise a set of methods and a model system for studying the development and maturation of the vertebrate central nervous system. I wanted to learn and create tools in biological imaging and molecular biology to apply in research on the developmental origins of health and disease (DOHaD). This growing field primarily focuses on metabolic or cardiovascular disorders originating from fetal or early post-natal lesions or environmental conditions. The initial manifestations of developmentally derived diseases occasionally appear during the first decade of life but their debilitating symptomatology is generally most evident in adulthood.

Zebrafish provide an ideal vertebrate model for initial animal studies of DOHaD because they possess many advantages, such as optical transparency during embryogenesis and early larval stages, high fecundity, and regular, year-round spawning behaviors, along with a short time to peak sexual maturity. Zebrafish are also becoming more common in toxicology research; they may be particularly useful in uncovering the link between environmental pollution and CNS disorders (Jacobson, Birkholz, McNamara, Bharate and George, 2010).

What Rohon-Beard Neurons Can Tell Us About A Changing Nervous System

Rohon-Beard neurons are present and functional throughout the early life of zebrafish and, as I have shown in Chapter 3, seem to persist in the adult. Unlike other sensory neurons, they are located within the spinal cord and as such are subject to the same exposures as other components of the neural tube. Defects in gene expression, exposure

to environmental pollution and mechanical lesions that cause known neural tube diseases are likely to also affect development, connectivity, and maturation of RB cells. Given their location in the dorsal-most section of the spinal cord, RBs are easily visualized by a variety of microscopy techniques and are readily approachable with microsurgical tools. In this way, studies aimed at altering early embryonic development specifically to manipulate RB neurons are easier to accomplish, and unexpected effects of such interventions are more likely to be identified.

Protein Kinase C α

The trapped gene highlighted in the present work, protein kinase C alpha (PKCα), may support RB neuron survival. We may categorize protein kinase C (PKC) isoforms by their activators, phosphatidylserine (PS), diacylglycerol (DAG), and calcium (Ca^{2+}) (Ohno and Nishizuka, 2002a). The "typical" PKCs use all three activators, while the "novel" and "atypical" subgroups, respectively, require 1) PS and DAG, or 2) PS only. The role of these activators in RB death and survival should be further explored.

PKCα may be involved in synapse maturation (Akinori, 1998; Miki, 1995) and PKCγ, also found in RB neurons (Patten, Sihra, Dhami, Coutts and Ali, 2007), has been implicated in long-term potentiation (LTP) (Miki, 1995). Each of these could be the mode of RB transdifferentiation and may be important in the mature function of RB neurons. Given the requirement of calcium for PKCα activity it seems possible that Ca^{2+} signaling or gradients may mediate longevity in RB cells.

The factors that promote death and survival in primary sensory neurons are still being elucidated. The mechanisms of RB death have only been partially explained. Molecular evidence supporting a role for caspase-3-dependent programmed cell death (PCD) (Williams, 2000) is perhaps the strongest, but interestingly, activity is actually required for elimination of the population via Na^+ currents in the Nav1.6 channel (Svoboda, Linares and Ribera, 2001).

In contrast, RB survival may be influenced by a complex set of cell signaling molecules such as cyclin-dependent kinase 5 (CDK5). Kanungo and Pant showed that supernumerary RBs were induced by over-expression of cdk5 mRNA and reduced drastically, but not entirely eliminated by siRNA of the same gene (Kanungo, Li, Zheng and Pant, 2006). This cyclin is not involved in cell cycle control; however, several workers have shown a diverse array of functions, ranging from neuroprotection to neurodegeneration. Developmentally, cdk5's activity is still uncertain, but it appears to promote neuronal survival and may interact indirectly with PKCα. In 2008, Sahin et al. showed that PKCα negatively regulates two essential cdk5 substrates to affect downstream survival of mouse embryonic striatal neurons (Sahin, Hawasli, Greene, Molkentin and Bibb, 2008). Zebrafish are a good organism in which to examine the role of these two proteins in brain and spinal cord neuron survival because *in vivo* imaging techniques and the ease of genetic manipulation would allow for studies on dynamic protein interaction.

Taken together, these results show that the survival and programmed death of RBs is a molecularly complex process. The contribution of various developmentally significant genes in the maintenance of this cell population, or until they expire, has yet to be explored.

For the reasons outlined above, the RB neuron and its sensory arbors are unique models for interrogating the developmental perturbations in the CNS that may lead to adult disease. The presence of a RB-like neuron in human embryos has been documented, but its longevity is unknown. The previous model of early-dying RB neurons suffocated any interest in a homologue in human adults and attempts to follow the longitudinal development of embryonic precursors in zebrafish and other vertebrates. I hope that others will track larval, juvenile, and adult RB lineages, and that the function of these cells will be characterized along with interest in searching for the human cognate.

Future Directions

The role of PKCα in RB survival warrants further investigation. Of particular interest is its possible effect on other signaling molecules, including the PKCα activators, Ca^{2+}, PS, and DAG. Additionally, a comparison of the involvement of sodium and calcium channels, and studies on Ca^{2+} intracellular concentrations, ionic flux, and tissue gradients in RB survival would shed light on how different ions acting in the same organ and circuits affect neuronal function and maturation, and CNS development generally. As in studies of NT3, it would be interesting to compare the survival of RBs subjected to anti-PKCα antibody and exogenous PKCα protein.

Interestingly, retinoic acid (RA) positively influences PKCα expression in mice via a retinoic acid response element (RARE) found in the murine homolog (Desai, Hirai, Karnes, Niles and Ohno, 1999). For example, increased RA expression is also associated with changes in hindbrain organization in embryonic mice. A future goal is to clone the promoter region of zebrafish PKCα to determine if a RARE exists.

The FT transgenic lines in this study would facilitate our understanding of the interaction between RA and PKCα in RB neuron development because fusion protein fluorescence gives a direct readout of changes in PKCα expression on the protein level. A simple experiment in which RA administration at different stages of development is compared to the effect on zebrafish embryonic hindbrain and RB neurons would further elucidate PKCα's role in patterning the CNS when it interacts with other known CNS affecters. Careful studies of PKCα-positive RB longevity, function, and morphology, along with spinal neuron patterning upon administration of RA, would further elucidate both the role of PKCα and RA in zebrafish spinal cord development.

With its strong fluorescent signal in axons and spinal neuron somata, FT lines ct7a and ct54a in combination with other transgenics, such as HuC::kaede or islet-1::GFP lines, would enable further dissection of spinal neuron patterning. The goal with these combinations would be to answer questions proximal to the present study on the role of PKCα in both RB and spinal cord development in zebrafish and to fit this within DOHaD models.

Zebrafish As A Model for Magnetosensation

Magnetosensation research has benefitted from the use of undomesticated, migratory birds (Wiltschko and Wiltschko, 2005), aquatic vertebrates (Walker et al., 2003), and insects (Wajnberg, Acosta-Avalos, Alves, de Oliveira, Srygley and Esquivel, 2010) to assay behavioral responses to magnetic field variations. Additionally, genetically tractable bacteria have elucidated the biosynthetic pathways and formation of components of the bacterial magnetic sensory system (Jogler and Schüler, 2009; Murat, Quinlan, Vali and Komeili, 2010). To date, however, the physiology and structure of magnetoreceptor cells and the intracellular signal transduction mechanism for magnetic stimuli have remained elusive. Moving forward, the importance of developing a systematic methodology for studying the behavioral output and anatomical basis of the magnetic sense on a gross level, together with the neurophysiologic, molecular and genetic mechanisms on the microscopic level in one animal subject is clear (Johnsen and Lohmann, 2005). Few studies have taken advantage of biology's model organisms (Cranfield, Dawe, Karloukovski, Dunin-Borkowski, de Pomerai and Dobson, 2004; McKay and Persinger, 2005; Muheim, Edgar, Sloan and Phillips, 2006; Saint-Pierre and Persinger, 2008), ideal candidates for dissecting the vertebrate magnetic sense.

The zebrafish is a relative newcomer to biological research, but it has quickly become an iconic model in developmental and neuro-genetic studies (Kullander, 2005; Rinkwitz, Mourrain and Becker, 2011; Weinstein, 2004). Available genomic, genetic, and imaging techniques in zebrafish are well validated and diverse, and the ease of creating new transgenic lines to study genetic and morphological features is remarkable (Cerda et al.,

2006; Cui, Yang, Kaufman, Agalliu and Hackett, 2003; Higashijima, Hotta and Okamoto, 2000; McLean and Fetcho, 2008; Megason, 2009; Trinh et al., 2011b; Udvadia and Linney, 2003; Wu, Zhang, Xiong, Luo, Cui, Hu, Yu, Su, Xu and Zhu, 2006). Electrophysiological methods in use for several decades are also gaining popularity as younger researchers invest time to learn and apply these techniques, along with histological and behavioral assays, to understand vertebrate nervous system development and function.

Characterizing the zebrafish magnetic receptor system in depth may elucidate the genetic and physiological mechanisms of magnetosensation in higher vertebrates. The small size of zebrafish embryos and their optical transparency during the first 7 days of development, when the entire larval central nervous system is formed and many adult structures are in place (Appel, 2000; Lewis and Eisen, 2003; Westerfield, 2000), lend themselves to anatomical studies at early stages to detect the location and electrophysiological characteristics of magnetoreceptor cells.

We showed that zebrafish as young as 4 days old possess large quantities of magnetite, and this amount increases dramatically over the rest of the juvenile period. Many migratory fish (Walker et al., 1985a), including several teleosts, are magnetosensory and appear to produce biogenic magnetite (Hanson and Westerberg, 1987). Zebrafish, also a teleost, possess magnetosensory capabilities, as demonstrated in an experiment in which adult animals were trained to detect and avoid magnetic fields (Shcherbakov et al., 2005). On the opposite end of the developmental spectrum, magnetic fields were shown to delay

enzymatically mediated hatching (Skauli, Reitan and Walther, 2000); embryos that fail to hatch on time exhibit physical abnormalities (Skauli et al., 2000), but this may be due more to physical restrictions than any magnetic field effects. Whether this early larval zebrafish magnetite in some way mediates hatching directly or indirectly is unclear. Future studies should include extracting neurophysiologic and molecular information from test animals at all developmental stages.

Why adult non-migratory animals like zebrafish possess magnetite, its means of production, and the developmental pathways of magnetoreception in vertebrates are not clear. Another question is why, if at all, two different mechanisms for magnetoreception exist—light-dependent and magnetite-based systems. Wiltschko and Wiltschko, have suggested that, at least in birds and possibly other organisms, both magnetite-based and optical pumping mechanisms operate (Wiltschko and Wiltschko, 2005). The compass and map senses, they argue, require animals to have magnetoreceptors with different levels of sensitivity to magnetic field intensity, and therefore, they cannot simultaneously detect changes in direction.

Here we have shown that zebrafish biomineralize magnetite and, although some may be located in the head where trigeminal innervation is expected, the vast majority of its stores are in areas more likely innervated by other sensory structures such as the lateral line, DRG or mature RB projections. Studies with this model organism should be able to answer some of these questions and clarify the developmental progression of magnetosensation in a non-migratory animal.

BIBLIOGRAPHY

Akinori, M. (1998). Subspecies of Protein Kinase C in The Rat Spinal Cord. *Progress in Neurobiology* **54**, 499-530.

Anderson, D. J. (1999). Lineages and transcription factors in the specification of vertebrate primary sensory neurons. *Current Opinion in Neurobiology* **9**, 517-524.

Appel, B. (2000). Zebrafish Neural Induction and Patterning. *Developmental Dynamics* **203**, 155-168.

Beard, J. (1889). On the early development of Lepidosteus osseous. *Proceedings of the Royal Society of London* **46**, 1108-1118.

Bennett, A. T. D. (1996). Do Animals Have Cognitive Maps? *The Journal of Experimental Biology* **199**, 219-224.

Blader, P., Plessy, C. and Stra¨hle, U. (2003). Multiple regulatory elements with spatially and temporally distinct activities control *neurogenin1* expression in primary neurons of the zebrafish embryo. *Mechanisms of Development* **120**, 211-218.

Briscoe, J., Pierani, A., Jessell, T. M. and Ericson, J. (2000). A Homeodomain Protein Code Specifies Progenitor Cell Identity and Neuronal Fate in The Ventral Neural Tube. *Cell* **101**, 435-445.

Buss, R. R., Sun, W. and Oppenheim, R. W. (2006). Adaptive Roles of Programmed Cell Death During Nervous System Development. *Annual Reviews of Neuroscience* **29**, 1-35.

Caron, S. J. C., Prober, D., Choy, M. and Schier, A. F. (2008). In vivo birthdating by BAPTISM reveals that trigeminal sensory neuron diversity depends on early neurogenesis. *Development* **135**, 3259-3269.

Cerda, G. A., Thomas, J. E., Allende, M. L., Karlstrom, R. O. and Palma, V. (2006). Electroporation of DNA, RNA, and Morpholinos into Zebrafish Embryos. *Methods* **39**, 207-211.

Clarke, J. D. W., Hayes, B. P., Hunt, S. P. and Roberts, A. (1984). Sensory Physiology, Anatomy and Immunohistochemistry of Rohon-Beard Neurones in Embryos Of *Xenopus Laevis*. *Journal of Physiology* **348**, 511-525.

Cole, L. K. and Ross, L. S. (2001). Apoptosis in the Developing Zebrafish Embryo. *Developmental Biology* **240**, 123-142.

Cornell, R. A. and Eisen, J. S. (2000). Delta signaling mediates segregation of neural crest and spinal sensory neurons from zebrafish lateral neural plate. *Development* **127**, 2873-2882.

Cornell, R. A. and Eisen, J. S. (2002). Delta/Notch signaling promotes formation of zebrafish neural crest by repressing Neurogenin 1 function. *Development* **129**, 2639-2648.

Cranfield, C. G., Dawe, A., Karloukovski, V., Dunin-Borkowski, R. E., de Pomerai, D. and Dobson, J. (2004). Biogenic Magnetite in The Nematode *Caenorhabditis elegans*. *Proceedings of the Royal Society of London Series B-Biological Sciences* **271**, S436-S439.

Cui, Z., Yang, Y., Kaufman, C. D., Agalliu, D. and Hackett, P. B. (2003). RecA-Mediated, Targeted Mutagenesis in Zebrafish. *Marine Biotechnology* **5**, 174-184.

D'Amico-Martel, A. and Noden, D. M. (1983). Contributions of Placodal and Neural Crest to Avian Cranial Peripheral Ganglia. *The American Journal of Anatomy* **166**, 445-468.

Desai, D. S., Hirai, S.-i., Karnes, J., William E. , Niles, R. M. and Ohno, S.-g. (1999). Cloning and Characterization of The Murine PKCα Promoter: Identification of A Retinoic Acid Response Element. *Biochemical and Biophysical Research Communications* **263**, 28-34.

Falkenberg, G., Fleissner, G., Schuchardt, K., Kuehbacher, M., Thalau, P., Mouritsen, H., Heyers, D., Wellenreuther, G. and Fleissner, G. (2010). Avian Magnetoreception: Elaborate Iron Mineral Containing Dendrites in the Upper Beak Seem to Be a Common Feature of Birds. *PLOS ONE* **5**.

Fleissner, G., Stahl, B., Thalau, P., Falkenberg, G. and Fleissner, G. (2007). A novel concept of Fe-mineral-based magnetoreception: histological and physicochemical data from the upper beak of homing pigeons. *Naturwissenschaften* **94**, 631-642.

Fong, L. E., Holzer, J. R., McBride, K. K., Lima, E. A. and Baudenbacher, F. (2005). High-resolution room-temperature sample scanning superconducting quantum interference device microscope configurable for geological and biomagnetic applications. *Review of Scientific Instruments* **76**, 9.

Furutani-Seiki, M., Jiang, Y.-J., Brand, M., Heisenberg, C.-P., Houart, C., Beuchle, D., van Eeden, F. J. M., Granato, M., Haffter, P., Hammerschmidt, M. et al. (1996). Neural degeneration mutants in the zebrafish, *Danio rerio*. *Development* **123**, 229-239.

Ghysen, A. and Dambly-Chaudiere. (2004). Development of the zebrafish lateral line. *Current Opinion in Neurobiology* **14**, 67-73.

Gong, Z., Ju, B. and Wan, H. (2001). Green Fluorescent Protein (GFP) Transgenic Fish and Their Applications. *Genetica* **111**, 213-225.

Gould, J. L. (1979). Do Honeybees Know What They Are Doing. *Natural History* **88**, 66-75.

Gould, J. L. and Kirschvink, J. L. (1978). Bees Have Magnetic Remanence. *Science* **201**, 1026-1028.

Griesbeck, O., Baird, G. S., Campbell, R. E., Zacharias, D. A. and Tsien, R. Y. (2001). Reducing the Environmental Sensitivity of Yellow Fluorescent Protein. *the Journal of Biological Chemistry* **276**.

Guillemot, F. (2007). Spatial and Temporal Specification of Neural Fates by Transcription Factor Codes. *Development* **134**, 3771-3780.

Hanson, M., Karlsson, L. and Westerberg, H. (1984). Magnetic Material In European Eel (Anguilla Anguilla L.). *Comparative Biochemistry and Physiology* **77A**, 221-224.

Hanson, M. and Westerberg, H. (1987). Occurrence of Magnetic Material in Teleosts. *Comparative Biochemistry and Physiology* **86A**, 169-172.

Helms, A. W., Battiste, J., Henke, R. M., Nakada, Y., Simplicio, N., Guillemot, F. and Johnson, J. E. (2005). Sequential Roles for Mash1 and Ngn2 in the Generation of Dorsal Spinal Cord Interneurons. *Development* **132**, 2709-2719.

Helms, A. W. and Johnson, J. E. (2003). Specification of Dorsal Spinal Cord Interneurons. *Current Opinion in Neurobiology* **13**, 42-49.

Higashijima, S., Hotta, Y. and Okamoto, H. (2000). Visualization of Cranial Motor Neurons in Live Transgenic Zebrafish Expressing Green Fluorescent Protein Under Control of The Islet-1 Promoter/Enhancer. *Journal of Neuroscience* **20**, 206-218.

Hirata, H., Nakano, Y. and Oda, Y. (2009). Phenotypic analysis of a new fish mutant harboring Rohon-Beard neuron defects. *Neuroscience Research* **65**, S135.

Hua, X. Y., Moore, A., Malkmus, S., Murray, S. F., Dean, N., Yaksh, T. L. and Butler, M. (2002). Inhibition of spinal protein kinase C alpha expression by an antisense oligonucleotide attenuates morphine infusion-induced tolerance. *Neuroscience* **113**, 99-107.

Humphrey, T. (1944). Primitive neurons in the embryonic human central nervous system. *Journal of Comparative Neurology* **81**, 1-45.

Humphrey, T. (1950). Intramedullary sensory ganglion cells in the roof plate area of the embryonic human spinal cord. *Journal of Comparative Neurology* **92**, 333-399.

Jacobson, S. M., Birkholz, D. A., McNamara, M. L., Bharate, S. B. and George, K. M. (2010). Subacute Developmental Exposure of Zebrafish to The Organophosphate Pesticide Metabolite, Chlorpyrifos-Oxon, Results in Defects in Rohon-Beard Sensory Neuron Development. . *Aquatic Toxicology* **100**, 101-111.

Jankowska, E. (2001). Spinal Interneuronal Systems: Identification, Multifunctional Character and Reconfiguration in Mammals. *The Journal of Physiology* **533**, 31-40.

Jessell, T. M. (2000). Neuronal Specification in the Spinal Cord: Inductive Signals and Transcriptional Codes. *Nature Reviews: Genetics* **1**, 20-29.

Jogler, C. and Schüler, D. (2009). Genomics, Genetics, and Cell Biology of Magnetosome Formation. *Annual Review of Microbiology* **63**, 501-521.

Johnsen, S. and Lohmann, K. J. (2005). The Physics and Neurobiology of Magnetoreception. *Nature Reviews: Neuroscience* **6**, 703-712.

Johnson, H. P., Lowrie, W. and Kent, D. V. (1975). Stability of Anhysteretic Remanent Magnetization in Fine and Coarse Magnetite and Maghemite Particles. *Geophysical Journal of the Royal Astronomical Society* **41**, 10.

Jones, D. S. and MacFadden, B. J. (1982). Induced Magnetization in The Monarch Butterfly, Danaus-Plexippus (Insecta, Lepidoptera). *Journal of Experimental Biology* **96**, 1-9.

Kalmijn, A. J. (1978). Electric and magneitc sensory world of sharks, skates and rays. In *Sensory Biology of Sharks, Skates and Rays*, (ed. F. S. Hodgson and R. F. Mathewson), pp. 507-528. Arlington, VA: Office of Naval Research.

Kanungo, J., Li, B.-S., Zheng, Y. and Pant, H. (2006). Cyclin-dependent kinase 5 influences Rohon-Beard neuron survival in zebrafish. *Journal of Neurochemistry* **99**, 251-259.

Kimmel, C. B., Hatta, K. and Eisen, J. S. (1991). Genetic control of primary neuronal development in zebrafish. *Development* **Supplemental**, 46-57.

Kimmel, C. B. and Westerfield, M. (1990). Primary neurons of the zebrafish. In *Signals and Sense*, (ed. G. M. Edelman W. E. Gall and M. W. Cowan), pp. 561-588. New York: Wiley-Liss.

Kimura, Y., Okamura, Y. and Higashijima, S. (2006). alx, a Zebrafish Homology of Chx10, Marks Ipsilateral Descending Excitatory Interneurons That Participate in The Regulation of Spinal Locomotor Circuits. *The Journal of Neuroscience* **26**, 5684-5697.

King, J., Banerjee, S. K., Marvin, J. and Ozdemir, O. (1982). A comparison of different magnetic methods for determining the relative grain size of magnetite in natural materials: some results from lake sediments. *Earth and Planetary Science Letters* **59**, 404-419.

Kirschvink, J. L. (1989). Magnetite Biomineralization and Geomagnetic Sensitivity in Higher Animals: An Update and Recommendations for Future Study. *Bioelectromagnetics* **10**, 239-259.

Kirschvink, J. L. and Gould, J. L. (1981). Biogenic Magnetite As A Basis For Magnetic Field Detection in Animals. *BioSystems* **13**, 181-201.

Kirschvink, J. L., Jones, D. S. and MacFadden, B. J. (1985). Magnetite Biomineralization and Magnetoreception in Organisms. In *Topics in Geobiology*, vol. 5 (ed. New York and London: Plenum Press.

Kirschvink, J. L., Kobayashi-Kirschvink, A. and Woodford, B. J. (1992a). Magnetite biomineralization in the human brain. *Proceedings of the National Academy of Science* **89**, 7683-7687.

Kirschvink, J. L., Kopp, R. E., Raub, T. D., Baumgartner, C. T. and Holt, J. W. (2008). Rapid, Precise, and High-Sensitivity Acquisition of Paleomagnetic and Rock-Magnetic Data: Development of a Low-Noise Automatic Sample Changing System for Superconducting Rock Magnetometers. *Geochemistry Geophysics Geosystems* **9**, 1-18.

Kirschvink, J. L., Kuwajima, T., Ueno, S., Kirschvink, S. J., Diaz-Ricci, J. C., Morales, A., Barwig, S. and Quinn, K. (1992b). Discrimination of low-frequency magnetic fields by honeybees: Biophysics and experimental tests. In *Sensory Transduction*, (ed. D. P. Corey and S. D. Roper), pp. 225-240. New York: Rockefeller University Press.

Kirschvink, J. L. and Lowenstam, H. A. (1979). Mineralization and Magnetization of Chiton Teeth-Paleomagnetic, Sedimentologic, and Biologic Implications of Organic Magnetite. *Earth and Planetary Science Letters* **44**, 193-204.

Kirschvink, J. L., Padmanabha, S., Boyce, C. K. and Oglesby, J. (1997). Measurement of the threshold sensitivity of honeybees to weak, extremely low-frequency magnetic fields. *The Journal of Experimental Biology* **200**, 1363-1368.

Kirschvink, J. L. and Walker, M. M. (1985). Particle-size considerations for magnetite-based magnetoreceptors. In *Magnetite Biomineralization and Magnetoreception in Organisms*, vol. 5 (ed. J. L. Kirschvink D. S. Jones and B. J. MacFadden), pp. 243-254. New York and London: Plenum Press.

Knaut, H., Blader, P., Strahle, U. and Schier, A. F. (2005). Assembly of Trigeminal Sensory Ganglia by Chemokine Signaling. *Neuron* **47**, 653-666.

Kollros, J. J. and Bovbjerg, A. M. (1997). Growth and Death of Rohon-Beard Cells in *Rana pipiens* and *Ceratophrys ornata*. *Journal of Morphology* **232**, 67-78.

Kopp, R. E., Raub, T. D., Schumann, D., Vali, H., Smirnov, A. V. and Kirschvink, J. L. (2007). Magnetofossil spike during the Paleocene-Eocene thermal maximum: Ferromagnetic resonance, rock magnetic, and electron microscopy evidence from Ancora, New Jersey, United States. *Paleoceanography* **22**, 1-7.

Kopp, R. E., Weiss, B. P., Maloof, A. C., Vali, H., Nash, C. Z. and Kirschvink, J. L. (2006). Chains, clumps, and strings: Magnetofossil taphonomy with ferromagnetic resonance spectroscopy. *Earth and Planetary Science Letters* **247**, 10 - 25.

Kullander, K. (2005). Genetics Moving to Neuronal Networks. *Trends in Neuroscience* **28**, 239.

Kuwada, J. Y., Bernhardt, R. R. and Nguyen, N. (1990). Development of Spinal Neurons and Tracts in the Zebrafish Embryo. *The Journal of Comparative Neurology* **302**, 617-628.

Lamborghini, J. E. (1987). Disappearance of Rohon-Beard Neurons From the Spinal Cord of Larval *Xenopus laevis*. *The Journal of Comparative Neurology* **264**, 47-55.
Lee, S. K. and Pfaff, S. L. (2001). Transcriptional Networks Regulating Neuronal Identity in The Developing Spinal Cord. *Nature Neuroscience* **4**, 1183-1191.
Lewis Katharine E., E. J. S. (2003). From cells to circuits: development of the zebrafish spinal cord. *Progress in Neurobiology* **69**, 419-449.
Lewis, K. E. (2005). How Do Genes Regulate Simple Behaviours? Understanding How Different Neurons in The Vertebrate Spinal Cord Are Genetically Specified. *Philosophical Transactions of The Royal Society B* **361**, 45-66.
Lewis, K. E. and Eisen, J. S. (2003). From Cells to Circuits: Development of The Zebrafish Spinal Cord. *Progress in Neurobiology* **69**, 419-449.
Lippert, P. C. and Zachos, J. C. (2007). A biogenic origin for anomalous fine-grained magnetic material at the Paleocene-Eocene boundary at Wilson Lake, New Jersey. *Paleoceanography* **22**, 1-8.
Lohmann, K. J. and Johnsen, S. (2000). The neurobiology of magnetoreception in vertebrate animals. *Trends in Neuroscience* **23**, 153-159.
Lohmann, K. J., Lohmann, C. M. F. and Putnam, N. F. (2007). Magnetic maps in animals: nature's GPS. *The Journal of Experimental Biology* **210**, 3697-3705.
Lowenstam, H. A. (1962). Magnetite in denticle capping in recent chitons (*Polyplacophora*). *Geological Society of America Bulletin* **73**, 435.
Lowrie, W. and Fuller, M. (1971). On the Alternating Field Demagnetization Characteristics of Multidomain Thermoremanent Magnetization in Magnetite. *Journal of Geophyiscal Research* **76**, 6339-6349.
McKay, B. E. and Persinger, M. A. (2005). Complex Magnetic Fields Enable Static Magnetic Field Cue Use for Rats in Radial Maze Tasks. *International Journal of Neuroscience* **115**, 625-648.
McLean, D. L., Fan, J., Higashijima, S., Hale, M. E. and Fetcho, J. R. (2007). A Topographic Map of Recruitment in Spinal Cord. *Nature* **446**.
McLean, D. L. and Fetcho, J. R. (2008). Using Imaging and Genetics in Zebrafish to Study Developing Spinal Circuits *In Vivo*. *Developmental Neurobiology* **68**, 817-834.
Megason, S. G. (2009). *In Toto* Imaging of Embryogenesis With Confocal Time-Lapse Microscopy. *Methods in Molecular Biology* **546**, 317-332.
Megason, S. G. and Fraser, S. E. (2003). Digitizing Life at the Level of the Cell: High-performance Laser-scanning Microscopy and Image Analysis for in toto Imaging of Development. *Mechanisms of Development* **120**, 1407-1420.
Miki, A. (1995). Developmental Changes in The Expression of alpha-, beta-, and gamma-Subspecies of Protein Kinase C at Synapses in The Ventral Horn of The Embryonic and Postnatal Rat Spinal Cord. *Brain Research Developmental Brain Research* **87**, 46-54.
Moore, A., Freake, S. M. and Thomas, I. M. (1990). Magnetic Particles in the Lateral Line of the Atlantic Salmon (*Salmo salar L.*). *Philosophical Transactions: Biological Sciences* **329**, 11-15.
Moore, A. and Riley, W. D. (2009). Magnetic particles associated with the lateral line of the European eel Anguilla anguilla. *Journal of Fish Biology* **74**, 1629-1634.

Moskowitz, B. M., Frankel, R. B. and Bazylinski, D. A. (1993). Rock magnetic criteria for the detection of biogenic magnetite. *Earth and Planetary Science Letters* **120**, 283-300.

Muheim, R., Edgar, N. M., Sloan, K. A. and Phillips, J. B. (2006). Magnetic Compass Orientation in C57BL/6J Mice. *Learning & Behavior* **34**, 366-373.

Murat, D., Quinlan, A., Vali, H. and Komeili, A. (2010). Comprehensive Genetic Dissection of The Magnetosome Gene Island Reveals The Step-Wise Assembly of A Prokaryotic Organelle. *Proceedings of the National Academy of Science* **107**, 5593-5598.

Nakano, Y., Fujita, M., Ogino, K., Saint-Amant, L., Kinoshita, T., Oda, Y. and Hirata, H. (2010). Biogensis of GPI-anchored proteins is essential for surface expression of sodium channels in zebrafish Rohon-Beard neurons to respond to mechanosensory stimulation. *Development* **137**, 1689-1698.

Nakao, T. and Ishizawa, A. (1987). Development of the spinal nerves in the lamprey: I. Rohon-Beard cells and interneurons. *Journal of Comparative Neurology* **256**, 342-355.

Ogura, M., Kato, M., Arai, N., Sasada, T. and Sakaki, Y. (1992). Magnetic particles in chum salmon (*Oncorhynchus keta*): extraction and transmission electron microscopy. *Canadian Journal of Zoology* **70** 874-877.

Ohno, S. and Nishizuka, Y. (2002a). Protein Kinase C Isotypes and Their Specific Functions: Prologue. *Journal of Biochemistry* **132**, 509-511.

Ohno, S.-g. and Nishizuka, Y. (2002b). Protein Kinase C Isotypes and Their Specific Functions: Prologue. *Journal of Biochemistry* **132**, 509-511.

Olivier, N., Luengo-Oroz, M., Duloquin, L., Faure, E., Savy, T., Veilleux, I., Solinas, X., Debarre, D., Bourgine, P., Santos, A. et al. (2010). Cell Lineage Reconstruction of Early Zebrafish Embryos Using Label-Free Nonlinear Microscopy. *Science* **329**, 976-971.

Parichy, D. M., Elizondo, M. R., Mills, M. G., Gordon, T. N. and Engeszer, R. E. (2009). Normal Table of Postembryonic Zebrafish Development: Staging by Externally Visible Anatomy of the Living Fish. *Developmental Dynamics* **238**, 2975-3015.

Park, H. C., Kim, C. H., Bae, Y. K., Yeo, S. Y., Kim, S. H., Hong, S. K., Shin, J., Yoo, K. W., Hibi, M., Hirano, T. et al. (2000). Analysis of Upstream Elements in The HuC Promoter Leads to The Establishment of Transgenic Zebrafish with Fluorescent Neurons. *Developmental Biology* **227**, 279-293.

Patten, S. A., Sihra, R. K., Dhami, K., Coutts, C. A. and Ali, D. W. (2007). Differential expression of PKC isoforms in developing zebrafish. *International Journal of Developmental Neuroscience* **25**, 155-164.

Penaloza, C., Lin, L., Lockshin, R. A. and Zakeri, Z. (2006). Cell death in development: shaping the embryo. *Histochemical Cell Biology* **126**, 149-158.

Presti, D. and Pettigrew, J. D. (1980). Ferromagnetic coupling to muscle receptors as a basis for geomagnetic field sensitivity in animals. *Nature* **285**, 99-101.

Reyes, R., Haendel, M., Grant, D., Melancon, E. and Eisen, J. S. (2004). Slow Degeneration of Zebrafish Rohon-Beard Neurons During Programmed Cell Death. *Developmental Dynamics* **229**, 30-41.

Ribera, A. B. and Nüsslein-Volhard, C. (1998). Zebrafish Touch-Insensitive Mutants Reveal an Essential Role for the Developmental Regulation of Sodium Current. *The Journal of Neuroscience* **18**, 9181-9191.

Rinkwitz, S., Mourrain, P. and Becker, T. S. (2011). Zebrafish: An Integrative System for Neurogenomics and Neurosciences. *Progress in Neurobiology* **93**, 231-243.
Ritz, T., Adem, S. and Schulten, K. (2000). A model for photoreceptor-based magnetoreception in birds. *Biophysical Journal* **78**, 707-718.
Ritz, T., Ahmad, M., Mouritsen, H., Wiltschko, R. and Wiltschko, W. (2010). Photoreceptor-based magnetoreception: optimal design of receptor molecules, cells, and neuronal processing. *Journal of the Royal Soceity Interface* **7**, S135-S146.
Rohon, J. V. (1884). Histogenese des Ruckenmarkes der Forelle. *Akad Wiss Math* **14**.
Sagasti, A., Guido, M. R., Raible, D. W. and Schier, A. F. (2005). Repulsive Interactions Shape the Morphologies and Functional Arrangements of Zebrafish Peripheral Sensory Arbors. *Current Biology* **15**, 804-814.
Sahin, B., Hawasli, A. H., Greene, R. W., Molkentin, J. D. and Bibb, J. A. (2008). Negative Regulation of Cyclin-Dependent Kinase 5 Targets by Protein Kinase C. *European Journal of Pharmacology* **581**, 270-275.
Saint-Amant, L. and Drapeau, P. (1998). Time Course of the Development of Motor Behaviors in the Zebrafish Embryo. *Journal of Neurobiology* **37**, 622-632.
Saint-Pierre, L. S. and Persinger, M. A. (2008). Behavioral Changes in Adult Rats After Prenatal Exposures to Complex, Weak Magnetic Fields. *Electromagnetic Biology and Medicine* **27**, 355-364.
Sapir, T., Geiman, E. J., Wang, Z., Velasquez, T., Mitsui, S., Yoshihara, Y., Frank, E., Alvarez, F. J. and Goulding, M. (2004). Pax6 and Engrailed 1 Regulate Two Distinct Aspects of Rental Cell Development. *The Journal of Neuroscience* **24**, 1255-1264.
Saueressig, H., Burrill, J. and Goulding, M. (1999). Engrailed-1 and Netrin-1 Regulate Axon Pathfinding by Association Interneurons That Project to Motor Neurons. *Development* **126**, 4201-4212.
Shcherbakov, D., Winklhofer, M., Petersen, N., Steidle, J., Hilbig, R. and Blum, M. (2005). Magnetosensation in Zebrafish. *Current Biology* **15**, R162.
Shirasaki, R. and Pfaff, S. L. (2002). Transcriptional Codes and The Control of Neuronal Identity. *Annual Review of Neuroscience* **25**, 251-281.
Sipple, B. A. (1998). The Rohon-Beard Cell: The Formation, Function, and Fate of A Primary Sensory System in The Embryonic Zebrafish, *Danio rerio*, vol. PhD (ed., pp. 47: Temple University).
Skauli, K. S., Reitan, J. B. and Walther, B. T. (2000). Hatching in Zebrafish (*Danio rerio*) Embryos Exposed to a 50 Hz Magnetic Field. *Bioelectromagnetics* **21**, 407-410.
Slatter, C. A. B., Kanji, H., Coutts, C. A. and Ali, D. W. (2004). Expession of PKC in the Developing Zebrafish, *Danio rerio*. *Journal of Neurobiology* **62**, 425-438.
Solov'yov, I. A. and Greiner, W. (2007). Theoretical Analysis of an Iron Mineral-Based Magnetoreceptor Model in Birds. *Biophysical Journal* **93**, 1493-1509.
Svoboda, K. R., Linares, A. E. and Ribera, A. B. (2001). Activity Regulates Programmed Cell Death of Zebrafish Rohon-Beard Neurons. *Development* **128**, 3511-3520.
Trinh, L. A., Hochgreb, T., Graham, M., Wu, D., Ruf, F., Jayasena, C., Saxena, A., Hawk, R., Gonzalez-Serricchio, A., Dixson, A. et al. (2011a). A versatile gene trap to visualize and interrogate the function of the vertebrate proteome., (ed., pp. 53. Pasadena: California Institute of Technology.

Trinh, L. A., Hochgreb, T., Graham, M., Wu, D., Ruf, F., Jayasena, C., Saxena, A., Hawk, R., Gonzalez-Serrichchio, A., Dixson, A. et al. (2011b). FlipTraps: Fluorescent Tagging and Cre-Mediated Mutagensis of Proteins at Their Endogenous Loci. *Genes & Development* **25**.

Udvadia, A. J. and Linney, E. (2003). Windows into Development: Historic, Current and Future Perspectives on Transgenic Zebrafish. *Developmental Biology* **256**, 1-7.

Vanderstraeten, J. and Gillis, P. (2010). Theoretical Evaluation of Magnetoreception of Power-Frequency Fields. *Bioelectromagnetics* **31**, 371-379.

Wajnberg, E., Acosta-Avalos, D., Alves, O. C., de Oliveira, J. F., Srygley, R. B. and Esquivel, D. M. S. (2010). Magnetoreception in Eusocial Insects: An Update. *Journal of the Royal Soceity Interface* **7**, S207-S225.

Walcott, C., Gould, J. L. and Kirschvink, J. L. (1979). Pigeons Have Magnets. *Science* **205**, 1027-1029.

Walker, M. M., Diebel, C. E. and Kirschvink, J. L. (2003). Detection and Use of The Earth's Magnetic Field by Aquatic Vertebrates. In *Sensory Processing in Aquatic Environments*, (ed. S. P. Collins and N. J. Marshall), pp. 53-74. New York: Springer-Verlag.

Walker, M. M., Kirschvink, J. L. and Dizon, A. E. (1985a). Magnetoreception and Biomineralization of Magnetite: Fish. In *Magnetite Biomineralization and Magnetoreception in Organisms*, vol. 5 (ed. J. L. Kirschvink D. S. Jones and B. J. MacFadden), pp. 417-437. New York and London: Plenum Press.

Walker, M. M., Kirschvink, J. L., Perry, A. and Dizon, A. E. (1985b). Detection, Extraction, and Characterization of Biogenic Magnetite. In *Magnetite Biomineralization and Magnetoreception in Organisms*, vol. 5 (ed. J. L. Kirschvink D. S. Jones and B. J. MacFadden), pp. 155-166. New York and London: Plenum Press.

Walker, M. M., Quinn, T. P., Kirschvink, J. L. and Groot, C. (1988). Production of Single-Domain Magnetite Throughout Life By Sockeye Salmon, *Oncorhynchus nerka*. *Journal of Experimental Biology* **140**, 51-63.

Weinstein, B. M. (2004). Something's Fishy in Bethesda: Zebrafish in The NIH Intramural Program. *Zebrafish* **1**, 12-20.

Weiss, B. P., Kim, S. S., Kirschvink, J. L., Koppe, R. E., Sankaran, M., Kobayashi, A. and Komeili, A. (2004). Ferromagnetic resonance and low-temperature magnetic tests for biogenic magnetite. *Earth and Planetary Science Letters* **224**, 73-89.

Westerfield, M. (1993). The Zebrafish Book. Eugene: University of Oregon Press.

Westerfield, M. (2000). The Zebrafish Book: A Guide for The Laboratory Use of Zebrafish (*Danio rerio*). Eugene: University of Oregon Press.

Williams, J. A., Barrios, A. Gatchalian, C., Rubin, L., Wilson, S.W., Holder, N. (2000). Programmed cell death in zebrafish Rohon Beard neurons is influenced by TrkC1/NT-3 signaling. *Developmental Biology* **226**, 220-230.

Wiltschko, R., Stapput, K., Ritz, T., Thalau, P. and Wiltschko, W. (2007). Magnetoreception in birds: different physical processes for two types of directional responses. *HFSP Journal* **1**, 41-48.

Wiltschko, R. and Wiltschko, W. (1995). Magnetic Orientation in Animals. Berlin, Heidelberg, New York: Springer Verlag.

Wiltschko, W. and Wiltschko, R. (2005). Magnetic Orientation and Magnetoreception in Birds and Other Vertebrates. *Journal of Comparative Physiology A* **191**, 675-693.

Winklhofer, M. and Kirschvink, J. L. (2010). A quantitative assessment of torque-transducer models for magnetoreception. *Journal of the Royal Soceity Interface*.
Wright, M. A. and Ribera, A. B. (2010). Brain-Derived Neurotrophic Factor Mediates Non-Cell-Autonomous Regulation of Sensory Neuron Position and Identity. *The Journal of Neuroscience* **30**, 14513-14521.
Wu, Y., Zhang, G., Xiong, Q., Luo, F., Cui, C., Hu, W., Yu, Y., Su, J., Xu, A. and Zhu, Z. (2006). Integration of Double-Fluorescence Expression Vectors into Zebrafish Genome for The Selection of Site-Directed Knockout/Knockin. *Marine Biotechnology* **8**, 304-311.
Youngstrom, K. A. (1944). Intramedullary sensory type ganglion cells in the spinal cord of human embryos. *Journal of Comparative Neurology* **81**, 47-53.
Zhou, Y., Yamamoto, M. and Engel, J. D. (2000). GATA2 is Required for the Generation of V2 Interneurons. *Development* **127**, 3829-3838.